8-1-1996

Modeling of road vehicle lateral dynamics

Joseph Kiefer

MODELING OF ROAD VEHICLE LATERAL DYNAMICS

by

Joseph R. Kiefer

A Thesis Submitted
in
Partial Fulfillment
of the
Requirements for the

MASTER OF SCIENCE
in

Mechanical Engineering

Approved by:

Professor _____
Dr. Kevin Kochersberger
Thesis Advisor

Professor _____
Dr. Alan Nye

Professor _____
Dr. Michael Hennessey

Professor _____
Dr. Charles Haines
Thesis Advisor

DEPARTMENT OF MECHANICAL ENGINEERING
COLLEGE OF ENGINEERING
ROCHESTER INSTITUTE OF TECHNOLOGY

AUGUST 1996

Disclosure Statement

Permission Granted

I, Joseph R. Kiefer, hereby grant permission to the Wallace Memorial Library of the Rochester Institute of Technology to reproduce my thesis entitled Modeling of Road Vehicle Lateral Dynamics in whole or in part. Any reproduction will not be for commercial use or profit.

August 16, 1996

_____

Joseph R. Kiefer

Abstract

The lateral dynamics of a road vehicle is studied through the development of a mathematical model. The vehicle is represented with two degrees of freedom, lateral and yaw. Equations of motion are derived for this vehicle model from basic principles of Newtonian mechanics. Both linear and non-linear models are developed.

In the linear model tire lateral forces are represented by an approximate linear relationship. Transfer functions are written for the vehicle system for various control and disturbance inputs. Steady-state and transient response characteristics and frequency response are studied, and numerical simulation of the model is performed.

In the non-linear model a detailed representation of tire lateral forces known as tire data nondimensionalization is utilized. Simulation is performed and compared with the linear model simulation to determine the range of applicability of the linear modeling assumptions.

Table of Contents

Disclosure Statement ii

Abstract iii

Table of Contents iv

List of Tables vi

List of Figures vii

List of Symbols x

Chapter 1 Introduction 1

Chapter 2 Literature Review 5

Chapter 3 Tire Behavior 10

3.1 Introduction 10

3.2 Lateral Force Mechanics 11

3.3 Linear Tire Model 14

3.4 Non-Linear Tire Model 14

Chapter 4 Two Degree-of-Freedom Vehicle Model 24

4.1 Introduction 24

4.2 Description of Model 25

4.2.1 Assumptions 26

4.2.2 Vehicle Parameters 27

4.2.3 Free-Body Diagram 28

4.3 Derivation of Equations of Motion 29

4.4 Derivation of Tire Slip Angles 31

4.5 Linear Model 33

4.5.1 Additional Assumptions 34

4.5.2 Vehicle Sideslip Angle 35

4.5.3 Tire Slip Angles 35

4.5.4 External Forces and Moments 36

4.5.5 Equations of Motion 37

4.5.6 Transfer Functions 39

4.5.7 Vehicle Sideslip Angle Gain 41

4.5.8 Yaw Velocity Gain 42

4.5.9 Front Tire Slip Angle Gain 42

4.5.10 Rear Tire Slip Angle Gain 43

4.5.11 Path Curvature Gain 43

4.5.12 Lateral Acceleration Steady-State Step Response Gain 44
4.5.13 Steady-State Steer Angle 45
4.5.14 Understeer Gradient 46
4.5.15 Stability Factor 48
4.5.16 Neutral Steer Point 48
4.5.17 Static Margin 49
4.5.18 Tangent Speed 50
4.5.19 Critical Speed 51
4.5.20 Characteristic Speed 51
4.5.21 Characteristic Equation 52
4.5.22 Undamped Natural Frequency 53
4.5.23 Damping Ratio 53
4.5.24 System Poles 55
4.5.25 System Zeros 55
4.5.26 Frequency Response 58
4.5.27 Simulation 65
4.6 Non-Linear Model 89
4.6.1 Model Equations 89
4.6.2 Simulation 90

Chapter 5 Conclusion 100

References 102

Appendix A Tire Model MATLAB Programs 105
A.1 MagicFit.m 105
A.2 MagicError.m 106
A.3 NLTire.m 107

Appendix B Two DOF Model Mathematica Session 108

Appendix C Two DOF Model MATLAB Programs 123
C.1 DOF2Control.m 123
C.2 DOF2Param.m 124
C.3 DOF2DependParam.m 126
C.4 SteerAngle.m 127
C.5 DOF2LFreq.m 129
C.6 DOF2LSim.m 130
C.7 DOF2LDE.m 132
C.8 DOF2NLSim.m 133
C.9 DOF2NLDE.m 135

Appendix D Relevant Literature 136

List of Tables

Table 3.1: Non-Linear Tire Model Parameters 17

Table 3.2: Experimental Tire Data 21

Table 4.1: Vehicle Parameters 28

Table 4.2: Linear Tire Model Parameters 36

Table 4.3: Steady-State Response Gains 45

Table 4.4: System Zeros 56

List of Figures

Figure 3.1: Tire Slip Angle 11

Figure 3.2: Tire Lateral Force Versus Slip Angle 12

Figure 3.3: Experimental Tire Data 21

Figure 3.4: Tire Cornering Coefficient 22

Figure 3.5: Tire Lateral Friction Coefficient 22

Figure 3.6: Tire Normalized Lateral Force 23

Figure 3.7: Reconstructed Tire Lateral Force 23

Figure 4.1: Vehicle Model 26

Figure 4.2: Free-Body Diagram 29

Figure 4.3: Kinematic Diagram 32

Figure 4.4: Gravitational Side Force 37

Figure 4.5: Natural Frequency vs. Vehicle Velocity 54

Figure 4.6: Poles and Zeros 57

Figure 4.7: Sideslip Angle / Steer Angle Frequency Response, V = 100 km/hr 61

Figure 4.8: Sideslip Angle / Aero Side Force Frequency Response, V = 100 km/hr 61

Figure 4.9: Sideslip Angle / Road Side Slope Frequency Response, V = 100 km/hr 62

Figure 4.10: Yaw Velocity / Steer Angle Frequency Response, V = 100 km/hr 62

Figure 4.11: Yaw Velocity / Aero Side Force Frequency Response, V=100 km/hr 63

Figure 4.12: Yaw Velocity / Road Side Slope Frequency Response, V = 100 km/hr 63

Figure 4.13: Sideslip Angle / Steer Angle Frequency Response, V = 30 km/hr 64

Figure 4.14: Sideslip Angle / Steer Angle Frequency Response, V = 49.84 km/hr 64

Figure 4.15: Simulation Steer Angle Inputs 67

Figure 4.16: Linear Step Steer Lateral Velocity Response 71

Figure 4.17: Linear Step Steer Yaw Velocity Response 71

Figure 4.18: Linear Step Steer Sideslip Angle Response 72

Figure 4.19: Linear Step Steer Front Tire Slip Angle Response 72

Figure 4.20: Linear Step Steer Rear Tire Slip Angle Response 73

Figure 4.21: Linear Step Steer Lateral Acceleration Response 73

Figure 4.22: Linear Ramp Step Steer Lateral Velocity Response 74

Figure 4.23: Linear Ramp Step Steer Yaw Velocity Response 74

Figure 4.24: Linear Ramp Step Steer Sideslip Angle Response 75

Figure 4.25: Linear Ramp Step Steer Front Tire Slip Angle Response 75

Figure 4.26: Linear Ramp Step Steer Rear Tire Slip Angle Response 76

Figure 4.27: Linear Ramp Step Steer Lateral Acceleration Response 76

Figure 4.28: Linear Ramp Square Steer Lateral Velocity Response 77

Figure 4.29: Linear Ramp Square Steer Yaw Velocity Response 77

Figure 4.30: Linear Ramp Square Steer Sideslip Angle Response 78

Figure 4.31: Linear Ramp Square Steer Front Tire Slip Angle Response 78

Figure 4.32: Linear Ramp Square Steer Rear Tire Slip Angle Response 79

Figure 4.33: Linear Ramp Square Steer Lateral Acceleration Response 79

Figure 4.34: Linear 1 Hz Sine Steer Lateral Velocity Response 80

Figure 4.35: Linear 1 Hz Sine Steer Yaw Velocity Response 80

Figure 4.36: Linear 1 Hz Sine Steer Sideslip Angle Response 81

Figure 4.37: Linear 1 Hz Sine Steer Front Tire Slip Angle Response 81

Figure 4.38: Linear 1 Hz Sine Steer Rear Tire Slip Angle Response 82

Figure 4.39: Linear 1 Hz Sine Steer Lateral Acceleration Response 82

Figure 4.40: Linear Step Aero Side Force Lateral Velocity Response 83

Figure 4.41: Linear Step Aero Side Force Yaw Velocity Response 83

Figure 4.42: Linear Step Aero Side Force Sideslip Angle Response 84

Figure 4.43: Linear Step Aero Side Force Front Tire Slip Angle Response 84

Figure 4.44: Linear Step Aero Side Force Rear Tire Slip Angle Response 85

Figure 4.45: Linear Step Aero Side Force Lateral Acceleration Response 85

Figure 4.46: Linear Step Road Side Slope Lateral Velocity Response 86

Figure 4.47: Linear Step Road Side Slope Yaw Velocity Response 86

Figure 4.48: Linear Step Road Side Slope Sideslip Angle Response 87

Figure 4.49: Linear Step Road Side Slope Front Tire Slip Angle Response 87

Figure 4.50: Linear Step Road Side Slope Rear Tire Slip Angle Response 88

Figure 4.51: Linear Step Road Side Slope Lateral Acceleration Response 88

Figure 4.52: Non-Linear Step Steer Lateral Velocity Response 94

Figure 4.53: Non-Linear Step Steer Yaw Velocity Response 94

Figure 4.54: Non-Linear Step Steer Sideslip Angle Response 95

Figure 4.55: Non-Linear Step Steer Front Tire Slip Angle Response 95

Figure 4.56: Non-Linear Step Steer Rear Tire Slip Angle Response 96

Figure 4.57: Non-Linear Step Steer Lateral Acceleration Response 96

Figure 4.58: Non-Linear Ramp Square Steer Lateral Velocity Response 97

Figure 4.59: Non-Linear Ramp Square Steer Yaw Velocity Response 97

Figure 4.60: Non-Linear Ramp Square Steer Sideslip Angle Response 98

Figure 4.61: Non-Linear Ramp Square Steer Front Tire Slip Angle Response 98

Figure 4.62: Non-Linear Ramp Square Steer Rear Tire Slip Angle Response 99

Figure 4.63: Non-Linear Ramp Square Steer Lateral Acceleration Response 99

List of Symbols[†]

$1/R$	Path curvature (1/m)
a	Distance from mass center to front axle (m)
$\mathbf{a_o}$	Acceleration of the origin of the vehicle-fixed coordinate system (m/s^2)
a_y	Acceleration of vehicle mass center in y-direction (m/s^2)
A_y	Acceleration of vehicle mass center in y-direction in units of "g" (g)
b	Distance from mass center to rear axle (m)
B_1	Magic Formula curve fit parameter
B_3	Tire cornering coefficient intercept (N/deg/N)
B_5	Tire lateral friction coefficient intercept
c	Distance from front axle to aerodynamic side force (m)
C_1	Magic Formula curve fit parameter
C_3	Tire cornering coefficient slope ($N/deg/N^2$)
C_5	Tire lateral friction coefficient slope
C_α	Tire cornering stiffness (N/rad)
C_f	Front tire cornering stiffness - two tires (N/rad)
C_r	Rear tire cornering stiffness - two tires (N/rad)
C_c	Tire cornering coefficient (N/deg)
d	Distance from front axle to neutral steer point (m)
D_1	Magic Formula curve fit parameter
E_1	Magic Formula curve fit parameter
f	Front axle weight fraction
$\mathbf{F}$	External force (N)

[†] By convention, scalar variables are italicized and vectors are boldfaced.

F_{ns}	Fictitious lateral force for finding neutral steer point (N)
F_y	Tire lateral force (N)
$\overline{F}_y$	Normalized tire lateral force
F_{ya}	Aerodynamic side force disturbance (N)
F_{yf}	Front tire lateral force - two tires (N)
F_{yg}	Gravitational side force disturbance (N)
F_{yr}	Rear tire lateral force - two tires (N)
F_z	Tire vertical load (N)
g	Acceleration due to gravity (m/s^2)
G	Linear momentum (kg-m/s)
H	Angular momentum (about mass center) ($kg\text{-}m^2/s$)
i	Unit vector in x-direction of vehicle-fixed coordinate system
I_{zz}	Total vehicle yaw mass moment of inertia ($kg\text{-}m^2$)
j	Unit vector in y-direction of vehicle-fixed coordinate system
k	Unit vector in z-direction of vehicle-fixed coordinate system
K	Stability factor (s^2/m^2)
K_{us}	Understeer gradient (rad)
L	Wheelbase (m)
m	Total vehicle mass (kg)
M	External moment (about mass center) (N-m)
N_r	Yaw damping derivative (N-m-s/rad)
N_β	Directional stability derivative (N-m/rad)
N_δ	Control moment derivative (N-m/rad)
r	Yaw velocity (rad/s)
R	Path radius (m)

$\mathbf{R}_f$	Position vector from vehicle mass center to front tire (m)
$\mathbf{R}_r$	Position vector from vehicle mass center to rear tire (m)
s	Laplace-domain variable
SM	Static margin
u	Forward velocity (m/s)
v	Lateral velocity (m/s)
V	Magnitude of vehicle velocity (m/s)
V_{char}	Characteristic speed (m/s)
V_{crit}	Critical speed (m/s)
$\mathbf{V}_f$	Velocity of front tire (m/s)
$\mathbf{V}_o$	Velocity of vehicle-fixed coordinate system (m/s)
$\mathbf{V}_r$	Velocity of rear tire (m/s)
V_{tan}	Tangent speed (m/s)
V_x	Component of velocity in x-direction (m/s)
V_y	Component of velocity in y-direction (m/s)
Y_r	Lateral force/yaw coupling derivative (N-s/rad)
Y_β	Damping-in-sideslip derivative (N/rad)
Y_δ	Control force derivative (N/rad)
α	Tire slip angle (rad)
$\overline{\alpha}$	Tire normalized slip angle
α_f	Front tire slip angle (rad)
α_r	Rear tire slip angle (rad)
β	Vehicle sideslip angle (rad)
δ	Front steer angle input (rad)
δ_{Acker}	Ackerman steer angle (rad)

δ_f	Front steer angle (rad)
δ_r	Rear steer angle (rad)
δ_{ss}	Steady-state steer angle for given path radius (rad)
$\overline{\psi}$	Magic Formula intermediate variable
θ	Road side slope (rad)
$\overline{\theta}$	Magic Formula intermediate variable
ζ	Damping ratio
μ_y	Tire lateral friction coefficient
ω_n	Undamped natural frequency (rad/s)
Ω	Angular velocity of vehicle-fixed coordinate system (rad/s)
Ω_z	Angular velocity of vehicle-fixed coordinate system about z-axis (rad/s)

1 Introduction

The first practical automobiles were built in 1886 by Karl Benz and Gottlieb Daimler.[1] The top speeds of these vehicles were only about fifteen miles per hour. With much of the automotive industry's early engineering effort devoted to developing faster vehicles, production car top speeds reached forty-five miles per hour by 1900 and eighty miles per hour by 1915. This year, Craig Breedlove will attempt to be the first man to travel faster than the speed of sound in a ground vehicle.

Since the top speeds of the first automobiles were relatively low, there was initially little concern with the dynamic behavior of the vehicles. However, as cars quickly became capable of achieving higher speeds, vehicle dynamics became an important concern for automotive engineers. Of primary importance from a safety standpoint was the behavior of vehicles in maneuvers such as turning and braking as top speeds increased. Also, since early roads were of very poor quality by today's standards, isolation of the driver and passengers from road disturbances became increasingly important.

The field of vehicle dynamics encompasses three basic modes of vehicle performance. Vertical dynamics, or ride dynamics, basically refers to the vertical response of the vehicle to road disturbances. Longitudinal dynamics involves the straight-line acceleration and braking of the vehicle. Lateral dynamics is concerned with the vehicle's turning behavior. Achieving acceptable performance in each of these modes is necessary in order for a vehicle to meet the requirements of the consumer, and the government, with regards to comfort, controllability, and safety. Vehicle dynamics needs to be considered throughout the entire design and development process from initial conceptualization through production if performance goals are to be met. Mathematical modeling is an excellent tool for engineers to use to design and develop vehicles that meet performance goals.

Traditionally there has been a relatively long cycle in the design and development process from the initial concept for a vehicle to its production. With such a long time from initial concept to production, vehicle designs can be out of style and obsolete by the time they reach production. Increasing competition from a globally expanding industry has driven automobile manufacturers to reduce the length of the design cycle. This allows manufacturers to respond more quickly to changes in market demand. In addition, reducing the length of the design cycle reduces the cost of developing a new vehicle.

One way that manufacturers can reduce design cycle length is by achieving the best possible design before any prototypes are built. The development of the digital computer and the techniques of computer-aided engineering such as solids modeling, finite element analysis, computational fluid dynamics, and multibody dynamics simulation have greatly facilitated this effort. As computer speeds continually increase and engineering software becomes more powerful, better vehicle designs can be obtained before prototypes are built, resulting in fewer prototypes and reduced development time and cost.

Mathematical modeling of vehicle dynamics helps engineers reduce the time it takes to achieve a design which will meet performance requirements for the consumer and for government regulations. A proposed design can be studied to determine if it can meet goals before any prototypes are built. The effects of design changes can be evaluated without building costly prototypes. Development engineers can use mathematical models to assist with the tuning of prototypes by identifying the changes which should be made to produce desired ride and handling characteristics.

Computer simulation offers a controlled, repeatable environment where the effects of individual parameters can be isolated without the influence of the variations in the environment. Simulation can remove the performance of the test driver from the picture to isolate the performance of the vehicle. In addition, simulation can be used to study maneuvers that could result in costly damage to the vehicle or danger to the test driver. An

example would be a maneuver resulting in roll over. Real time driving simulators can be used to train drivers and to evaluate driver performance in crash avoidance maneuvers or when drowsy or under the influence of alcohol. Many of the new safety and comfort related technologies such anti-lock brakes, traction control, stability control, and variable damping would be very difficult, if not impossible, to develop without the use of simulation. Computer simulation has many useful applications in the field of vehicle dynamics.

Vehicle dynamics models can have a wide range of complexity. Models can consider just a single mode of performance (vertical, longitudinal, lateral) or a combination of modes. Depending upon its purpose, a model must include representations of appropriate systems of the vehicle. Effects of the suspension system, steering system, powertrain system, braking system, or tires may need to be modeled. Representations of these systems can be linear or non-linear, quasi-static or dynamic depending upon the accuracy required. Control of the vehicle can be open-loop or it can be closed-loop if an appropriate representation of the driver is available. The vehicle model used must be suitable for the maneuvers it will simulate.

The subject of this thesis is the modeling of road vehicle lateral dynamics. As such, it is concerned with the turning behavior of the vehicle in response to control and disturbance inputs. A simple two degree-of-freedom vehicle model popularly known in the literature as the bicycle model is used in this study. Despite its simplicity, the two degree-of-freedom model can be very useful in demonstrating the interaction of major parameters such as tire properties, inertia properties, mass center location, wheelbase, and forward speed.

Chapter 2 is a review of vehicle dynamics literature relating to lateral dynamics. Since the majority of the forces acting on a vehicle are developed by the tires, an overview of tire lateral force mechanics is provided in Chapter 3 along with a description of the two

tire models used in this thesis. Both a linear tire model and a non-linear tire model are used in this study. The non-linear model is based on a method called tire data nondimensionalization.

Chapter 4 presents the main focus of this research, the development and application of the two degree-of-freedom vehicle model. Equations of motion are derived from basic principles of Newtonian mechanics. The model is then developed in two forms, linear and non-linear. In the linear model transfer functions are written and used to derive various measures of steady-state and transient response and to examine the frequency response of the vehicle to control and disturbance inputs. In addition, the response of the linear model to various inputs is simulated by integrating the differential equations of motion. Also, simulation of the non-linear model is performed and the results are compared with those of the linear model. Conclusions are drawn regarding the range of applicability of the linear model.

2 Literature Review

As mentioned in Chapter 1 as the top speeds of automobiles increased rapidly in the early part of this century vehicle dynamics became an important consideration to engineers. A large body of vehicle dynamics literature currently exists covering all aspects of vertical, longitudinal, and lateral performance. Fundamental to understanding lateral vehicle dynamics is knowledge of the mechanism of tire lateral force generation, and much has been written on this topic.

One of first papers concerning road vehicle lateral dynamics was written in 1908 by William Lanchester.[2] In this work Lanchester discussed the steering behavior of automobiles. However, complete understanding of turning behavior was hampered in the early years by a lack of understanding of tire mechanics. In 1925 George Broulhiet published a paper titled "The Suspension and the Automobile Steering Mechanism" which described tire lateral force generation in terms of the slip angle concept which is still used today and forms the basis for nearly all lateral vehicle dynamics models. Following this development tire dynamometers were built which could measure the forces generated by a tire under various conditions. These advancements paved the way for others to develop detailed explanations and models of turning behavior.

One of the early pioneers in vehicle dynamics research was Maurice Olley. He was responsible for the introduction of the independent front suspension in the United States for Cadillac and described the operation of the system in the 1934 SAE paper "Independent Wheel Suspension: Its Whys and Whererfores." A report written in 1937 titled "Suspension and Handling" reviewed the research in lateral dynamics during the preceding years and covered much of what is understood today.[3] Olley was active in vehicle dynamics from the early 1930's through his retirement in 1955. During the period of the

early 1960's he published a series of documents know today as "Olley's Notes"[4,5] which summarized his extensive knowledge of suspension systems and handling.

One of the most significant works concerning lateral vehicle dynamics was written in 1956 by Leonard Segal.[6] Segal, who worked at Cornell Aeronautical Laboratory, applied to the road vehicle many of the analytical techniques which had been developed for aircraft dynamics. In this work, entitled "Theoretical Prediction and Experimental Substantiation of the Response of the Automobile to Steering Control," Segal developed equations of motion for a linear three degree-of-freedom (yaw, lateral, and roll) model of vehicle turning behavior. Since digital computers were not available for his research, it was necessary to have a linear model for which transfer functions could be written and closed-form solutions found. Segal used the stability derivative technique in the derivation of the equations of motion and described the concepts of stability factor, neutral steer point, and static margin. Segal backed his modeling efforts with experimental testing of a vehicle and concluded that a linear model was sufficiently accurate for lateral motions of a reasonable magnitude.

A second paper "Design Implications of a General Theory of Automobile Stability and Control" written by David Whitcomb and William Milliken, also of Cornell Aeronautical Laboratory, was presented at the same time as Segal's paper as part of a five paper series "Research in Automobile Stability and Control and in Tyre Performance."[7] This paper studied the vehicle as a linear two degree-of-freedom system. This enabled the authors to utilize a large body of established techniques for the analysis of second order dynamic systems.

These papers preceded a great deal of research in lateral vehicle dynamics which has provided engineers today with a comprehensive understanding of the subject. Several textbooks have been written covering the subject of vehicle dynamics. Among these are *Car Suspension and Handling* (Bastow and Howard, 1993),[8] *Elementary Vehicle Dynamics*

(Cole, 1972),[9] *Tyres, Suspension and Handling* (Dixon, 1991),[10] *Vehicle Dynamics* (Ellis, 1969),[11] *Road Vehicle Dynamics* (Ellis, 1989),[12] *Fundamentals of Vehicle Dynamics* (Gillespie, 1992),[1] *Race Car Vehicle Dynamics* (Milliken and Milliken, 1995),[13] *Fundamentals of Vehicle Dynamics* (Mola, 1969),[14] *The Automotive Chassis: Engineering Principles* (Reimpell and Stoll, 1996),[15] *Mechanics of Vehicles* (Taborek, 1957),[16] and *Theory of Ground Vehicles* (Wong, 1993).[17] Most of these books utilize a two degree-of-freedom vehicle model when explaining turning behavior.

Another significant contribution to the literature was made in 1976 by Bundorf and Leffert.[18] In this work the cornering compliance concept is described. With this technique the contributions of various vehicle systems and characteristics to understeer are determined and added to estimate the total understeer of the vehicle. This allows engineers to see the effects of steering and suspension compliances, roll steer, tire cornering stiffnesses, tire camber stiffnesses, tire aligning torque, and lateral load transfer on understeer without developing the detailed vehicle models that would be necessary to simulate these effects directly. Since the computing hardware and software needed to analyze sufficiently detailed models was not readily available at the time, this concept was a significant advancement.

Since the work of Segal in 1956 many vehicle models have been developed which expand on his model. The dynamics of other systems such as the steering system have been integrated into the vehicle models. Lateral dynamics models have been expanded to include longitudinal and vertical degrees of freedom. Non-linearities, particularly in tire force generation, have been included in the models. Some examples in the literature can be found in works by Allen,[19] Heydinger,[20] and Xunmao.[21]

With the 1970's came the development of multibody dynamics codes. These software programs allow the parts of mechanisms, or in this case vehicles, to be modeled individually and connected using joints. By modeling each suspension component individually a very accurate kinematic representation of a complete vehicle can be obtained.

Examples of the application of multibody codes to vehicle dynamics can be found in the literature.[22,23] As computer processing speeds increase, the use of multibody codes for vehicle dynamics simulations becomes more practical. The biggest disadvantage with the use of these codes is the large amount of information that is required to construct the models. The dimensions, mass properties, and in some cases stiffnesses of each relevant component must be known to build an accurate model. Commercial multibody codes used for vehicle dynamics simulation include ADAMS, DADS, and Mechanica Motion.

Paramount to the development of successful vehicle dynamics models has been the development of accurate representations of tire behavior. Much effort has been devoted to this task and the results can be found in the literature. One the first attempts at a theoretical model of tire behavior was done by von Schlippe and Dietrich in 1941. They represented the tire by a massless taut string on an elastic foundation and predicted forces based on the geometry and material properties of the tire. Most of the major advancements in tire models have occurred within the last fifteen years as digital computers have become readily available. A comprehensive analysis of tire mechanics was performed under a government contract by Clarke in 1981.[24] In 1990 a detailed theoretical tire model was developed by Gim and Nikravesh.[25] However, most of the popular tire models in existence today are based primarily upon empirical data. These models involve curve fitting of experimentally measured tire data. One of the most popular empirical tire models known as the "Magic Formula" was published by Bakker, Nyborg, and Pacejka in 1987.[26] Other useful tire models include those by Radt[27] and Allen.[28] The development of accurate tire models has been critical to the success of vehicle dynamics modeling.

There exists a large body a literature regarding vehicle dynamics. The last forty years in particular have seen many significant developments on the topic. Models of vehicles and tires have been developed to the point where very accurate simulations of lateral dynamic response can be performed. The advent of the digital computer has greatly

enhanced the ability of engineers to develop and utilize these models for practical gains. A list of relevant sources from the vehicle dynamics literature reviewed during this research is provided in Appendix D.

3 Tire Behavior

3.1 Introduction

With the exception of gravitational and aerodynamic forces, all of the forces acting on a road vehicle are applied to the vehicle through its tires. In supporting the vehicle the ground applies vertical forces to the tires. When the vehicle changes speed or direction as a result of control inputs, the forces and moments which produce these accelerations are, in general, applied to the vehicle by the ground through the tires. Thus, to model the dynamics of road vehicles it is necessary to have a suitable representation of tire behavior. Two tire models are used in this thesis: a simple linear model and a more accurate, more widely applicable non-linear model.

The requirements of a tire model vary depending upon the aspects of vehicle performance which are being modeled and the accuracy required. In general, there are three force components and three moment components acting on a tire due to its interaction with the ground. In a complete model of vehicle dynamics where the longitudinal, lateral, and vertical motions of the vehicle are being studied, all six of these components must be included to accurately model the effect of the tires on the dynamics of the vehicle. However, this thesis is concerned only with the lateral dynamics of the vehicle. The simple vehicle model which is studied has only lateral and rotational degrees of freedom in the horizontal plane. Thus only forces in the lateral direction and moments about the vertical axis of the vehicle need to be considered. The moment acting on the tire itself about its vertical axis is called the tire aligning moment. The effect of the aligning moments of the tires on the overall dynamics of the vehicle is generally small compared to the effect of the lateral forces of the tires. In the vehicle model which is presented here the aligning moments of the tires are neglected. Thus the only aspect of tire behavior which is modeled is lateral force generation.

3.2 Lateral Force Mechanics

The mechanics of the lateral force generation of a tire is a complex process. A complete discussion of this process is beyond the scope of this thesis. Many thorough discussions of the mechanics of force generation exist in the literature.[1,13,17] The lateral force F_y generated by a pneumatic tire depends upon many variables including road surface conditions, tire carcass construction, tread design, rubber compound, size, pressure, temperature, speed, vertical load, longitudinal slip, inclination angle, and slip angle. For a given tire on unchanging, dry road surface conditions, vertical load and slip angle are the variables having the largest effect and are the variables considered for the tire models used in this thesis.

The tire slip angle is represented by the symbol α and is defined by SAE as "the angle between the *X'* axis and the direction of travel of the center of tire contact."[29] This

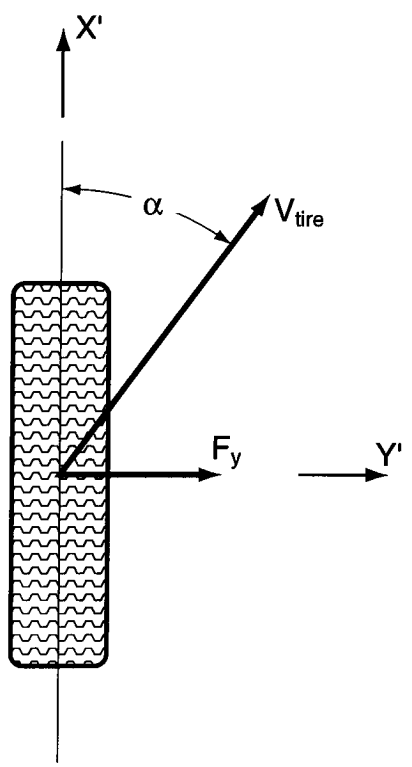

Figure 3.1: Tire Slip Angle

definition references the SAE tire axis system.[29] The origin of this system is at the center of the tire contact patch. The *X'* axis is the intersection of the plane of the wheel and the plane of the ground and is positive in the forward direction. The Z' axis is perpendicular to the plane of the road and is positive in the downward direction. The *Y'* axis is in the plane of the road and oriented to form a right-hand Cartesian coordinate system. The tire slip angle, lateral force, and tire axis system are shown in Figure 3.1. A positive slip angle and lateral force are shown. Simply stated, the slip angle is the angle between the direction the wheel is pointing and the direction it is traveling at a given instant in time.

The lateral force produced by a tire is a non-linear function of, among other variables, vertical load and slip angle. A typical lateral force versus slip angle curve for a single vertical load is shown in Figure 3.2. At low slip angles the curve is approximately linear. Here the lateral force generated depends primarily on the tire construction, tread design, and tire pressure. There is little sliding occurring between the tire and ground within the contact patch. Lateral force is developed as a result of deformation of the tire.

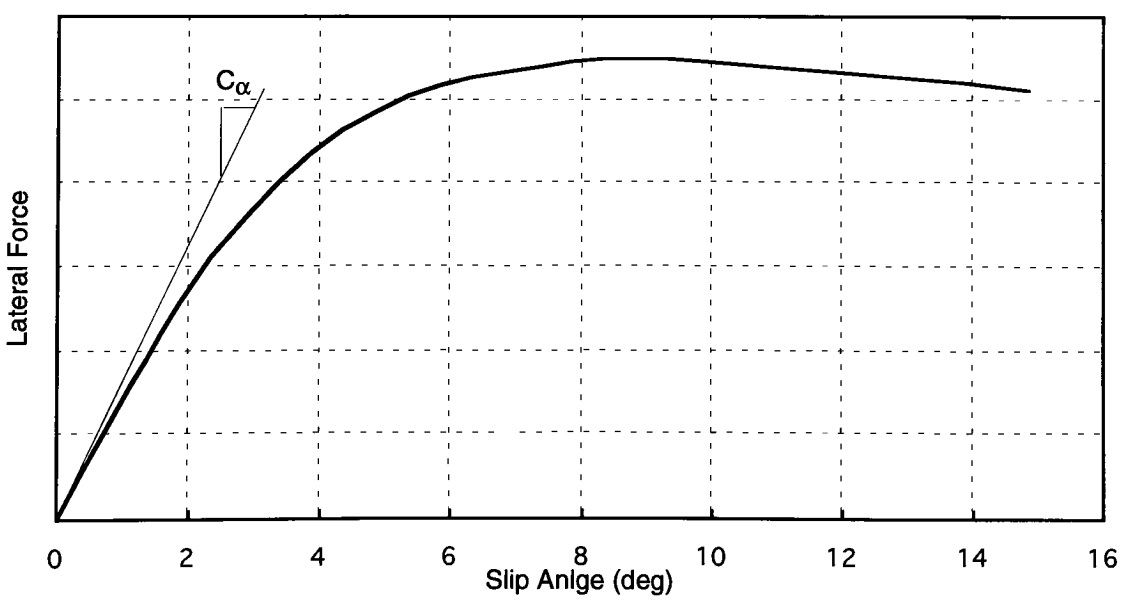

Figure 3.2: Tire Lateral Force Versus Slip Angle

The initial slope of lateral force versus slip angle curve is the cornering stiffness C_α of the tire. The cornering stiffness is often used as a linear approximation to the relationship between lateral force and slip angle (see Section 3.3). The cornering stiffness can be normalized by dividing by the vertical load. This quantity is the cornering coefficient C_c of the tire. The cornering stiffness and the cornering coefficient both vary with the vertical load on the tire. In general, the cornering stiffness increases with vertical load, while the cornering coefficient decreases. Both of these quantities are used in the tire models used in this thesis.

As the slip angle increases the slope of the lateral force curve decreases until the lateral force reaches a maximum. At this maximum the lateral force divided by the vertical force is the tire lateral friction coefficient μ_y. The lateral friction coefficient usually decreases as the vertical load on the tire increases. Beyond the slip angle at which the peak lateral force occurs, the lateral force begins to decrease. At high slip angles a larger portion of the contact patch is sliding than at low slip angles. Here the lateral force produced depends largely upon the tire rubber compound, the road surface, and the interface between them.

The curve shown in Figure 3.2 represents steady-state tire lateral force characteristics. Because of the elasticity and damping inherent in a pneumatic tire it is actually a dynamic system within itself. When a change in slip angle occurs, the change in lateral force lags behind. Although the effects of tire dynamics can be modeled by including an additional differential equation in the vehicle model for each tire, the effects are generally small below input frequencies of 3 Hz.[6] Tire dynamics are typically modeled when simulating emergency crash avoidance maneuvers such as a sudden lane change. Tire dynamics are neglected in the models of this thesis.

3.3 Linear Tire Model

As mentioned above the initial slope of the lateral force versus slip angle curve for a single vertical load is the cornering stiffness C_α of the tire at that load. Under certain conditions this characteristic can be used as a reasonable representation of tire behavior. Inspection of Figure 3.2 reveals that at small slip angles, the lateral force curve is nearly linear. Thus at sufficiently small slip angles, the lateral force produced by a tire can be approximated by the expression

$$F_y = C_\alpha \alpha \tag{3.1}$$

where

$$C_\alpha = \left.\frac{\partial F_y}{\partial \alpha}\right|_{\alpha=0^\circ} \tag{3.1}$$

When combined with other assumptions regarding the vehicle, linearization of the lateral force versus slip angle relationship permits modeling of the vehicle as a linear system. Since there is a wide variety of powerful, well-developed analysis techniques for linear systems, much can be learned about vehicle lateral dynamics from the study of a linear model. The range of applicability of the linear tire model is examined by comparison of simulations of linear and non-linear models in Section 4.6.2.

3.4 Non-Linear Tire Model

When tire slip angles become high the linear tire model does not accurately predict tire lateral force. At a high slip angle the linear model predicts a force which is higher than the actual tire force. A non-linear tire model is necessary to accurately determine tire lateral force at high slip angles.

As discussed in Chapter 2, several approaches to modeling tire behavior can be found in the literature. Some models are purely empirical, based upon curve fitting of experimentally measured tire data. Other models are primarily theoretical, with some

parameters determined experimentally, such as the stiffness of the tire. Each type of model has advantages and disadvantages. The type of tire model used in this thesis is the former, based entirely on empirical data. This type of tire model is used because of its limited complexity and its suitability to the tire data which is available to the researcher.

The tire model chosen for this study is called tire data nondimensionalization and was originated by Hugo Radt.[13,27,30] While this technique is able to predict tire aligning moment, longitudinal force, and lateral force for combined lateral slip, camber, and longitudinal slip, only the lateral force due to lateral slip is of interest in this thesis. The effects of camber on lateral force are being ignored, and the vehicle model assumes a constant forward velocity, so it is not necessary to consider longitudinal tire force. In this study tire aligning moments are considered to have a negligible effect on the overall dynamics of the vehicle.

There are two main steps in using the tire data nondimensionalization technique. The first step is preprocessing experimental tire data to determine the parameters for the tire model. The second step is using the model to calculate the tire lateral force for a given vertical load and slip angle. In a vehicle dynamics simulation, the first step would typically be done before running the simulation. The second step would be done at each time step during the simulation based on instantaneous values of tire vertical load and slip angle.

The tire data used for this study is based on experimental data provided by the manufacturer for a production passenger vehicle tire. The tire data is shown in tabular form at the end of this section in Table 3.2 and is plotted in Figure 3.3. Lateral force versus slip angle curves are available for vertical loads of 2793 N, 4190 N, 5587 N, 6984 N, and 8380 N. The slip angle varies from 0° to 15°. At each of the vertical loads the lateral force at 0° slip angle is not zero as might be expected. This is due to conicity and/or ply steer in the tire. Conicity arises from asymmetries in tire construction, while ply steer results from errors in the angles of the belt cords in the tire. Both conicity and ply steer depend upon

quality control in the manufacturing process and can be random in nature, varying from tire to tire. Since these effects are not important for the vehicle models under consideration here, these effects have been eliminated from the experimental data by shifting each of the lateral force curves to the left until they intersect the origin of the plot. This zeroed data is used in all subsequent analysis.

Preprocessing the experimental data is done by normalizing the data and then curve fitting the normalized data. The first step in normalizing the data is to determine the tire cornering coefficient C_c at each load. Since the cornering stiffness is the initial slope of the lateral force versus slip angle curve, and since the cornering coefficient is the cornering stiffness divided by the vertical load, the cornering coefficient can be approximated at each load by dividing the lateral force at 1° slip angle by the vertical load. Thus, from the experimental data the cornering coefficient at a single load is

$$C_c = \frac{C_\alpha}{F_z} \approx \frac{F_y\big|_{\alpha=1°}}{F_z} \tag{3.2}$$

The cornering coefficients at each load are plotted in Figure 3.4. As can be seen from the figure, the relationship between cornering coefficient and vertical load is approximately linear. For this tire the cornering coefficient as a function of vertical load can be represented as

$$C_c = B_3 + C_3 F_z \tag{3.3}$$

Values of the constants B_3 and C_3 are listed below in Table 3.1. This expression can be used to predict the cornering coefficient for an arbitrary load during a simulation.

Next the lateral friction coefficient μ_y at each load must be found. This is done by dividing the maximum lateral force for a given vertical load by the vertical load itself. Thus for a single vertical load, the lateral friction coefficient is

Table 3.1: Non-Linear Tire Model Parameters

Parameter	Symbol	Value
Tire cornering coefficient intercept	B_3	0.333
Tire cornering coefficient slope	C_3	-1.352×10^{-5}
Tire lateral friction coefficient intercept	B_5	1.173
Tire lateral friction coefficient slope	C_5	-3.696×10^{-5}
Magic Formula curve fit parameter	B_1	0.5835
Magic Formula curve fit parameter	C_1	1.7166
Magic Formula curve fit parameter	D_1	1.0005
Magic Formula curve fit parameter	E_1	0.2517

$$\mu_y = \frac{F_y\big|_{\max}}{F_z} \tag{3.4}$$

The lateral friction coefficients at each load are plotted in Figure 3.5. As with the cornering coefficients, the relationship between lateral friction coefficient and vertical load is approximately linear for this tire. The lateral friction coefficient can be expressed as

$$\mu_y = B_5 + C_5 F_z \tag{3.5}$$

Values of the constants B_5 and C_5 are provided in Table 3.1. This expression is used during simulation to predict the lateral friction coefficient for an arbitrary vertical load.

With the cornering coefficient and lateral friction coefficient known at each load for the experimental data, the normalized slip angle $\bar{\alpha}$ can be calculated at each data point from the expression

$$\bar{\alpha} = \frac{C_c \tan(\alpha)}{\mu_y} \tag{3.6}$$

Similarly, the normalized lateral force $\bar{F}_y$ at each data point is

$$\bar{F}_y = \frac{F_y}{\mu_y F_z} \tag{3.7}$$

When the normalized lateral force is plotted against the normalized slip angle at each data point, the results lie on a single curve as shown in Figure 3.6. The normalized data are then curve fit. While various functions could be used to fit this data, a popular function for fitting tire data known as the "magic formula" is used here.[26] The magic formula is a combination of trigonometric functions and has the ability to accurately fit tire data curves of various shapes such as lateral force, longitudinal force, and aligning moment. The normalized lateral force is fit to the function

$$\overline{F}_y = D_1 \sin\left(\overline{\theta}\right) \tag{3.8}$$

where

$$\overline{\theta} = C_1 \operatorname{atan}\left(B_1 \overline{\psi}\right) \tag{3.9}$$

and

$$\overline{\psi} = \left(1 - E_1\right)\overline{\alpha} + \frac{E_1 \operatorname{atan}\left(\mathrm{B}_1 \overline{\alpha}\right)}{B_1} \tag{3.10}$$

The parameters B_1, C_1, D_1, and E_1 must be determined to provide the best fit to the normalized experimental data. The curve fitting is implemented in the MATLAB script *MagicFit.m.* This script reads the normalized lateral force versus slip angle data from a file and uses the MATLAB Optimization Toolbox function *leastsq* to do a non-linear least squares fit. The *leastsq* function calls the function *MagicError.m* which computes the errors between each data point and the curve fit function. The parameters B_1, C_1, D_1, and E_1 are found to minimize the sum of the squares of these errors. *MagicFit.m* and *MagicError.m* are listed in Appendix A.1 and Appendix A.2 respectively. Values for the curve fit parameters are given in Table 3.1, and the function is plotted in Figure 3.6 along with the normalized data. It can be seen from the plot that a good fit to the data has been obtained.

With a function for the normalized lateral force in terms of normalized slip angle now available, the tire lateral force can be calculated for any combination of vertical load

and slip angle. First, the cornering coefficient and lateral friction coefficient are calculated from the vertical load using Eq. (3.3) and Eq. (3.5). Second, the normalized slip angle is calculated from the slip angle, the cornering coefficient, and the lateral friction coefficient using Eq. (3.6). Next, the normalized lateral force is calculated from the normalized slip angle using Eq. (3.10), Eq. (3.9), and Eq. (3.8). The tire lateral force can then be found from the normalized lateral force, the lateral friction coefficient, and the vertical load as

$$F_y = \overline{F}_y \mu_y F_z \tag{3.11}$$

This procedure is implemented in the MATLAB function *NLTire.m* which is listed in Appendix A.3. The function takes the tire vertical load and slip angle as inputs and outputs the lateral force. Plots of lateral force versus slip angle from this function for vertical loads of 2793 N, 4190 N, 5587 N, 6984 N, and 8380 N are shown in Figure 3.7 as solid lines along with the experimental data points.

The non-linear tire model implemented in this section accurately reproduces the experimentally determined lateral force versus slip angle relationship of the tire used in this study. This model is capable of predicting the lateral force produced by the tire at high slip angles. Thus the tire model is suitable for inclusion in a model of vehicle lateral dynamics where high tire slip angles are obtained. While this tire model only determines lateral force due to slip angle, it can be extended to predict aligning moment due to slip angle, lateral force and aligning moment due to camber, and longitudinal force due to longitudinal slip.

It should be noted that due to sign conventions in the SAE tire axis system and in the SAE vehicle coordinate system, a positive tire lateral force is produced by a negative slip angle. The description of the models in this chapter assumed that a positive slip angle produced a positive lateral force for convenience. However, when the tire models are integrated into the vehicle model appropriate care must be taken to ensure compatibility with

the sign convention required by the vehicle model. In the linear tire model the cornering stiffness must be negative to meet sign convention requirements.

Table 3.2: Experimental Tire Data

Slip Angle (deg)	Lateral Force @ Vertical Load (N)				
	2793	4190	5587	6984	8380
0	-89	-156	-245	-334	-378
1	737	1001	1223	1357	1458
2	1388	2024	2558	2869	3025
3	1935	2847	3603	4115	4404
4	2358	3403	4359	5026	5449
5	2647	3803	4849	5649	6183
6	2802	4026	5182	6005	6672
7	2910	4175	5350	6230	6950
8	2965	4241	5470	6330	7110
9	2969	4258	5490	6370	7166
10	2950	4246	5450	6352	7180
11	2930	4222	5400	6322	7153
12	2890	4168	5350	6291	7111
13	2840	4099	5282	6235	7050
14	2780	4037	5200	6160	6978
15	2750	3977	5121	6090	6900

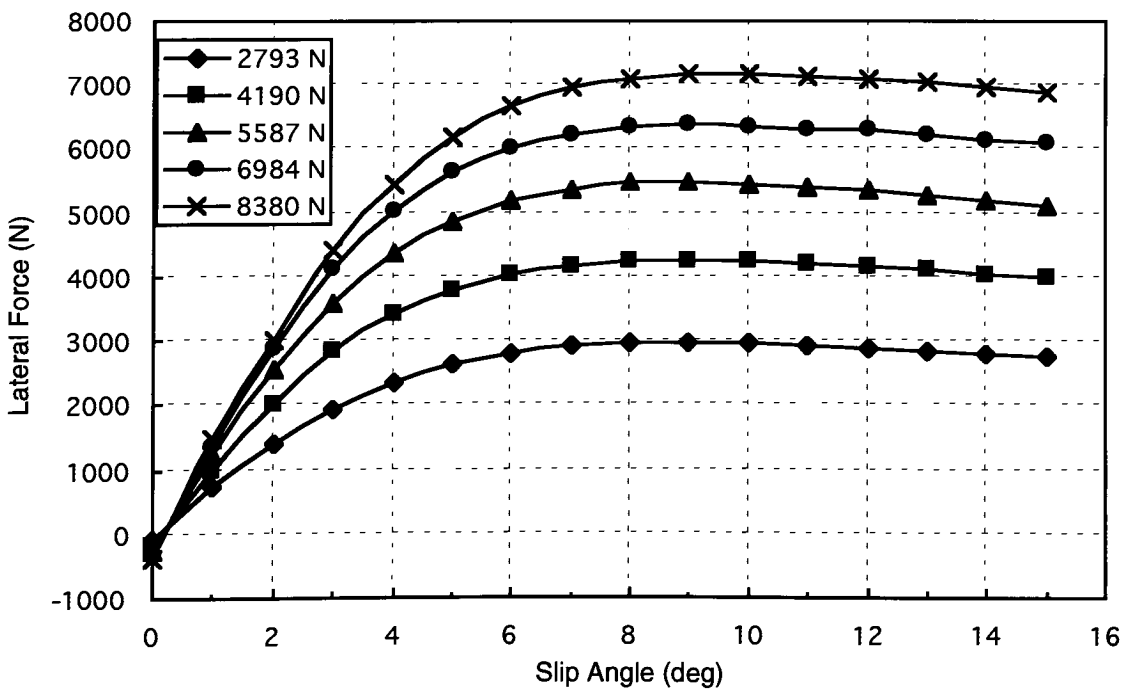

Figure 3.3: Experimental Tire Data

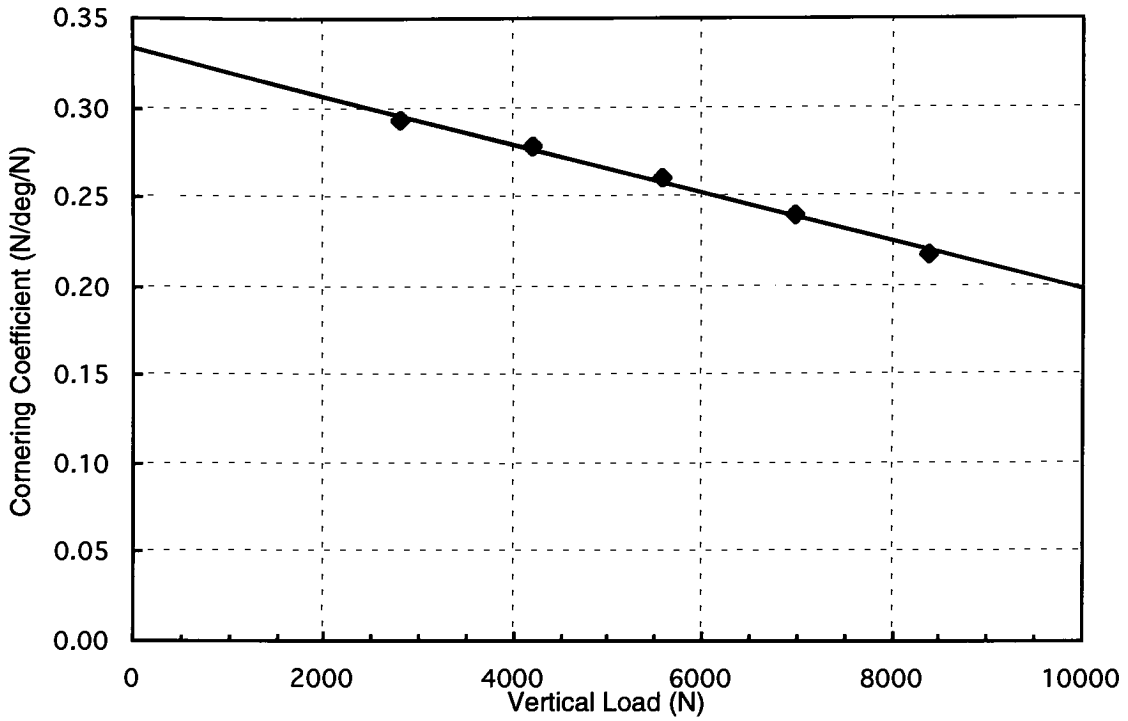

Figure 3.4: Tire Cornering Coefficient

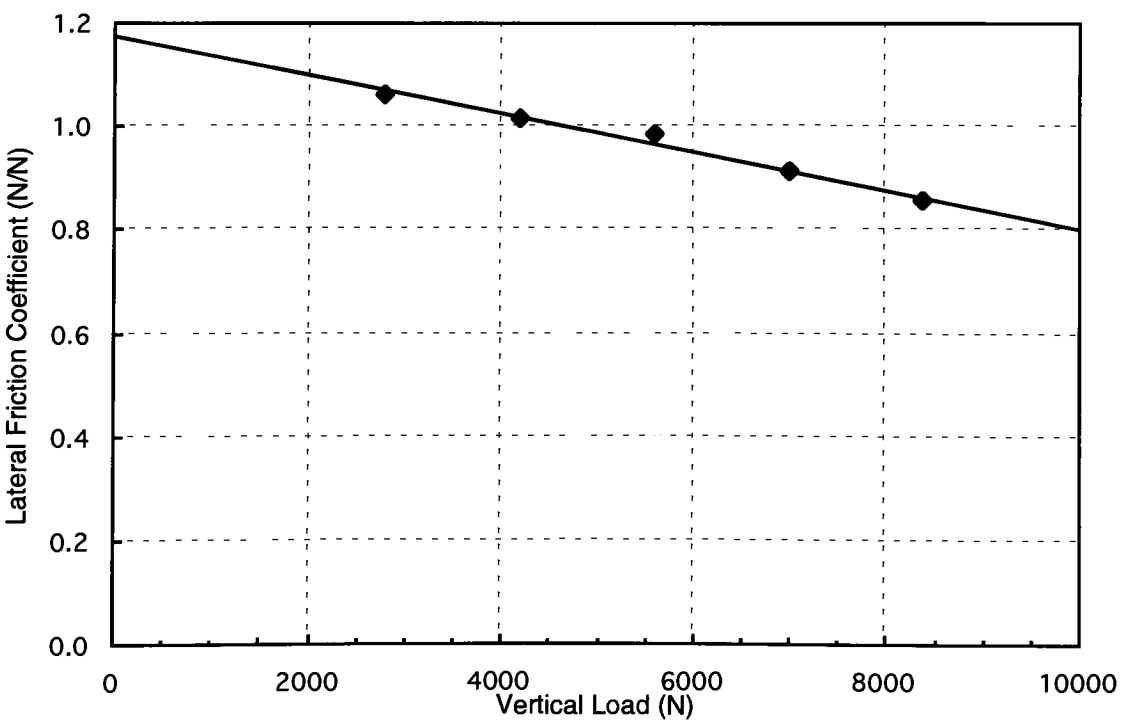

Figure 3.5: Tire Lateral Friction Coefficient

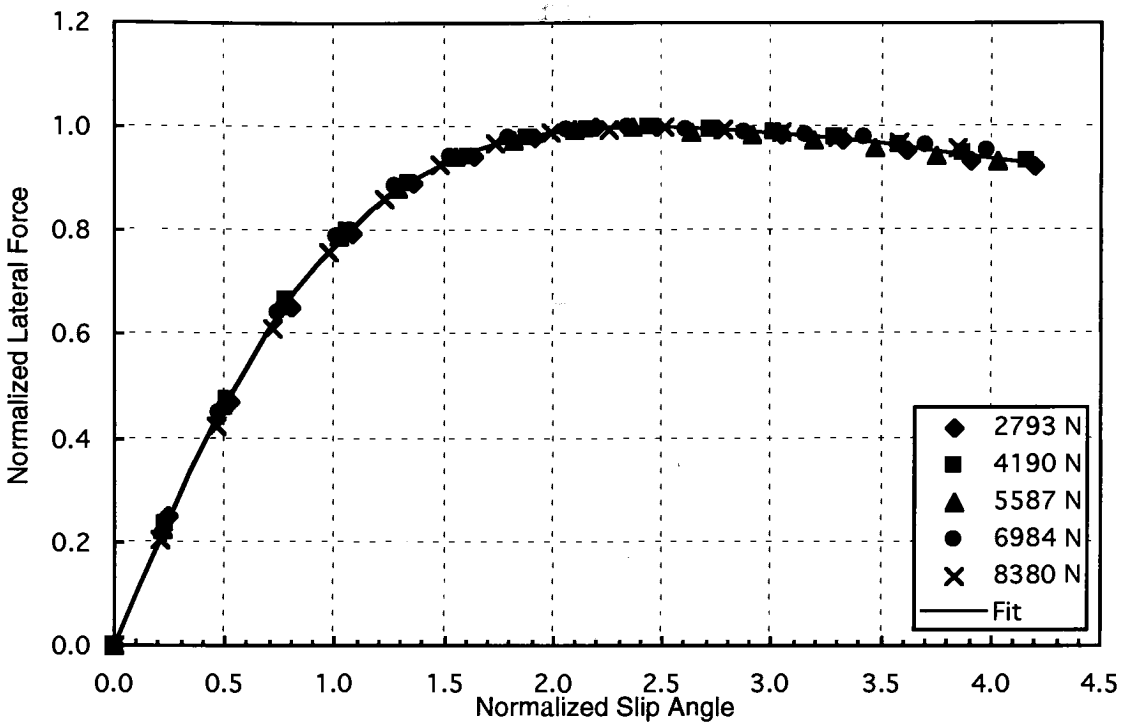

Figure 3.6: Tire Normalized Lateral Force

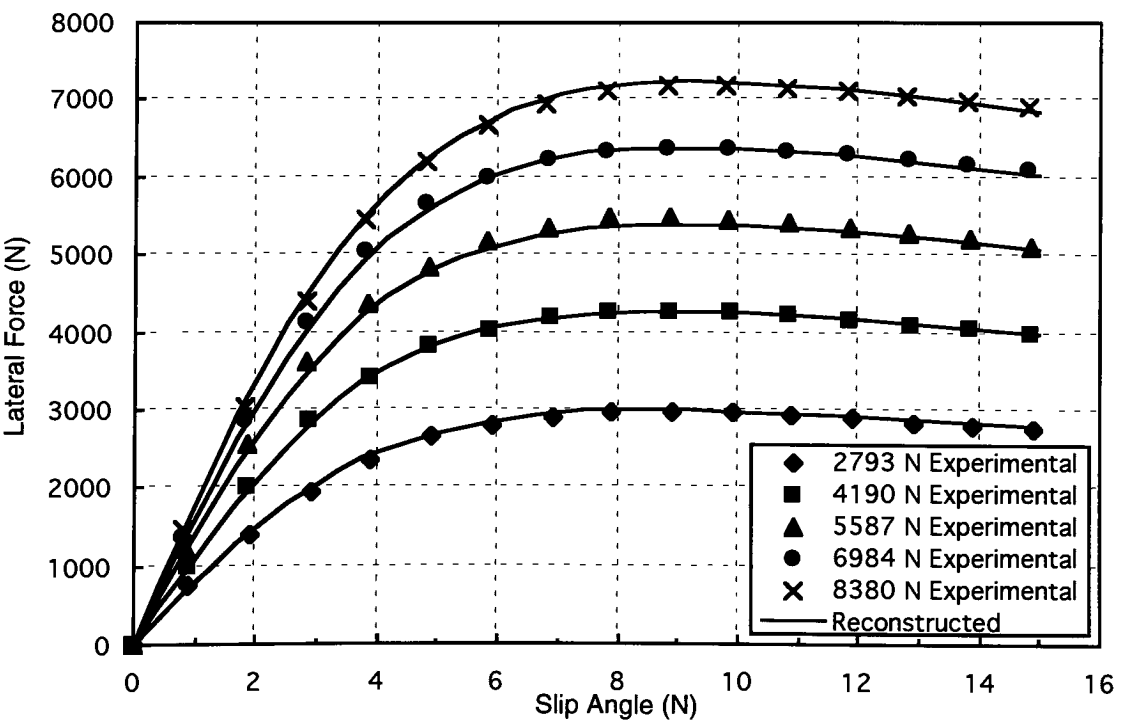

Figure 3.7: Reconstructed Tire Lateral Force

4 Two Degree-of-Freedom Vehicle Model

4.1 Introduction

Under normal driving conditions the driver and vehicle form a closed-loop system. The driver observes the motion of the vehicle and provides control inputs to produce the desired motion. However, this work is concerned primarily with predicting the open-loop lateral response of a road vehicle to control and disturbance inputs.

The simplest model which can realistically be used to examine the lateral response of a road vehicle is the two degree-of-freedom (DOF) "bicycle" model. As noted in Chapter 2, this model has been used extensively in the literature to study road vehicle lateral response. Although this model greatly simplifies the vehicle system, much can be learned about vehicle lateral response through its use. The model demonstrates the effects of major design and operational parameters such as tire properties, inertia properties, mass center location, wheelbase, and forward speed. Conclusions of practical significance regarding road vehicle lateral directional control and stability can be drawn using this simple model.[17]

In this chapter the two degree-of-freedom vehicle model is described in detail. The equations of motion are derived from basic principles of dynamics. Next, relationships for the tire slip angles are derived from the vehicle kinematics. From here the model is developed in two forms, linear and non-linear.

In the linear form of the model, additional assumptions are made which simplify the kinematic relationships and tire mechanics. This simplification allows powerful linear systems analysis techniques to be used to gain significant insight into the lateral dynamics of road vehicles. Transfer functions for the response of the vehicle to steering control, aerodynamic side force, and road side slope are developed. Several measures of steady-state and transient response are derived. Next, the frequency response of the vehicle is examined using bode plots. Finally, vehicle response is simulated for a variety of steering

inputs and for the disturbance inputs by integrating the differential equations of motion with respect to time.

In the non-linear form of the model, full non-linear kinematics and a non-linear tire model are used. The tire model, as described in Section 3.4, accounts for the non-linear, vertical load-dependent lateral force versus slip angle relationship. Simulation of the model response to steering inputs is performed and the results are compared to the linear model simulation.

4.2 Description of Model

The two degree-of-freedom model used in this chapter is shown in Figure 4.1. The vehicle is modeled as a single lumped mass rigid body and has lateral velocity v and yaw velocity r degrees of freedom. The forward velocity u is assumed to be constant. The pair of tires at each end of the vehicle is represented by a single tire at the centerline of the car. The vehicle has a wheel base L, a mass m, and a yaw mass moment of inertia I_{zz}, with its mass center located a distance a front the front axle and a distance b from the rear axle.

Rotation of the front tire about the vertical axis relative to the body is permitted and is measured by the front steer angle δ, with clockwise rotation considered positive. The front steer angle is the only control input considered. In this work position control is assumed. Position control is defined by SAE as "that mode of vehicle control wherein inputs or restraints are placed upon the steering system in the form of displacements at some control point in the steering system (front wheels, Pitman arm, steering wheel), independent of the force required."[29] This is in contrast to force control where inputs are in the form of forces or moments and are independent of displacement.

The standard SAE vehicle-fixed coordinate system x-y-z is used to describe the motion of the vehicle. The x-axis is positive in the forward direction, the y-axis is positive to the right, and the z-axis is positive down. The origin for the coordinate system is at the

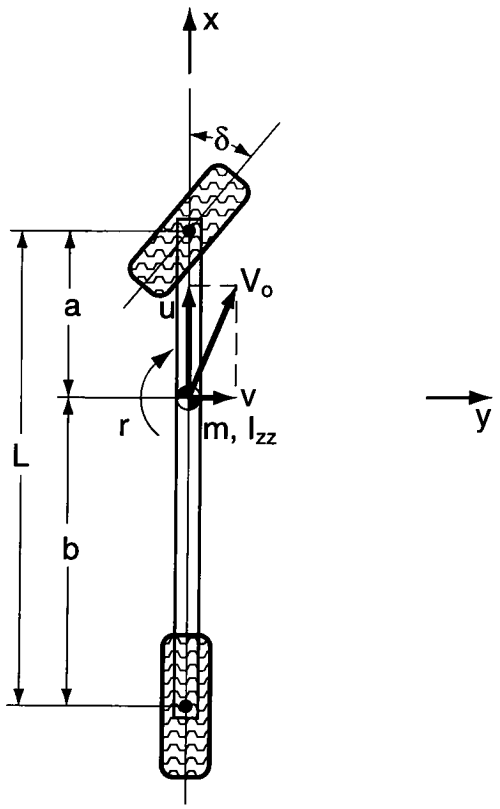

Figure 4.1: Vehicle Model

vehicle mass center, and the coordinate system translates and rotates with the vehicle. Motion is only permitted in the *x-y* plane.

4.2.1 Assumptions

Several simplifying assumptions are made to facilitate the development of the model:

- Constant vehicle parameters
- Constant vehicle forward velocity
- Motion in *x-y* plane only (ignore vertical, rolling, and pitching motions of sprung mass)
- Vehicle is rigid

- Vehicle is symmetrical about z-x plane
- Road surface is smooth
- Ignore effects of drive line
- Ignore longitudinal gravity effects (ignore road slope in longitudinal direction)
- Ignore all longitudinal forces (tire driving/braking forces, tire rolling resistance, aerodynamic drag)
- Ignore suspension system kinematics and dynamics
- Ignore steering system kinematics and dynamics
- Position control for steering input
- Ignore tire steer due to roll of sprung mass
- Ignore tire steer due to chassis compliance
- Ignore tire slip angles resulting from lateral tire scrub
- Ignore lateral and longitudinal load transfer (vertical tire forces remain constant)
- Tire properties are independent of time and forward velocity
- Ignore tire lateral forces due to camber, conicity, and ply steer.
- Ignore tire aligning moments
- Ignore effect of longitudinal tire slip on tire lateral force
- Ignore tire dynamics (no delay in lateral force generation)
- Ignore tire deflections

4.2.2 Vehicle Parameters

The nominal values of the vehicle parameters used for the two degree-of-freedom model in this study are given in Table 4.1. The International System of metric units (SI) is

used for all calculations. The base units are meter (m), kilogram (kg), and second (s). Force is measured in the derived unit newton (N). For convenience, the fraction of weight on the front axle f is used to define the position of the mass center along the wheelbase. The mass center location parameters a and b are then calculated from f and L. These parameters are representative of a production automobile.

Table 4.1: Vehicle Parameters

Parameter	Symbol	Value	
Vehicle mass	m	1775	kg
Yaw moment of inertia	I_{zz}	1960	kg-m^2
Front axle weight fraction	f	0.52	
Wheelbase	L	2.372	m
Distance from mass center to front axle	a	1.139	m
Distance from mass center to rear axle	b	1.233	m
Distance from front axle to aerodynamic side force	c	1.25	m

4.2.3 Free-Body Diagram

There are three types of external forces acting on a vehicle which are considered in this model: tire lateral forces, aerodynamic side force, and gravitational side force. The tire lateral forces F_{yf} and F_{yr} occur due to tire slip angles. The aerodynamic side force F_{ya} is a disturbance input acting at a distance c behind the front axle. This type of force acts on a vehicle when it encounters a crosswind. The gravitational side force F_{yg} is a disturbance input acting at the vehicle mass center and resulting from a side slope in the road. All forces are considered to be positive when acting in the positive y-direction. These forces are shown acting on the vehicle in Figure 4.2.

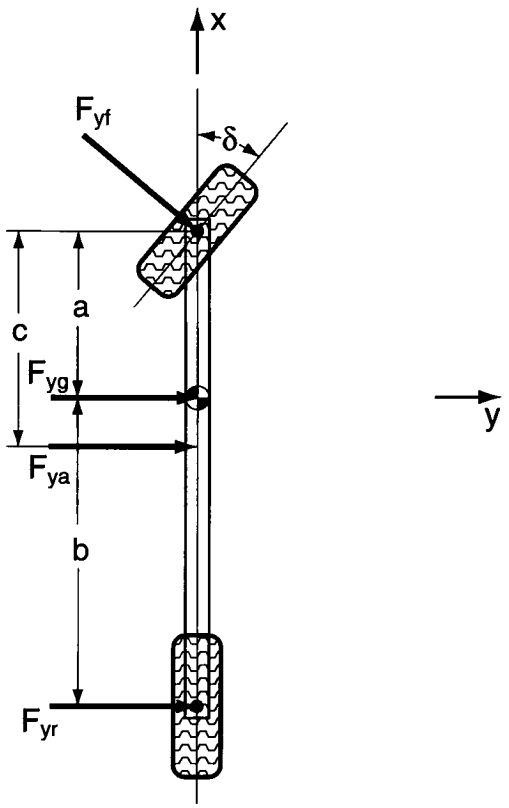

Figure 4.2: Free-Body Diagram

4.3 Derivation of Equations of Motion

The equations of motion for the two degree-of-freedom vehicle are derived using basic principles of Newtonian mechanics for rigid body motion relative to translating and rotating coordinate systems.[31] The basic equations relating the forces and moments acting on a rigid body to the acceleration of the body are

$$\begin{aligned} \sum \mathbf{F} &= \dot{\mathbf{G}} \\ \sum \mathbf{M}_G &= \dot{\mathbf{H}}_G \end{aligned} \tag{4.1}$$

where $\mathbf{F}$ and $\mathbf{M}_G$ are external forces and moments about the mass center (in vector form) acting on the body, and $\mathbf{G}$ and $\mathbf{H}_G$ are the linear and angular momenta of the body (also in vector form) measured relative to an inertial reference frame. Since in this model only

motion in the *x*-*y* plane is considered and all longitudinal (*x*-direction) forces are being ignored, Eq. (4.1) become

$$\begin{aligned} \sum F_y &= ma_y \\ \sum M_z &= I_{zz}\dot{\Omega}_z \end{aligned} \tag{4.2}$$

Since the *x*-*y*-*z* coordinate system is fixed to the vehicle with its origin at the vehicle mass center, the translational velocity of the vehicle mass center and rotational velocity of the vehicle are identical to those of the *x*-*y*-*z* system. From Figure 4.1, the velocity $\mathbf{V}_o$ of the origin of the *x*-*y*-*z* system is

$$\mathbf{V}_o = u\mathbf{i} + v\mathbf{j} \tag{4.3}$$

and the angular velocity Ω is

$$\Omega = r\mathbf{k} \tag{4.4}$$

Since the *x*-*y*-*z* system is rotating, the unit vectors are changing with time. Thus the acceleration $\mathbf{a}_o$ of the origin expressed in an inertial reference frame coincident with the *x*-*y*-*z* system is

$$\begin{aligned} \mathbf{a}_o &= \left.\frac{d\mathbf{V}_o}{dt}\right|_{xyz} + \Omega \times \mathbf{V}_o \\ &= (\dot{u} - vr)\mathbf{i} + (\dot{v} + ur)\mathbf{j} \end{aligned} \tag{4.5}$$

Similarly, the angular acceleration of the x-y-z system relative to the inertial frame is

$$\begin{aligned} \dot{\Omega} &= \left.\frac{d\Omega}{dt}\right|_{xyz} + \Omega \times \Omega \\ &= \dot{r}\mathbf{k} \end{aligned} \tag{4.6}$$

Thus the acceleration values of interest are

$$\begin{aligned} a_y &= \dot{v} + ur \\ \dot{\Omega}_z &= \dot{r} \end{aligned} \tag{4.7}$$

These values apply both to the vehicle-fixed *x*-*y*-*z* coordinate system and to the vehicle mass center.

The external forces acting on the vehicle are shown in their positive sense in Figure 4.2. A positive steer angle results in positive tire lateral forces. From the free-body diagram, it is seen that

$$\begin{aligned} \sum F_y &= F_{yf}\cos\delta + F_{yr} + F_{ya} + F_{yg} \\ \sum M_z &= aF_{yf}\cos\delta - bF_{yr} - (c-a)F_{ya} \end{aligned} \tag{4.8}$$

Substitution of Eq. (4.7) and Eq. (4.8) in Eq. (4.2) yields the equations of motion for the two degree-of-freedom vehicle:

$$\begin{aligned} F_{yf}\cos\delta + F_{yr} + F_{ya} + F_{yg} &= m(\dot{v} + ur) \\ aF_{yf}\cos\delta - bF_{yr} - (c-a)F_{ya} &= I_{zz}\dot{r} \end{aligned} \tag{4.9}$$

Here u is the vehicle forward velocity and is a constant. The state variables are the lateral velocity v and the yaw velocity r. F_{yf} and F_{yr} are the front and rear tire lateral forces. F_{ya} and F_{yg} are the aerodynamic side force and gravitational side force disturbance inputs, while the control input is the front steer angle δ.

4.4 Derivation of Tire Slip Angles

As discussed in Chapter 3, the lateral force produced by a tire depends upon, among other things, the vertical load on the tire and the slip angle of the tire. In this model the vertical load remains constant, but the front and rear tire slip angles vary as functions of the lateral velocity v and the yaw velocity r, which are the system state variables. Thus it is necessary to develop expressions for the front and rear tire slip angles, α_f and α_r, in terms of v and r.

Figure 4.3 is a kinematic diagram of the vehicle showing the tire velocity vectors and tire slip angles. Each slip angle is shown in its positive sense as the angle between the tire and the tire velocity vector. A positive slip angle implies a clockwise rotation from the tire to its velocity vector. However, for a positive steer input as shown in the figure, the tire

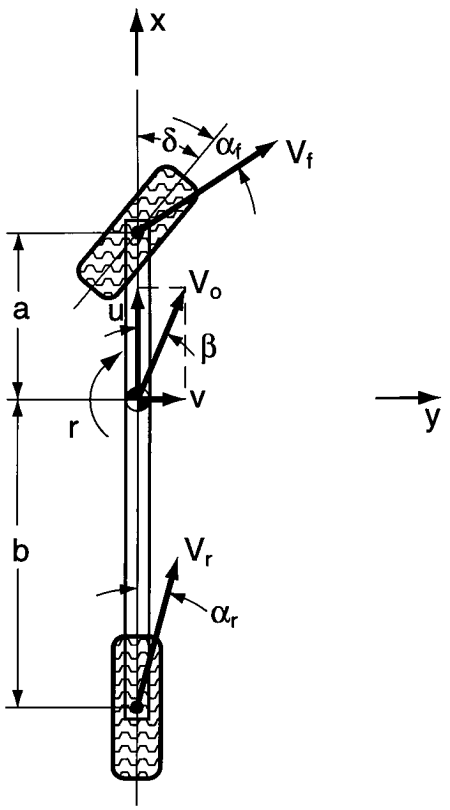

Figure 4.3: Kinematic Diagram

velocity vector is actually a counter-clockwise rotation from the tire, so slip angles are negative. In summary, a positive steer input results in negative tire slip angles.

The first step in determining the tire slip angles is finding the tire velocities. Since the translational and rotational velocities of the vehicle-fixed *x-y-z* coordinate system are already known from Eq. (4.3) and Eq. (4.4), it is convenient to use the principle of relative motion to derive the tire velocities.[31] The velocities $\mathbf{V}_f$ and $\mathbf{V}_r$ of the front and rear tires respectively are

$$\begin{aligned} \mathbf{V}_f &= \mathbf{V}_o + \Omega \times \mathbf{R}_f \\ \mathbf{V}_r &= \mathbf{V}_o + \Omega \times \mathbf{R}_r \end{aligned} \tag{4.10}$$

where $\mathbf{R}_f$ and $\mathbf{R}_r$ are position vectors from the vehicle mass center to the front and rear tires:

$$\begin{aligned} \mathbf{R}_f &= a\mathbf{i} \\ \mathbf{R}_r &= -b\mathbf{i} \end{aligned} \tag{4.11}$$

Thus the tire velocities are

$$\begin{aligned} \mathbf{V}_f &= u\mathbf{i} + (v + ar)\mathbf{j} \\ \mathbf{V}_r &= u\mathbf{i} + (v - br)\mathbf{j} \end{aligned} \tag{4.12}$$

In general, if the velocity and steer angle of the *i*th tire are known, the slip angle is

$$\alpha_i = \text{atan}\left(\frac{V_{yi}}{V_{xi}}\right) - \delta_i \tag{4.13}$$

where V_x and V_y are the x- and y-components of the velocity of the tire. Since steer of the rear tire is not permitted in this model, the tire slip angles are, in their general non-linear form,

$$\begin{aligned} \alpha_f &= \text{atan}\left(\frac{v + ar}{u}\right) - \delta \\ \alpha_r &= \text{atan}\left(\frac{v - br}{u}\right) \end{aligned} \tag{4.14}$$

4.5 Linear Model

Thus far the general non-linear equations of motion and tire slip angle relationships have been derived for the two degree-of-freedom vehicle. If additional assumptions are made to linearize the model, analysis techniques for linear systems may be used to gain more insight into road vehicle lateral dynamics. In this section, tire slip angles and lateral forces are assumed to be linear functions. Other research has shown that these assumptions are valid for vehicle lateral accelerations up to about 0.35 g, which corresponds to the linear range of the tire lateral force versus slip angle relationship.[13] Most automobile driving is done within this range, so results from the linear model are applicable over a wide range of driving situations.

It is common in modeling of vehicle lateral dynamics, particularly with linear models, to use the vehicle sideslip angle β instead of the lateral velocity v to describe the lateral motion of the vehicle. The vehicle sideslip angle is the angle between the vehicle-fixed x-axis and the vehicle velocity vector $\mathbf{V}_a$ as shown in Figure 4.3. Similar to Eq. (4.14) for tire slip angles, the vehicle sideslip angle is

$$\beta = \text{atan}\left(\frac{v}{u}\right) \tag{4.15}$$

A positive vehicle sideslip angle implies clockwise rotation from the x-axis to the velocity vector. For a given steer angle, the sideslip angle may be positive or negative, depending upon the forward speed.† In this thesis the vehicle sideslip angle is used in place of lateral velocity when finding transfer functions, steady-state response measures, transient response measures, and frequency response. However, since simulation of the non-linear model is more straightforward with lateral velocity as a state variable, simulation of the linear model is also performed with lateral velocity as a state variable to facilitate parallel development of the two simulation models.

Once the linearized equations of motion are written, transfer functions for the state variables in terms of the control and disturbance inputs are developed. From these transfer functions, measures of steady-state and transient response are derived and the frequency response is examined. Simulation of the model is performed for various steering and disturbance inputs.

4.5.1 Additional Assumptions

The following assumptions are made for the linear two degree-of-freedom model in addition to those listed in Section 4.2.1:

† See Section 4.5.18 for more information.

- Linear tire lateral force versus slip angle relationship
- Small steer angle, tire slip angles, vehicle sideslip angle, and road side slope angle.

4.5.2 Vehicle Sideslip Angle

With the small angle assumption, Eq. (4.15) for the vehicle sideslip angle becomes

$$\beta \approx \frac{v}{u} \tag{4.16}$$

However, if the vehicle sideslip angle is small then

$$\begin{gathered} \cos(\beta) = \frac{u}{V} \approx 1 \\ \text{or} \\ u \approx V \end{gathered} \tag{4.17}$$

where V is the magnitude of the vehicle velocity $\mathbf{V}_o$. Now Eq. (4.16) becomes

$$\beta \approx \frac{v}{V} \tag{4.18}$$

4.5.3 Tire Slip Angles

With the small angle assumption, the tire slip angles become

$$\begin{aligned} \alpha_f &= \frac{v + ar}{u} - \delta \\ \alpha_r &= \frac{v - br}{u} \end{aligned} \tag{4.19}$$

Furthermore, if vehicle sideslip angle is used in place of lateral velocity, then the tire slip angles can be expressed as

$$\begin{aligned} \alpha_f &= \beta + \frac{a}{V} r - \delta \\ \alpha_r &= \beta - \frac{b}{V} r \end{aligned} \tag{4.20}$$

4.5.4 External Forces and Moments

From the free-body diagram of the two degree-of-freedom model in Figure 4.2 it is seen that the four external forces acting on the vehicle are the front tire lateral force F_{yf}, the rear tire lateral force F_{yr}, the aerodynamic side force F_{ya}, and the gravitational side force F_{yg}.

With the assumption that tire lateral forces are linear functions of tire slip angle, the linear tire model of Section 3.3 can be employed. From Eq. (3.1) the tire lateral forces are

$$\begin{aligned} F_{yf} &= C_f \alpha_f \\ F_{yr} &= C_r \alpha_r \end{aligned} \tag{4.21}$$

where C_f and C_r are the front and rear tire cornering stiffnesses and are the effective cornering stiffnesses of both tires on an axle. Thus, for example, C_f is twice the cornering stiffness of a single front tire. As a result, F_{yf} and F_{yr} are the sums of the tire lateral forces of both tires on an axle. Since the tire slip angles are negative for a positive steer angle, the cornering stiffnesses must also be negative in order to produce the positive lateral forces required by the sign convention. For further explanation of this tire model see Section 3.3. Values for tire cornering stiffnesses for the vehicle studied are obtained though the application of Eq. (3.3) and are given in Table 4.2.

Table 4.2: Linear Tire Model Parameters

Parameter	Symbol	Value	
Front tire cornering stiffness (two tires)	C_f	-2461	N/deg
Rear tire cornering stiffness (two tires)	C_r	-2311	N/deg

The aerodynamic side force F_{ya} is in general a function of the relative air speed squared, the side force coefficient, and a reference area.[32] However, for simplicity the side force itself is used as the disturbance input to the system. The aerodynamic side force is positive when acting on the vehicle in the positive y-direction.

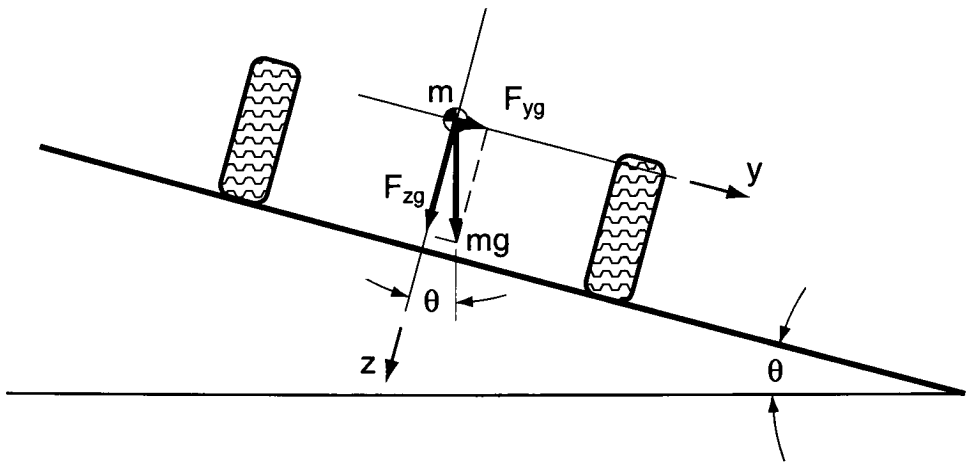

Figure 4.4: Gravitational Side Force

The gravitational side force F_{yg} is a function of the side slope in the road and is shown in Figure 4.4. The gravitational side force is positive when acting on the vehicle in the positive y-direction. Thus the gravitational side force can be expressed as

$$F_{yg} = mg\sin\theta \tag{4.22}$$

where g is the acceleration due to gravity and θ is the road side slope, which is positive for a road which is sloping down on the right side of the vehicle as shown in the figure. If the assumption of a small road side slope angle is used, then Eq. (4.22) simplifies to

$$F_{yg} = mg\theta \tag{4.23}$$

With the gravitational side force expressed in terms of the road side slope, the side slope θ can now be considered to be the disturbance input instead of the force itself.

4.5.5 Equations of Motion

With substitution of the tire slip angles from Eq. (4.20), the tire lateral forces from Eq. (4.21), and the gravitational side force from Eq. (4.23) into Eq. (4.9), the linearized equations of motion become

$$\begin{aligned}\left(C_f + C_r\right)\beta + \frac{aC_f - bC_r}{V} r - C_f\delta + F_{ya} + mg\theta &= mV\dot{\beta} + mVr \\ \left(aC_f - bC_r\right)\beta + \frac{a^2C_f + b^2C_r}{V} r - aC_f\delta - (c-a)F_{ya} &= I_{zz}\dot{r}\end{aligned} \tag{4.24}$$

The assumption that the steer angle is small has also been applied to reduce the equations to the above form. This assumption is generally valid for maneuvers at moderate to high speeds. For very low speed maneuvers, such as parking, large steer angles are often required.

To simplify manipulation of the equations of motion, the external force and moment terms of the left sides of Eq. (4.24) can be rewritten in terms of stability derivatives. This technique has been used extensively by early researchers in automobile lateral dynamics such as Leonard Segal, David Whitcomb, and William Milliken.[6,7,13] In addition to simplifying the equations of motion, the derivatives themselves have physical meaning which can give further insight into road vehicle lateral dynamics.

The stability derivatives are the rates of change of the external forces or external moments acting on the vehicle with respect to β, r, or δ. There are three stability derivatives associated with lateral force and three associated with yaw moment. The equations of motion in stability derivative form are

$$\begin{aligned}Y_\beta\beta + Y_r r + Y_\delta\delta + F_{ya} + mg\theta &= mV\dot{\beta} + mVr \\ N_\beta\beta + N_r r + N_\delta\delta - (c-a)F_{ya} &= I_{zz}\dot{r}\end{aligned} \tag{4.25}$$

where the stability derivatives are defined as follows:

$$
\begin{aligned}
Y_\beta &= C_f + C_r && \text{Damping} - \text{in} - \text{Sideslip} \\
Y_r &= \frac{aC_f - bC_r}{V} && \text{Lateral Force/Yaw Coupling} \\
Y_\delta &= -C_f && \text{Control Force} \\
N_\beta &= aC_f - bC_r && \text{Directional Stability} \\
N_r &= \frac{a^2C_f + b^2C_r}{V} && \text{Yaw Damping} \\
N_\delta &= -aC_f && \text{Control Moment}
\end{aligned}
\tag{4.26}
$$

In the two degree-of-freedom model under consideration the stability derivatives are all constants. As such, the equations of motion can be manipulated in stability derivative from without loss of generality.

By noting that the tire cornering stiffnesses C_f and C_r are always negative by definition, the signs of the stability derivatives can be obtained. The damping-in-sideslip derivative Y_β and yaw damping derivative N_r are always negative. The control force derivative Y_δ and control moment derivative N_δ are always positive. The lateral force/yaw coupling derivative Y_r and directional stability derivative N_β are both either positive or negative depending on the relative magnitudes of aC_f and bC_r. If aC_f is greater than the bC_r, then the derivatives are positive and the vehicle understeers. If aC_f is less than bC_r, then the derivatives are negative and the vehicle is oversteer. If the terms are equal, the derivatives are zero and the vehicle is neutral steer. Understeer, oversteer, and neutral steer are discussed in more detail in Section 4.5.14.

4.5.6 Transfer Functions

Now that the equations of motion are available in a simple, compact form, transfer functions can easily be found relating the outputs β and r to the inputs δ, θ, and F_{ya}. From these inputs and outputs six transfer functions can be formed. The transfer functions can be used to examine many aspects of system response such as steady-state response, frequency

response, and poles and zeros. The derivation of the transfer functions and all analytical expressions for measures of system response is done using Mathematica. The Mathematica session for the two degree-of-freedom vehicle is included in Appendix B.

To find the transfer functions the equations of motion are first written in the Laplace domain assuming that the initial conditions are zero:

$$\begin{bmatrix} s-\frac{Y_\beta}{mV} & 1-\frac{Y_r}{mV} \\ -\frac{N_\beta}{I_{zz}} & s-\frac{N_r}{I_{zz}} \end{bmatrix} \begin{pmatrix} \beta(s) \\ r(s) \end{pmatrix} = \begin{pmatrix} \frac{Y_\delta}{mV} \\ \frac{N_\delta}{I_{zz}} \end{pmatrix} \delta(s) + \begin{pmatrix} \frac{1}{mV} \\ \frac{a-c}{I_{zz}} \end{pmatrix} F_{ya}(s) + \begin{pmatrix} \frac{g}{V} \\ 0 \end{pmatrix} \theta(s) \tag{4.27}$$

From these Laplace-domain equations of motion, the transfer functions for vehicle sideslip angle are found to be

$$\frac{\beta}{\delta}(s) = \frac{\frac{Y_\delta}{mV}s - \frac{N_r Y_\delta + N_\delta(mV - Y_r)}{I_{zz}mV}}{s^2 - \left(\frac{N_r}{I_{zz}} + \frac{Y_\beta}{mV}\right)s + \frac{N_r Y_\beta + N_\beta(mV - Y_r)}{I_{zz}mV}} \tag{4.28}$$

$$\frac{\beta}{F_{ya}}(s) = \frac{\frac{1}{mV}s + \frac{(c-a)(mV - Y_r) - N_r}{I_{zz}mV}}{s^2 - \left(\frac{N_r}{I_{zz}} + \frac{Y_\beta}{mV}\right)s + \frac{N_r Y_\beta + N_\beta(mV - Y_r)}{I_{zz}mV}} \tag{4.29}$$

$$\frac{\beta}{\theta}(s) = \frac{\frac{g}{V}s - \frac{gN_r}{I_{zz}V}}{s^2 - \left(\frac{N_r}{I_{zz}} + \frac{Y_\beta}{mV}\right)s + \frac{N_r Y_\beta + N_\beta(mV - Y_r)}{I_{zz}mV}} \tag{4.30}$$

Similarly, the transfer functions for yaw velocity are

$$\frac{r}{\delta}(s) = \frac{\frac{N_\delta}{I_{zz}}s + \frac{N_\beta Y_\delta - N_\delta Y_\beta}{I_{zz}mV}}{s^2 - \left(\frac{N_r}{I_{zz}} + \frac{Y_\beta}{mV}\right)s + \frac{N_r Y_\beta + N_\beta(mV - Y_r)}{I_{zz}mV}} \tag{4.31}$$

$$\frac{r}{F_{ya}}(s)=\frac{\dfrac{a-c}{I_{zz}}s+\dfrac{Y_\beta(c-a)+N_\beta}{I_{zz}mV}}{s^2-\left(\dfrac{N_r}{I_{zz}}+\dfrac{Y_\beta}{mV}\right)s+\dfrac{N_rY_\beta+N_\beta(mV-Y_r)}{I_{zz}mV}} \tag{4.32}$$

$$\frac{r}{\theta}(s)=\frac{\dfrac{gN_\beta}{I_{zz}V}}{s^2-\left(\dfrac{N_r}{I_{zz}}+\dfrac{Y_\beta}{mV}\right)s+\dfrac{N_rY_\beta+N_\beta(mV-Y_r)}{I_{zz}mV}} \tag{4.33}$$

The above transfer functions for the lateral dynamics of the two degree-of-freedom vehicle can be used to examine steady-state behavior. For each of the three types of inputs, the steady-state step input response gains in vehicle sideslip angle, yaw velocity, tire slip angles, path curvature, and lateral acceleration are found. The steer angle required to produce a given turn radius is calculated. In addition, measures of steady-state vehicle behavior such as understeer gradient, stability factor, neutral steer point, static margin, tangent speed, critical speed, and characteristic speed are defined and expressed in terms of the stability derivatives.

The steady-state step response of vehicle sideslip angle and yaw velocity can be found for each of the three inputs by applying the Final Value Theorem to the transfer functions.[33] Before the Final Value Theorem can be applied, however, the stability of the system must be verified. The system is stable if none of the poles have positive real parts. Expressions for the system poles are derived in Section 4.5.24.

4.5.7 Vehicle Sideslip Angle Gain

Application of the Final Value Theorem to the vehicle sideslip angle transfer functions for steer angle, aerodynamic side force, and road side slope (Eq. (4.28), Eq. (4.29), and Eq. (4.30) respectively) gives the following steady-state response gains:

$$\left.\frac{\beta}{\delta}\right|_{ss} = -\frac{N_r Y_\delta + N_\delta (mV - Y_r)}{N_r Y_\beta + N_\beta (mV - Y_r)} \tag{4.34}$$

$$\left.\frac{\beta}{F_{ya}}\right|_{ss} = \frac{(c-a)(mV - Y_r) - N_r}{N_r Y_\beta + N_\beta (mV - Y_r)} \tag{4.35}$$

$$\left.\frac{\beta}{\theta}\right|_{ss} = -\frac{mgN_r}{N_r Y_\beta + N_\beta (mV - Y_r)} \tag{4.36}$$

Results for the sideslip angle response gains and for the response gains that follow are given in Table 4.3. The vehicle and tire parameters used for the calculations are given in Table 4.1 and Table 4.2, and the vehicle forward speed is 100 km/hr.

4.5.8 Yaw Velocity Gain

Similarly, the yaw velocity steady-state response gains are

$$\left.\frac{r}{\delta}\right|_{ss} = \frac{N_\beta Y_\delta - N_\delta Y_\beta}{N_r Y_\beta + N_\beta (mV - Y_r)} \tag{4.37}$$

$$\left.\frac{r}{F_{ya}}\right|_{ss} = \frac{Y_\beta (c-a) + N_\beta}{N_r Y_\beta + N_\beta (mV - Y_r)} \tag{4.38}$$

$$\left.\frac{r}{\theta}\right|_{ss} = \frac{mgN_\beta}{N_r Y_\beta + N_\beta (mV - Y_r)} \tag{4.39}$$

4.5.9 Front Tire Slip Angle Gain

Once steady-state values of vehicle sideslip angle and yaw velocity are known the steady-state tire slip angles can be found using Eq. (4.20). The front tire slip angle gains are

$$\left.\frac{\alpha_f}{\delta}\right|_{ss} = \frac{a\left(N_\beta Y_\delta - N_\delta Y_\beta\right) - V(mV - Y_r)\left(N_\beta + N_\delta\right) - VN_r\left(Y_\beta + Y_\delta\right)}{V\left(N_r Y_\beta + N_\beta (mV - Y_r)\right)} \tag{4.40}$$

$$\left.\frac{\alpha_f}{F_{ya}}\right|_{ss} = \frac{V(c-a)(mV-Y_r)+a(c-a)Y_\beta + aN_\beta - VN_r}{V\left(N_rY_\beta + N_\beta(mV-Y_r)\right)} \tag{4.41}$$

$$\left.\frac{\alpha_f}{\theta}\right|_{ss} = \frac{mg\left(aN_\beta - VN_r\right)}{V\left(N_rY_\beta + N_\beta(mV-Y_r)\right)} \tag{4.42}$$

4.5.10 Rear Tire Slip Angle Gain

Similarly, the steady-state rear tire slip angle gains are

$$\left.\frac{\alpha_r}{\delta}\right|_{ss} = \frac{-VN_\delta(mV-Y_r)-b\left(N_\beta Y_\delta - N_\delta Y_\beta\right)-VN_rY_\delta}{V\left(N_rY_\beta + N_\beta(mV-Y_r)\right)} \tag{4.43}$$

$$\left.\frac{\alpha_r}{F_{ya}}\right|_{ss} = \frac{V(c-a)(mV-Y_r)-b(c-a)Y_\beta - bN_\beta - VN_r}{V\left(N_rY_\beta + N_\beta(mV-Y_r)\right)} \tag{4.44}$$

$$\left.\frac{\alpha_r}{\theta}\right|_{ss} = \frac{-mg\left(bN_\beta + VN_r\right)}{V\left(N_rY_\beta + N_\beta(mV-Y_r)\right)} \tag{4.45}$$

4.5.11 Path Curvature Gain

Another response measure of interest is the curvature of the path that the vehicle follows when subject to one of the inputs. The path curvature *1/R* is the reciprocal of the path radius and can be found by dividing the yaw velocity by the vehicle velocity.

$$1/R = \frac{r}{V} \tag{4.46}$$

The path curvature gains for each of the inputs are

$$\left.\frac{1/R}{\delta}\right|_{ss} = \frac{N_\beta Y_\delta - N_\delta Y_\beta}{V\left(N_rY_\beta + N_\beta(mV-Y_r)\right)} \tag{4.47}$$

$$\left.\frac{1/R}{F_{ya}}\right|_{ss} = \frac{Y_\beta(c-a)+N_\beta}{V\left(N_rY_\beta + N_\beta(mV-Y_r)\right)} \tag{4.48}$$

$$\left.\frac{1/R}{\theta}\right|_{ss} = \frac{mgN_\beta}{V\left(N_r Y_\beta + N_\beta (mV - Y_r)\right)} \tag{4.49}$$

4.5.12 Lateral Acceleration Steady-State Step Response Gain

Lateral acceleration is an important measure of vehicle cornering performance. Lateral acceleration is typically expressed in units of "g". The linear vehicle model being considered here is valid for lateral accelerations up to approximately 0.35 g. Beyond that level, non-linearities, particularly in tire lateral force mechanics, become significant. Most passenger car driving is done below this limit, although a typical passenger car may be able to attain maximum lateral accelerations of approximately 0.7-0.8 g with standard street tires. Race cars without the aid of aerodynamic downforce reach over 1.2 g with special tires designed specifically for racing, while race cars with aerodynamic downforce have been known to exceed 4 g lateral acceleration. The steady-state lateral acceleration A_y expressed in units of "g" is

$$A_y = \frac{rV}{g} \tag{4.50}$$

The lateral acceleration gains for each of the inputs are

$$\left.\frac{A_y}{\delta}\right|_{ss} = \frac{V\left(N_\beta Y_\delta - N_\delta Y_\beta\right)}{g\left(N_r Y_\beta + N_\beta (mV - Y_r)\right)} \tag{4.51}$$

$$\left.\frac{A_y}{F_{ya}}\right|_{ss} = \frac{V\left(Y_\beta (c-a) + N_\beta\right)}{g\left(N_r Y_\beta + N_\beta (mV - Y_r)\right)} \tag{4.52}$$

$$\left.\frac{A_y}{\theta}\right|_{ss} = \frac{mVN_\beta}{N_r Y_\beta + N_\beta (mV - Y_r)} \tag{4.53}$$

Table 4.3: Steady-State Response Gains

V = 100 km/hr

Response	Steer Angle (δ)	Aerodynamic Side Force (F_{ya})	Road Side Slope (θ)
Vehicle sideslip angle (β)	-1.52 ° /°	2.82×10^{-4} ° /N	0.0615 ° /°
Yaw velocity (r)	0.197 rad/s /°	-7.07×10^{-6} rad/s /N	2.15×10^{-4} rad/s /°
Front tire slip angle (α_f)	-2.05 ° /°	2.66×10^{-4} ° /N	0.0620 ° /°
Rear tire slip angle (α_r)	-2.02 ° /°	3.00×10^{-4} ° /N	0.0609 ° /°
Path curvature ($1/R$)	7.10×10^{-3} 1/m /°	-2.54×10^{-7} 1/m /N	7.76×10^{-6} 1/m /°
Lateral acceleration (A_y)	0.559 g /°	-2.00×10^{-5} g /N	6.11×10^{-4} g /°

4.5.13 Steady-State Steer Angle

The steady-state steer angle required for the vehicle to turn at a constant path radius R can be found by solving the yaw velocity gain for steer angle input expression of Eq. (4.37) for the steer angle δ. After some manipulation, the steer angle is

$$\delta_{ss} = \frac{L}{R} + \frac{mV^2 N_\beta}{R\left(N_\beta Y_\delta - N_\delta Y_\beta\right)} \tag{4.54}$$

Substitution of the stability derivative definitions into this expression yields

$$\delta_{ss} = \frac{L}{R} + \left(\frac{a}{C_r} - \frac{b}{C_f}\right)\frac{m}{L}\frac{V^2}{R} \tag{4.55}$$

Examination of the kinematics of a turning vehicle indicates that the steer angle can also be expressed in terms of the tire slip angles as[17]

$$\delta_{ss} = \frac{L}{R} - \alpha_f + \alpha_r \tag{4.56}$$

From Eq. (4.55) it can be seen that as the vehicle velocity approaches zero the steer angle becomes

$$\delta_{Ack\,er} = \frac{L}{R} \tag{4.57}$$

This steer angle is known as the Ackerman steer angle and is the steer angle required to negotiate a turn of path radius R at low vehicle velocity. At low speeds the lateral acceleration, tire slip angles, and tire lateral forces are negligible and turning behavior is governed solely by geometry considerations.

For the vehicle used in this study the Ackerman steer angle for a 50 m radius turn is 2.72 °. The steer angle required to negotiate the turn at 100 km/hr is 2.82 °.

4.5.14 Understeer Gradient

A common measure of vehicle turning behavior is the understeer gradient, or understeer coefficient, K_{us}. The understeer gradient, assuming a constant radius turn, is basically the rate of change of steer angle with lateral acceleration.[1] The definition of the understeer gradient can be seen in the steady-state steer angle expression for a constant radius turn from Eq. (4.54):

$$\delta_{ss} = \frac{L}{R} + K_{us}\frac{V^2}{gR} \tag{4.58}$$

Thus the understeer gradient, expressed in units of radians, is

$$K_{us} = \frac{mgN_\beta}{N_\beta Y_\delta - N_\delta Y_\beta} \tag{4.59}$$

or substituting the stability derivative definitions

$$K_{us} = \left(\frac{a}{C_r} - \frac{b}{C_f}\right)\frac{mg}{L} \tag{4.60}$$

The understeer gradient is a measure of the amount of understeer or oversteer a vehicle has. If to maintain a constant path radius the steer angle must increase as vehicle forward velocity, and hence lateral acceleration, increases, the understeer gradient is positive and the vehicle is said to be understeer. If the steer angle must decrease, the understeer gradient is negative and the vehicle is oversteer. If the steer angle does not

change the understeer gradient is zero and the vehicle is neutral steer. The understeer of a vehicle can also be obtained from relationship between the front and rear tire slip angles. If the magnitude of the front tire slip angle is greater than the rear, the vehicle is understeer. If the rear tire slip angle is greater, the vehicle is oversteer. If the slip angles are equal, the vehicle is neutral steer.

For this simple model the understeer gradient is a function of tire cornering stiffnesses and the weight distribution. Other vehicle characteristics which influence the understeer gradient include lateral load transfer distribution, roll camber, roll steer, lateral force compliance steer, tire aligning moments, tire longitudinal forces, steering system compliance, and differential type.

The understeer gradient of a vehicle can be measured experimentally. The two most common methods of testing are the constant radius test and the constant speed test.[17] In the constant radius test the forward velocity of the vehicle is varied as the car is driven on a constant path radius. The steer angle is varied to maintain the constant radius. The understeer gradient is then calculated as the rate of change of steer angle with lateral acceleration:

$$K_{us} = \frac{\mathrm{d}\delta}{\mathrm{d}A_y} \tag{4.61}$$

In the constant speed test the vehicle forward velocity is held constant while the path radius is varied and the steer angle required to attain the radius is measured. The understeer gradient from the constant speed test is

$$K_{us} = \frac{\mathrm{d}\delta}{\mathrm{d}A_y} - \frac{gL}{V^2} \tag{4.62}$$

Most passenger cars have understeer gradients between 1 and 10 deg. Understeer is designed into passenger cars to assure directional stability over a wide range of operating conditions. The vehicle used for this example has an understeer gradient of 0.0626 deg,

indicating that the vehicle has a very small amount of understeer in the linear response range.

4.5.15 Stability Factor

A second measure of vehicle cornering behavior is the stability factor.[6] The definition of the stability factor comes from the yaw velocity gain for steer angle input expression of Eq. (4.37). This expression can be rewritten as

$$\left.\frac{r}{\delta}\right|_{ss} = \frac{V/L}{1+KV^2} \tag{4.63}$$

where the K is the stability factor. Solving Eq. (4.63) for K and substituting Eq. (4.37),

$$K = \frac{mN_\beta}{L\left(N_\beta Y_\delta - N_\delta Y_\beta\right)} \tag{4.64}$$

or substituting the stability derivative definitions,

$$K = \frac{m}{L^2}\left(\frac{a}{C_r} - \frac{b}{C_f}\right) \tag{4.65}$$

If K is positive the vehicle is understeer, while if K is negative it is oversteer. The sample vehicle has a stability factor of 4.69×10^{-5} s^2/m^2. Since the stability factor is positive, the vehicle is understeer.

4.5.16 Neutral Steer Point

The neutral steer point is "the point along the chassis at which an external lateral force can be applied which produces no steady-state yaw velocity."[13] On a real vehicle there is actually a neutral steer line, but for this simple model which does not account for body roll and roll steer effects there is only a neutral steer point. To find the neutral steer point a transfer function can be written relating the yaw velocity to a fictitious lateral force F_{ns} applied to the vehicle at a distance d behind the front axle. As in Section 4.5.8 the Final

Value Theorem can be used to find the steady-state yaw velocity gain for the fictitious lateral force.

$$\left.\frac{r}{F_{ns}}\right|_{ss} = \frac{Y_\beta(d-a)+N_\beta}{N_r Y_\beta + N_\beta(mV-Y_r)} \tag{4.66}$$

Setting this yaw velocity gain equal to zero and solving for d,

$$d = a - \frac{N_\beta}{Y_\beta} \tag{4.67}$$

Substituting the stability derivative definitions, the neutral steer point is located at a distance behind the front axle of

$$d = \frac{C_r L}{C_f + C_r} \tag{4.68}$$

If the neutral steer point is behind the mass center, the vehicle is understeer, while if it is in front of the mass center the vehicle is oversteer. The sample vehicle has a neutral steer point located at a distance of 1.149 m behind the front axle. Since the mass center is located 1.139 m behind the front axle, the neutral steer point is behind the mass center and the vehicle is understeer.

4.5.17 Static Margin

Another way of describing understeer is with the static margin. The static margin SM is the distance between the mass center and the neutral steer point, normalized by the wheelbase.[13]

$$SM = -\frac{N_\beta}{LY_\beta} \tag{4.69}$$

or, substituting the stability derivative definitions,

$$SM = -\frac{aC_f - bC_r}{L(C_f + C_r)} \tag{4.70}$$

If the static margin is positive, the vehicle is understeer. If it is negative the vehicle is oversteer. The sample vehicle has a static margin of 0.00428, indicating that the vehicle is understeer.

4.5.18 Tangent Speed

At low speed in a steady-state turn the rear axle travels on a smaller circle than the front axle. As speed is increased the radius of travel of the rear axle increases and surpasses that of the front. Thus at high speed the rear axle travels on a larger circle than the front in a steady-state turn. The speed at which the front and rear axles travel on circles of the same radius is called the tangent speed V_{tan}. At the tangent speed the vehicle sideslip angle is zero. For a right turn, below the tangent speed the vehicle sideslip angle is positive, while above the tangent speed it is negative. The tangent speed can be found by multiplying the steady-state sideslip angle gain for steer angle of Eq. (4.34) by the steady-state steer angle for a constant radius turn of Eq. (4.54), setting that product equal to zero, and solving for the vehicle velocity V.

$$V_{\tan} = \frac{N_\delta Y_r - N_r Y_\delta}{m N_\delta} \tag{4.71}$$

However, since the yaw velocity stability derivatives Y_r and N_r are both functions of velocity, it is necessary to substitute the stability derivative definitions and solve for V. When this is done the tangent speed is

$$V_{\tan} = \sqrt{-\frac{bLC_r}{am}} \tag{4.72}$$

The sample vehicle used in this study has a tangent speed of 49.8 km/hr. Below this speed the vehicle sideslip angle is positive for a right turn. Above this speed it is negative.

4.5.19 Critical Speed

Consideration of Eq. (4.37) for steady-state yaw velocity gain for steer angle input reveals that the yaw velocity gain could become infinite if the denominator were zero. The speed at which this happens is called the critical speed. The critical speed can be found by setting the denominator of Eq. (4.37) equal to zero and solving for V. In terms of the stability derivatives, the critical speed is

$$V_{crit} = \frac{N_\beta Y_r - N_r Y_\beta}{m N_\beta} \tag{4.73}$$

However, the stability derivatives Y_r and N_r are functions of velocity. Therefore, it is necessary to substitute the stability derivative definitions and solve for V. The critical speed is then

$$V_{crit} = \sqrt{\frac{C_f C_r L^2}{m\left(bC_r - aC_f\right)}} \tag{4.74}$$

At this speed the vehicle is unstable. A small steering input produces a theoretically infinite yaw velocity response. Given that the tire cornering stiffnesses are negative by definition, it can be seen from Eq. (4.74) that a critical speed only exists if bC_r is greater than aC_f. In Section 4.5.5 it is noted that when this condition exists the vehicle is oversteer. Thus a vehicle has a critical speed only if it is oversteer. When an oversteer vehicle reaches its critical speed it becomes directionally unstable. The more oversteer a vehicle has, the lower its critical speed. The critical speed for a neutral speed vehicle is infinite, and the critical speed does not exist for an understeer vehicle.

Since the sample vehicle is understeer, it does not have a critical speed.

4.5.20 Characteristic Speed

While an understeer vehicle has no critical speed, the characteristic speed is defined in a similar manner to indicate the level of understeer present in the vehicle. The

characteristic speed is the speed at which the steer angle required to produce any steady-state turn radius is twice the Ackerman steer angle. The characteristic speed can be found by setting the steady-state steer angle of Eq. (4.54) equal to twice the Ackerman steer angle of Eq. (4.57) and solving for the velocity V. Since the solution to this equation is a function of stability derivatives which depend on velocity, the stability derivative definitions must be substituted and the resulting equation solved for V. The characteristic speed is then

$$V_{char} = \sqrt{\frac{C_f C_r L^2}{m\left(aC_f - bC_r\right)}} \tag{4.75}$$

The characteristic speed is seen to have the same form as the critical speed, but with the sign of the denominator reversed. A characteristic speed only exists if aC_f is greater than bC_r. Since, from Section 4.5.5, this is the condition for an understeer vehicle, only understeer vehicles have a characteristic speed. Neutral steer vehicles have an infinite characteristic speed and oversteer vehicles have no characteristic speed. The more understeer a vehicle has, the lower its characteristic speed.

The sample vehicle has a characteristic speed of 525 km/hr. Since the characteristic speed is very high, the vehicle has a small amount of understeer.

4.5.21 Characteristic Equation

The measures of system response derived in Section 4.5.7 through Section 4.5.20 are all measures of steady-state system response. The lateral transient response of the two degree-of-freedom road vehicle is now examined.

From the Laplace-domain equations of motion of Eq. (4.27), the characteristic equation for the system is

$$s^2 - \left(\frac{N_r}{I_{zz}} + \frac{Y_\beta}{mV}\right)s + \frac{N_r Y_\beta + N_\beta\left(mV - Y_r\right)}{I_{zz} mV} = 0 \tag{4.76}$$

From this characteristic equation, the undamped natural frequency, damping ratio, and poles of the system can be found.

4.5.22 Undamped Natural Frequency

From the characteristic equation of Eq. (4.76) the natural frequency of the system is

$$\omega_n = \sqrt{\frac{N_r Y_\beta + N_\beta (mV - Y_r)}{I_{zz} mV}} \tag{4.77}$$

Substituting the stability derivative definitions yields

$$\omega_n = \sqrt{\frac{L^2 C_f C_r}{I_{zz} mV^2} + \frac{aC_f - bC_r}{I_{zz}}} \tag{4.78}$$

With the expression in this form the effects of various parameters on undamped natural frequency, and consequently, system response time can be seen. From the first term the natural frequency decreases with the yaw moment of inertia, the mass, and the square of the forward velocity of the vehicle. In addition, it increases with the product of tire cornering stiffnesses and with the square of the wheelbase. The numerator of the second term is the directional stability N_β. This term is positive if the vehicle is understeer, negative if it is oversteer, and zero if it is neutral steer. Thus from this model, all else being equal, an understeer vehicle has a higher natural frequency and lower response time than an oversteer vehicle.

The sample vehicle has an undamped natural frequency of 1.01 Hz at a forward speed of 100 km/hr. The natural frequency decreases as vehicle velocity increases as shown in Figure 4.5.

4.5.23 Damping Ratio

The damping ratio of the system can also be obtained from the characteristic equation. In terms of the stability derivatives the damping ratio is

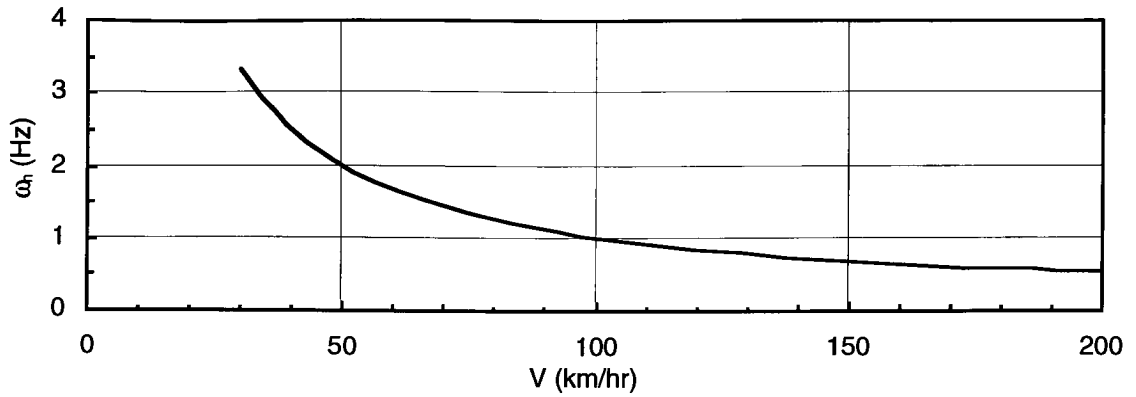

Figure 4.5: Natural Frequency vs. Vehicle Velocity

$$\zeta = -\frac{I_{zz}Y_\beta + mVN_r}{2\sqrt{I_{zz}mV\left(N_rY_\beta + N_\beta\left(mV - Y_r\right)\right)}} \tag{4.79}$$

If the stability derivatives are substituted the damping ratio becomes

$$\zeta = -\frac{I_{zz}\left(C_f + C_r\right) + m\left(a^2C_f + b^2C_r\right)}{2\sqrt{I_{zz}m\left(L^2C_fC_r + mV^2\left(aC_f - bC_r\right)\right)}} \tag{4.80}$$

Depending on the values of the parameters, the vehicle may be underdamped, critically damped, or overdamped. Neutral steer vehicles tend to be close to critically damped, with understeer vehicles tending toward underdamped and oversteer vehicles tending toward overdamped.[13] As with other dynamic systems, the damping ratio affects the response time and overshoot of the road vehicle to lateral control and disturbance inputs.

At a forward speed of 100 km/hr the sample vehicle has a damping ratio of 0.990, indicating that the vehicle is very slightly underdamped. Damping ratio decreases as vehicle velocity increases. This vehicle is overdamped below a speed of approximately 63.7 km/hr.

4.5.24 System Poles

The poles of the system can be found by solving the characteristic equation of Eq. (4.76) for s. Doing this yields the poles

$$p_{1,2} = \frac{mVN_r + I_{zz}Y_\beta \pm \sqrt{\left(mVN_r + I_{zz}Y_\beta\right)^2 - 4I_{zz}mV\left(N_rY_\beta + N_\beta\left(mV - Y_r\right)\right)}}{2I_{zz}mV} \tag{4.81}$$

The location of the poles in the s-plane provides an indication of system response. During the design stage the vehicle parameters may be manipulated to place the poles such that the desired system response is obtained. The pole locations also provide an indication of system stability. If there are any poles in the right half of the s-plane (i.e., they have positive real components), the system is unstable.

At a forward speed of 100 km/hr the sample vehicle has poles of $-6.301 \pm 0.918i$. Since the poles are complex conjugates, the vehicle is underdamped. Furthermore, since the real part of the poles is negative, the system is stable. As speed decreases the poles move together until they meet on the real axis at -9.897 at a vehicle speed of 63.7 km/hr. At this speed the vehicle is critically damped. As speed increases from 100 km/hr the poles move farther apart and approach the imaginary axis. However, even at a forward speed of 300 km/hr the poles remain in the left half of the s-plane, indicating that the vehicle remains stable for reasonable speeds.

4.5.25 System Zeros

Further insight into the nature of system response can be obtained by examining the system zeros. The system zeros can be found for each input and state variable combination by setting the numerator of the corresponding transfer function equal to zero and solving for s. The transfer functions are given in Eq. (4.28) through Eq. (4.33).

The zero for sideslip angle response to steer angle input is

$$z_{\beta/\delta} = \frac{N_r Y_\delta + N_\delta (mV - Y_r)}{I_{zz} Y_\delta} \tag{4.82}$$

The zero for sideslip angle response to aerodynamic side force input is

$$z_{\beta/F_{ya}} = \frac{N_r - (c-a)(mV - Y_r)}{I_{zz}} \tag{4.83}$$

The zero for sideslip angle response to road side slope angle input is

$$z_{\beta/\theta} = \frac{N_r}{I_{zz}} \tag{4.84}$$

The zero for yaw velocity response to steer angle input is

$$z_{r/\delta} = \frac{N_\delta Y_\beta - N_\beta Y_\delta}{mVN_\delta} \tag{4.85}$$

The zero for yaw velocity response to aerodynamic side force is

$$z_{r/F_{ya}} = \frac{N_\beta + Y_\beta (c-a)}{mV(c-a)} \tag{4.86}$$

There is no zero for yaw velocity response to road side slope since s does not appear in numerator of this transfer function. This is due to the fact that the gravitational side force acts at the mass center and therefore results in no external yaw moment on the vehicle.

The system zeros for the sample vehicle with a forward speed of 100 km/hr are given in Table 4.4.

Table 4.4: System Zeros

V = 100 km/hr

Response	Steer Angle	Aerodynamic Side Force	Road Side Slope
Vehicle sideslip angle	21.53	-9.86	-7.06
Yaw velocity	-5.59	-5.04	-

The effect that zeros have on response depends upon their location relative to the poles.[33] The closer a zero is to a pole, the larger the effect. A zero that is in the right half of the *s*-plane (i.e., is positive in sign) is called a nonminimum-phase zero. The nonminimum-phase zero can cause the response to initially start in the opposite direction. This response can be seen in the lateral velocity and sideslip angle response to steer angle input which is simulated in Section 4.5.27. Plots of the poles and zeros for each input and output combination are provided in Figure 4.6 for the sample vehicle with a forward speed of 100 km/hr.

The values of all of the zeros increase with vehicle speed. The sideslip angle / steer angle zero is negative at low speeds and positive at high speed. This zero changes sign when the vehicle speed reaches its tangent speed. All other zeros remain negative for reasonable values of vehicle speed.

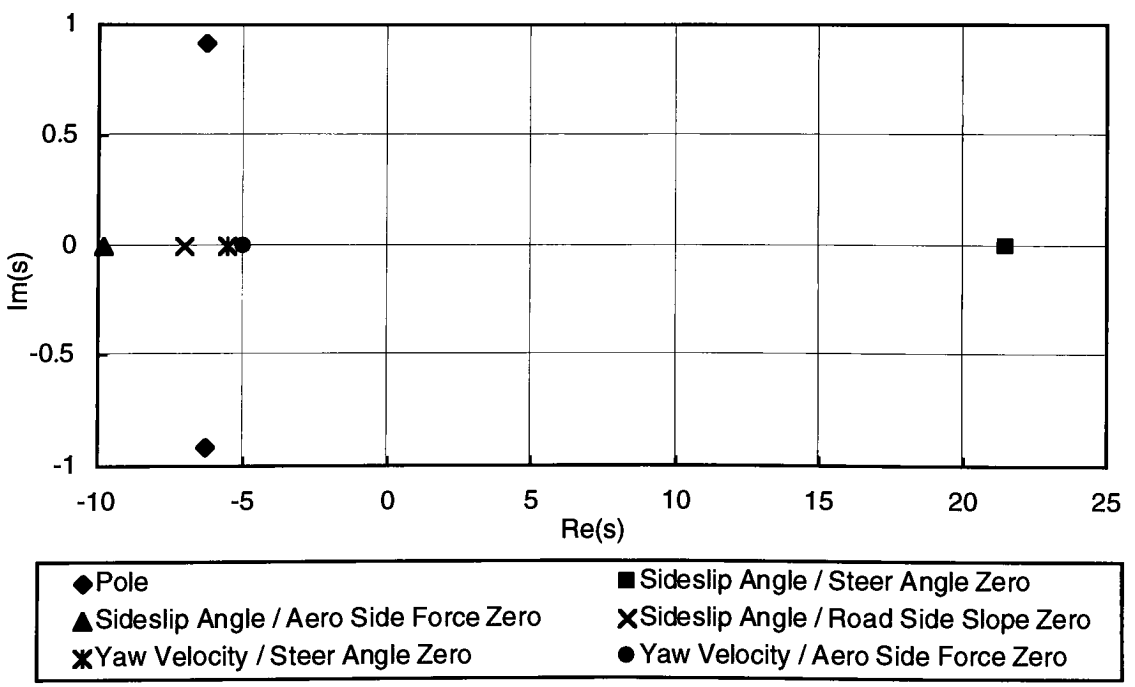

Figure 4.6: Poles and Zeros

4.5.26 Frequency Response

It is also interesting to examine the frequency response of the vehicle. A driving event where frequency response may be of particular interest is a slalom test where the vehicle is driven through regularly spaced cones by means of a sinusoidal steering input. The frequency of the input required to negotiate the slalom depends upon the vehicle speed and the cone spacing. The performance of the vehicle in the slalom may be influenced by the magnitude of the input frequency relative to the natural frequency of the vehicle. Sinusoidal steering inputs may also be used in emergency maneuvers such as a double lane change. Examining the frequency response of the vehicle may provide an indication of its performance in such a maneuver. Since it is generally desirable to minimize the response of a vehicle to disturbances such as side winds and road side slope, frequency response techniques can be used to examine the response of the vehicle to periodic disturbance inputs.

Phase lags in response to steering input require the driver to adjust his input to obtain the desired response, making the vehicle more difficult to drive. Smaller phase lags tend to improve vehicle controllability.[21] The frequency response of the sample vehicle with a forward velocity of 100 km/hr is examined using the bode plotting capability of the MATLAB Controls Toolbox. The gain and phase responses of vehicle sideslip angle and yaw velocity to steer angle, aerodynamic side force, and road side slope are plotted in Figure 4.7 through Figure 4.12. The MATLAB script *DOF2LFreq.m,* which is listed in Appendix C.5, is used to facilitate plotting of the frequency response. The script generates gain and phase versus input frequency for the two degree-of-freedom model. *DOF2LFreq.m* calls the scripts *DOF2Control.m*, which sets program execution parameters; *DOF2Param.m*, which sets vehicle and input magnitude parameters; and

DOF2DependParam.m, which calculates vehicle parameters which depend on other parameters. These scripts are listed in Appendix C.1 through Appendix C.3.

The frequency response of a road vehicle changes as forward velocity changes. For most of the responses the magnitude of the gain changes while the general shape of the curves remain approximately constant. There is little change in the phase plot for most of the responses. The sideslip angle / steer angle response is the only response which experiences significant change in the shape of the gain and phase plots as forward velocity changes. The sideslip angle / steer angle frequency response is influenced strongly by the magnitude of the forward speed relative to the tangent speed of the vehicle. This is a result of the sideslip angle / steer angle zero changing sign at the tangent speed. The sideslip angle / steer angle frequency response is plotted in Figure 4.13 and Figure 4.14 for forward speeds of 30 km/hr and 49.84 km/hr respectively.

At 30 km/hr the gain is flat up to approximately 1 Hz at 0.33 deg/deg and the phase goes from 0° at 0.1 Hz to -90° at 100 Hz. The phase response is typical of a second order system with a negative zero. At 49.84 km/hr, the tangent speed, the gain approaches zero as the frequency approaches zero as expected from the definition of tangent speed. However, there is a significant peak in the gain at approximately 2 Hz, which is the undamped natural frequency at 49.84 km/hr. The phase goes from 90° at 0.1 Hz to -90° at 100 Hz, crossing zero at the undamped natural frequency. The frequency response at 100 km/hr is shown in Figure 4.7. The phase goes from 180° at 0.1 Hz to -90° at 100 Hz. There is a 180° phase lead at low frequency because above the tangent speed a positive steady-state steer angle produces a negative sideslip angle as shown in Section 4.5.18.

Also of interest is the yaw velocity / road side slope phase response. The phase goes from 0° at 0.1 Hz to -180° at 100 Hz. The phase response of this transfer function differs from the others due to the lack of a zero.

At low frequencies the gains for each input and output combination approach the values of the steady-state step input response gains shown in Table 4.3 for a forward velocity V = 100 km/hr.

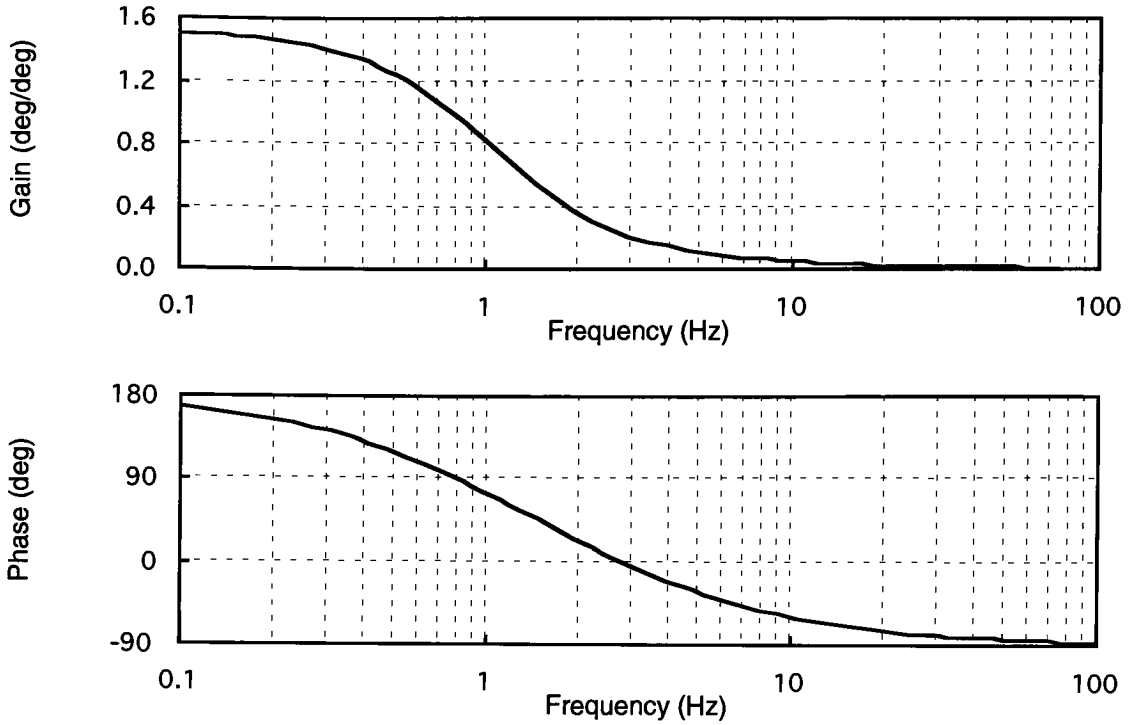

Figure 4.7: Sideslip Angle / Steer Angle Frequency Response, V = 100 km/hr

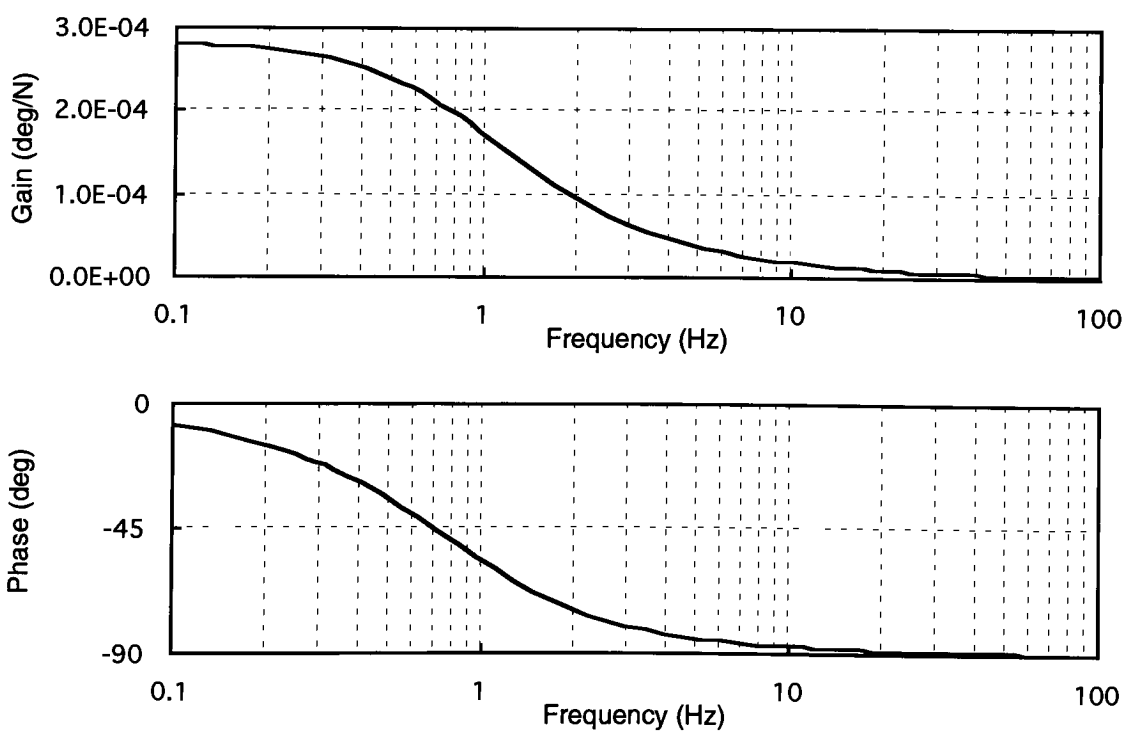

Figure 4.8: Sideslip Angle / Aero Side Force Frequency Response, V = 100 km/hr

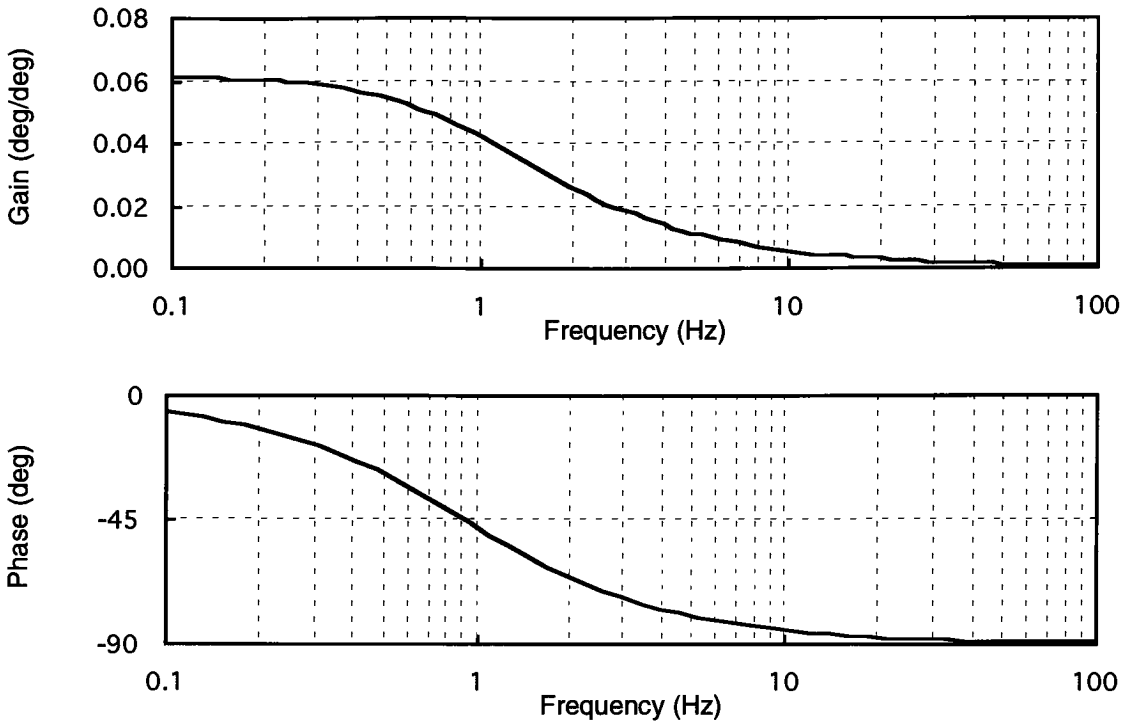

Figure 4.9: Sideslip Angle / Road Side Slope Frequency Response, V = 100 km/hr

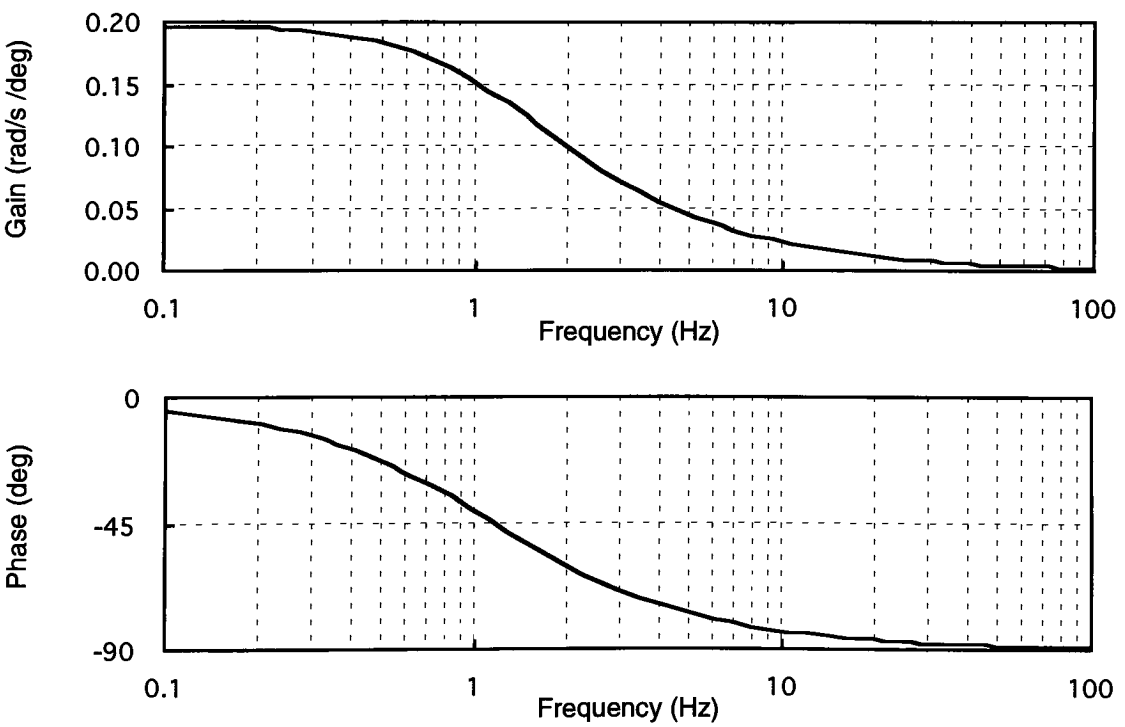

Figure 4.10: Yaw Velocity / Steer Angle Frequency Response, V = 100 km/hr

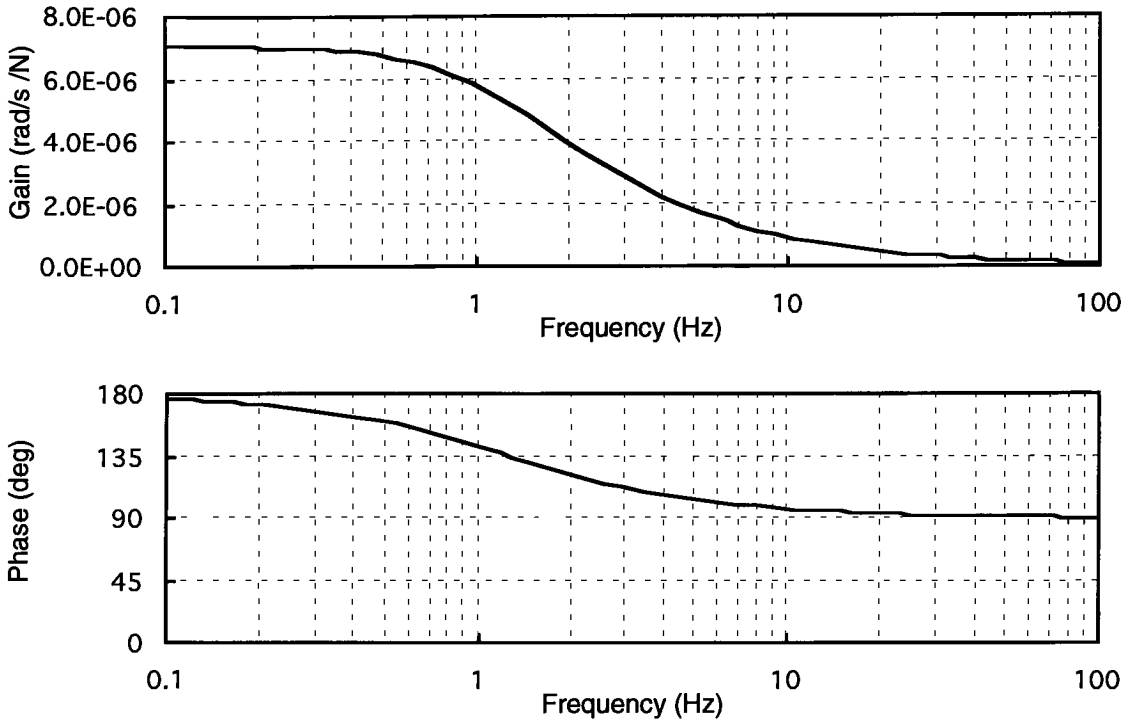

Figure 4.11: Yaw Velocity / Aero Side Force Frequency Response, V=100 km/hr

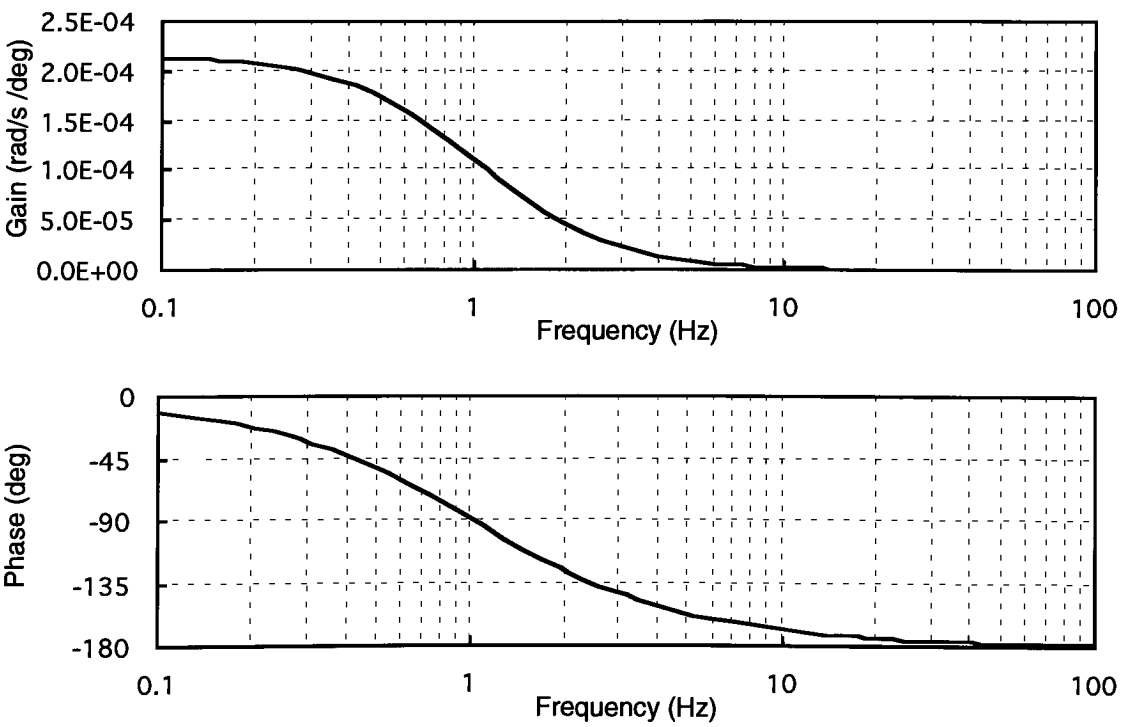

Figure 4.12: Yaw Velocity / Road Side Slope Frequency Response, V = 100 km/hr

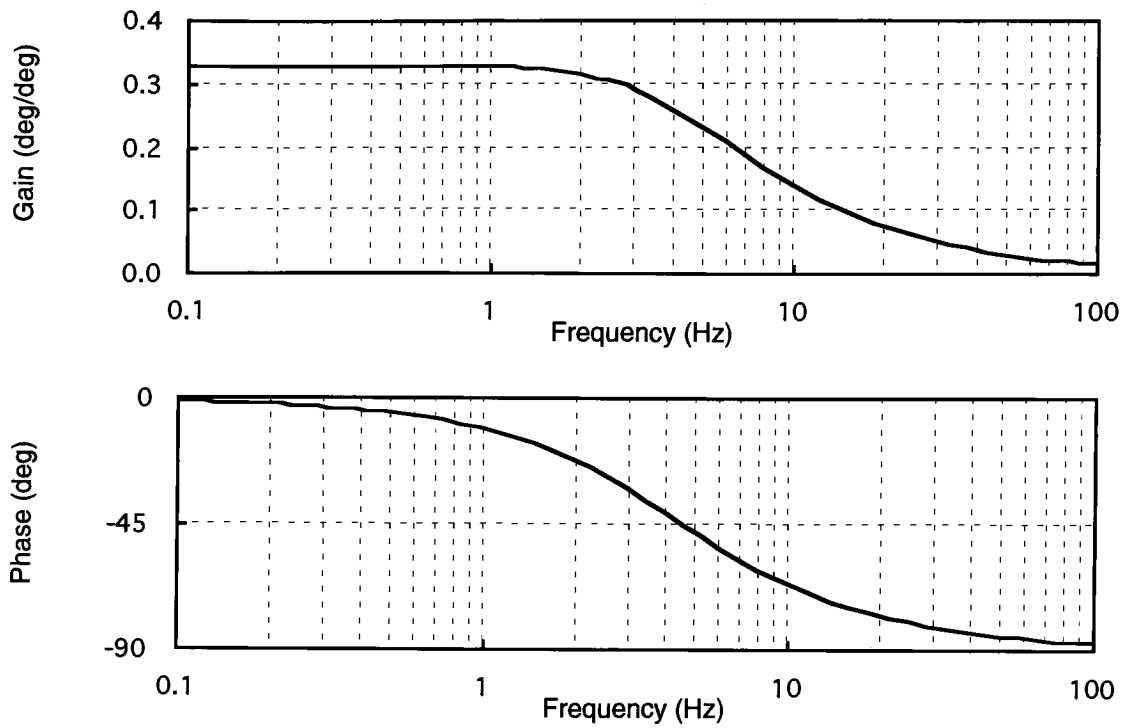

Figure 4.13: Sideslip Angle / Steer Angle Frequency Response, V = 30 km/hr

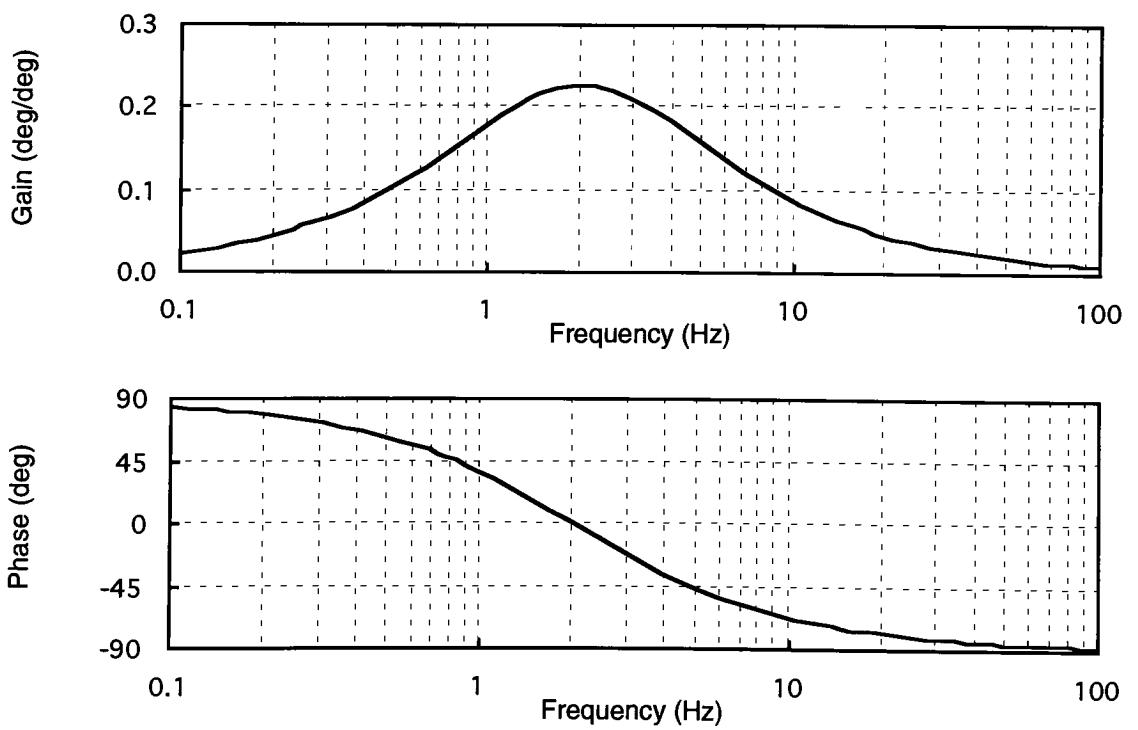

Figure 4.14: Sideslip Angle / Steer Angle Frequency Response, V = 49.84 km/hr

4.5.27 Simulation

Another tool that is very useful in analyzing vehicle lateral dynamics is numerical simulation. Simulation is done by integrating the differential equations of motion with respect to time and can be used to predict the response of the vehicle to arbitrary control and disturbance inputs. Non-linearities are generally much easier to handle with numerical simulation than with the analytical techniques used up to this point in this chapter.

To maintain consistency with the non-linear model simulation which follows in Section 4.6, the lateral velocity v is used as a state variable for the linear model simulation instead of the sideslip angle β. Since the equations of motion were originally derived in terms of yaw velocity and lateral velocity and then simplified to be in terms of yaw velocity and sideslip angle, the model has been returned to its original, more general, form.

The equations of motion in their general, non-linear form are given by Eq. (4.9). With the small steer angle assumption used for the linear model the equations become

$$\begin{aligned} F_{yf} + F_{yr} + F_{ya} + F_{yg} &= m(\dot{v} + ur) \\ aF_{yf} - bF_{yr} - (c-a)F_{ya} &= I_{zz}\dot{r} \end{aligned} \tag{4.87}$$

Expressions for the tire slip angles, tire lateral forces, and gravitational side force are derived in Section 4.5.3 and Section 4.5.4 using the small angle assumption and are repeated here for convenience.

$$\begin{aligned} \alpha_f &= \frac{v + ar}{u} - \delta \\ \alpha_r &= \frac{v - br}{u} \end{aligned} \tag{4.19}$$

$$\begin{aligned} F_{yf} &= C_f \alpha_f \\ F_{yr} &= C_r \alpha_r \end{aligned} \tag{4.21}$$

$$F_{yg} = mg\theta \tag{4.23}$$

Outputs from the simulation are time histories of lateral velocity, yaw velocity, vehicle sideslip angle, tire slip angles, and lateral acceleration. Inputs can be a step steer, ramp step steer, ramp square steer, sine steer, step aerodynamic side force, or step road side slope.

The simulation is implemented in the MATLAB script *DOF2LSim.m,* which is listed in Appendix C.6. Integration of the differential equations of motion is done using the built-in MATLAB function *ode23*, which uses second and third order Runge-Kutta formulas.[34] The function *ode23* returns the state variables v and r over the time interval specified for the simulation.

At each time step the *ode23* function calls the function *DOF2LDE.m* which calculates the state derivatives $\dot{v}$ and $\dot{r}$ based upon the instantaneous values of the state variables v and r. First, the instantaneous steer angle is calculated by the function *SteerAngle.m*, which is listed in Appendix C.4, based upon the current time, the type of input selected, the magnitude of the input, and the values of the input duration parameters. Any arbitrary steer input, including steer inputs measured experimentally during vehicle testing, could easily be implemented in this function. Use of measured steer input data facilitates experimental validation of the model.

After the steer angle is calculated, the tire slip angles are calculated from the current values of the state variables v and r which are passed as parameters into *DOF2LDE.m.* The tire lateral forces are then calculated from the slip angles using Eq. (4.21). Finally, the state derivatives are calculated as

$$\begin{aligned} \dot{v} &= \frac{F_{yf} + F_{yr} + F_{ya} + F_{yg}}{m} - ur \\ \dot{r} &= \frac{aF_{yf} - bF_{yr} - (c-a)F_{ya}}{I_{zz}} \end{aligned} \tag{4.88}$$

Eq. (4.88) are obtained by solving Eq. (4.87) for $\dot{v}$ and $\dot{r}$. A listing of *DOF2LDE.m* is provided in Appendix C.7.

To illustrate the effect of forward velocity on response, simulations are performed at low speed (30 km/hr), at the tangent speed (49.84 km/hr), at normal highway speed (100 km/hr), and at high speed (150 km/hr). The simulations are run until steady-state is reached. Initial conditions for the simulations are zero. Lateral velocity, yaw velocity, sideslip angle, front tire slip angle, rear tire slip angle, and lateral acceleration are plotted for each input studied.

The inputs used for the simulation are a 1° step steer, a 1° ramp step steer with a ramp time of 0.2 sec, a 1° ramp square steer with a ramp time of 0.2 sec and a dwell time of 1.0 sec, a 1° sine steer with a period of 1 sec, a 10000 N step aerodynamic side force, and a 1° step road side slope. The ramp step steer, ramp square steer, and sine steer inputs are shown in Figure 4.15. The steer input is a positive steer angle, indicating a right turn.

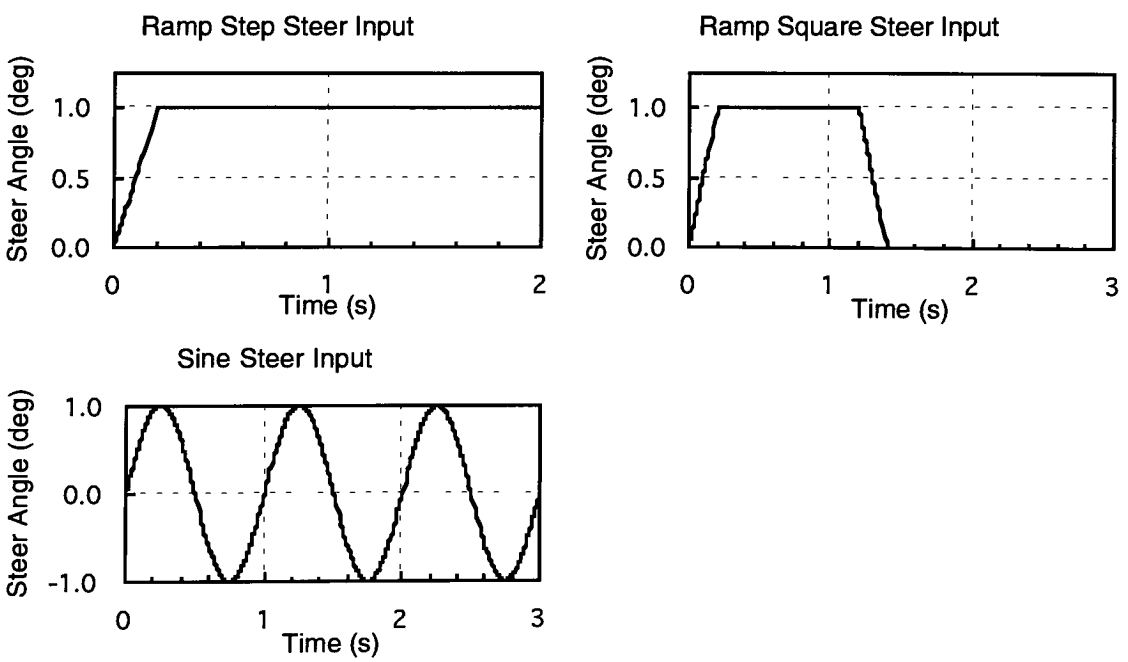

Figure 4.15: Simulation Steer Angle Inputs

The aerodynamic side force input is applied in the positive y-direction, and the road side slope is positive, which means that the road slopes down to the right.

Simulation results for the step steer input are plotted in Figure 4.16 through Figure 4.21. The response times increase with forward speed. The steady-state lateral velocity and sideslip angle are positive below the tangent speed, zero at the tangent speed, and negative above the tangent speed. This agrees with the definition of the tangent speed presented in Section 4.5.18. Above the tangent speed the lateral velocity and sideslip angle also initially begin to increase from zero becoming positive and then decrease to negative values. This is a result of the system zero being positive when the forward speed is greater than the tangent speed. As explained in Section 4.5.25 a system with a positive zero is a nonminimum-phase system and typically exhibits the type of step response shown here, initially in the opposite direction to the steady-state value. The front tire slip angles show response similar to the sideslip angle, but with initial values of -1° due to the 1° step steer. The lateral acceleration has a non-zero initial value due to the rate of change of lateral velocity when the step steer occurs. The steady-state values of yaw velocity, sideslip angle, front tire slip angle, rear tire slip angle, and lateral acceleration agree with the steady-state response gains presented in Table 4.3. In addition, the steady-state sideslip angles and yaw velocities agree with the values approached at low frequency in the frequency response plots of Figure 4.7, Figure 4.10, Figure 4.13, and Figure 4.14.

Ramp step steer simulation results are plotted in Figure 4.22 through Figure 4.27. The ramp step steer response is similar to the step steer response and lags it slightly as expected. The steady-state values are identical to those of the step response. The lateral velocity and sideslip angle still exhibit the non-minimum phase system response above the tangent speed, but the magnitude of the initial response is less than it is for the step steer. Unlike with the step input, the front tire slip angle and lateral acceleration are initially zero

for the ramp step input. At 30 km/hr and 49.84 km/hr there are peaks in the front tire slip angle response at 0.2 sec which is when the ramping of the steer input is completed.

The responses to the ramp square steer input are plotted in Figure 4.28 through Figure 4.33. The ramp square steer response is identical to the ramp step response up until the time that the steer input is ramped back down to zero. At the lower speeds the responses reach steady-state before the ramp down. However, at 150 km/hr the ramp down occurs before steady-state has been reached. As with the ramp step response the front tire slip angles experience overshoot at 30 km/hr and 49.84 km/hr as the ramp up is completed.

The sine steer results are shown in Figure 4.34 through Figure 4.39. The sine steer input had a frequency of 1 Hz. From visual inspection of the plots it is seen that the steady-state yaw velocity and sideslip angle gains and phases agree with those obtained for 1 Hz from the frequency response in Figure 4.7, Figure 4.10, Figure 4.13, and Figure 4.14. The response amplitude increases with forward velocity in all cases except the lateral velocity and sideslip angle. As expected from the definition of tangent speed, at 49.84 km/hr the lateral velocity and sideslip angle amplitudes are less than those at 30 km/hr.

Results from the aerodynamic side force step input simulation are provided in Figure 4.40 through Figure 4.45. The magnitude of the responses increases with forward velocity. Since the center of aerodynamic pressure is located behind the neutral steer point, a positive aerodynamic side force produces a negative yaw velocity. The steady-state yaw velocity, sideslip angle, front tire slip angle, rear tire slip angle, and lateral acceleration responses at 100 km/hr agree with the steady-state gains in Table 4.3. In addition, the steady-state yaw velocity and sideslip angle at 100 km/hr agree with the frequency response gains of Figure 4.8 and Figure 4.11 as the input frequency approaches zero. The sideslip angles, front tire slip angles, rear tire slip angles, and lateral acceleration curves have higher slopes at lower speeds indicating that the response is faster at lower speeds.

Road side slope step input results are plotted in Figure 4.46 through Figure 4.51. The lateral velocity, yaw velocity, and lateral acceleration responses increase with forward velocity, while the sideslip angle, front tire slip angle, and rear tire slip angle decrease. Again, the steady-state yaw velocity, sideslip angle, front tire slip angle, rear tire slip angle, and lateral acceleration at 100 km/hr obtained with the simulation agree with the steady-state gains of Table 4.3, and the steady-state yaw velocity and sideslip angle agree with frequency response gains of Figure 4.9 and Figure 4.12 as the input frequency approaches zero.

The linear two degree-of-freedom model is useful for characterizing and predicting the response of the automobile to control and disturbance inputs. Although this model greatly simplifies the vehicle system, much can be learned about road vehicle lateral dynamics through its study. The effects of changing vehicle and tire parameters on system response can quickly be studied. Powerful linear analysis techniques based on system transfer functions can be readily applied to the vehicle model to gain significant insight into system behavior. The results from the linear model are generally valid for lateral accelerations up to 0.35 g, which constitutes most of normal passenger car driving. Beyond this level a non-linear tire model is required to accurately simulate tire behavior at high slip angles.

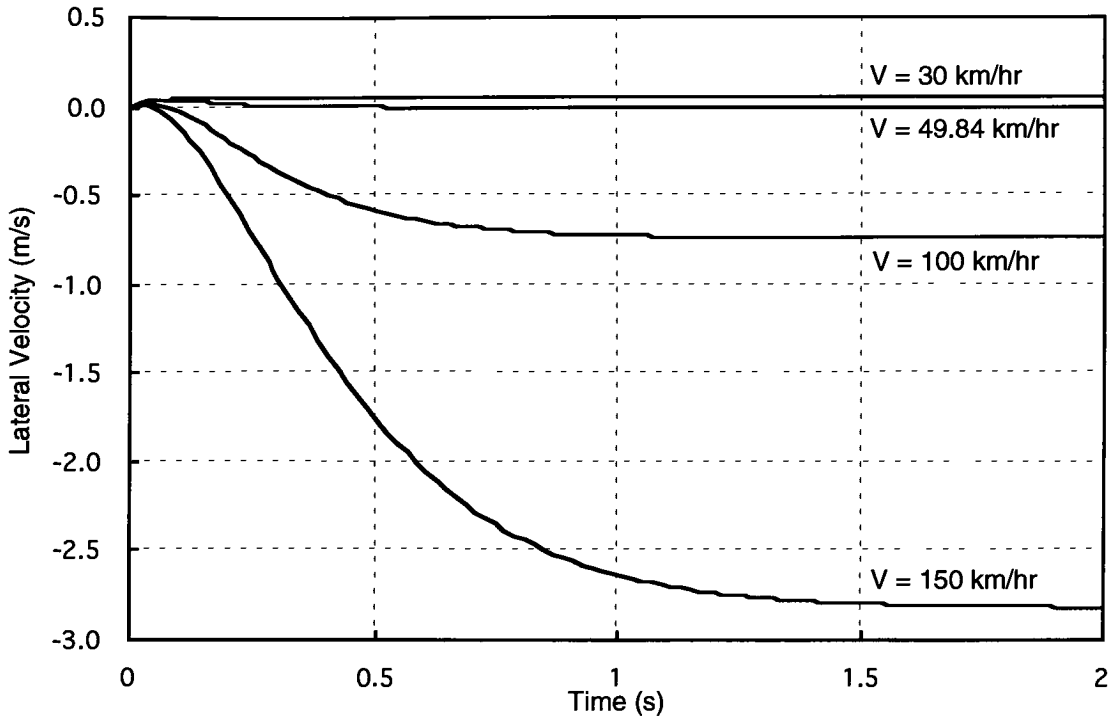

Figure 4.16: Linear Step Steer Lateral Velocity Response

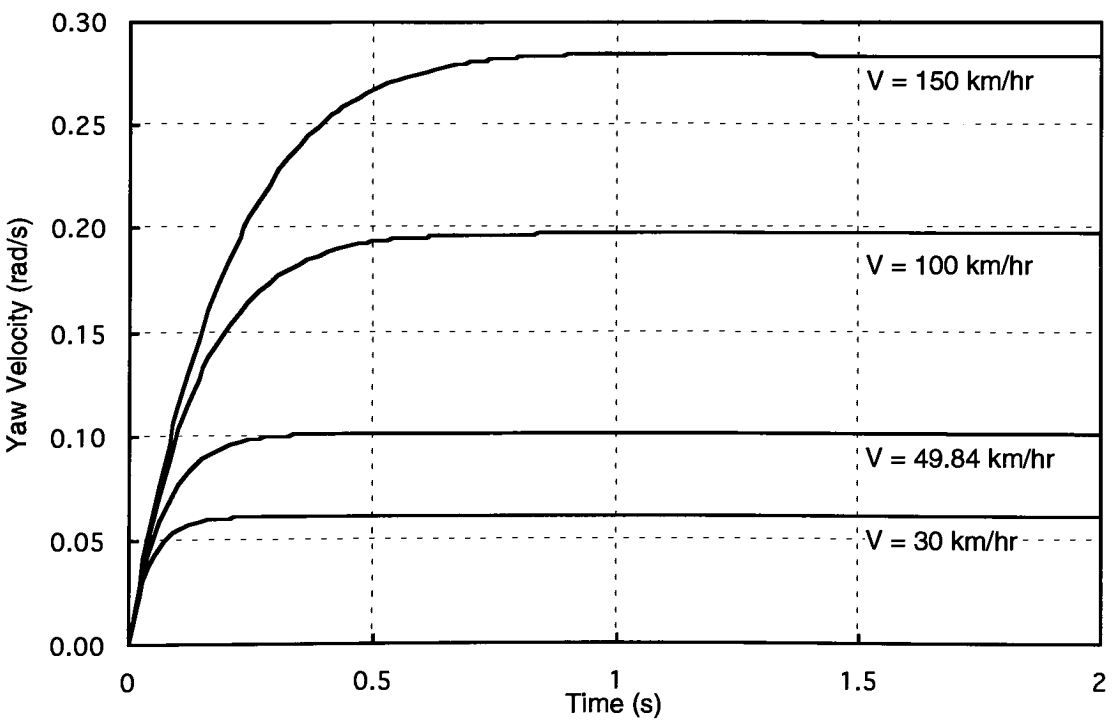

Figure 4.17: Linear Step Steer Yaw Velocity Response

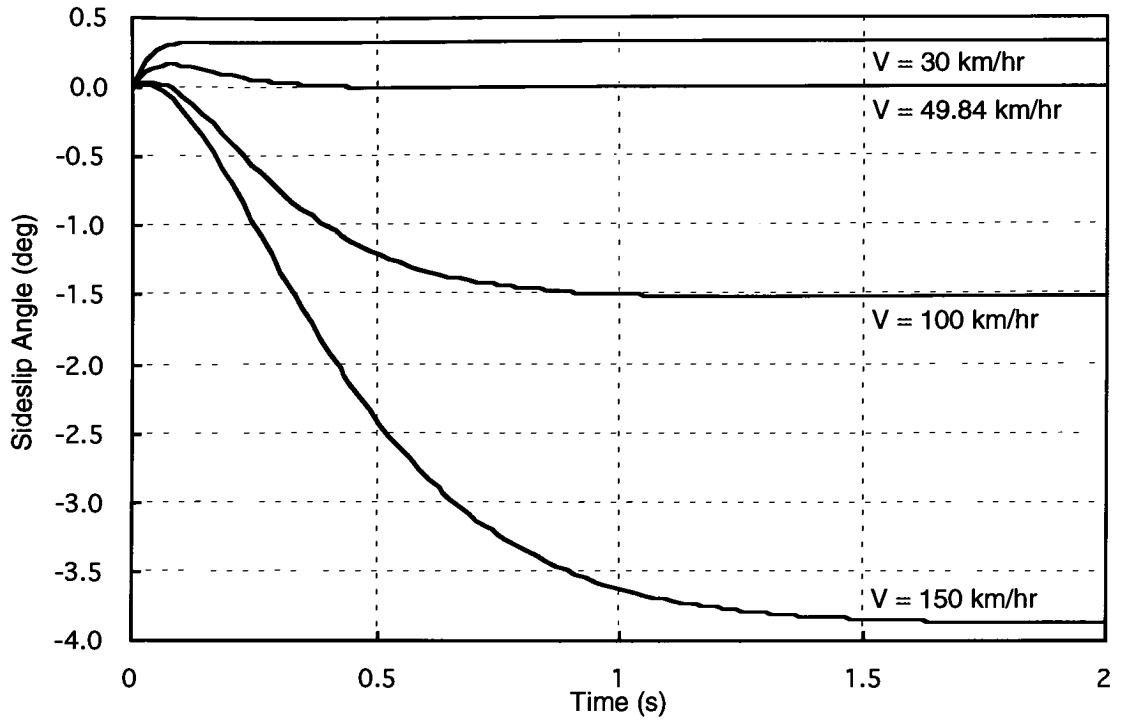

Figure 4.18: Linear Step Steer Sideslip Angle Response

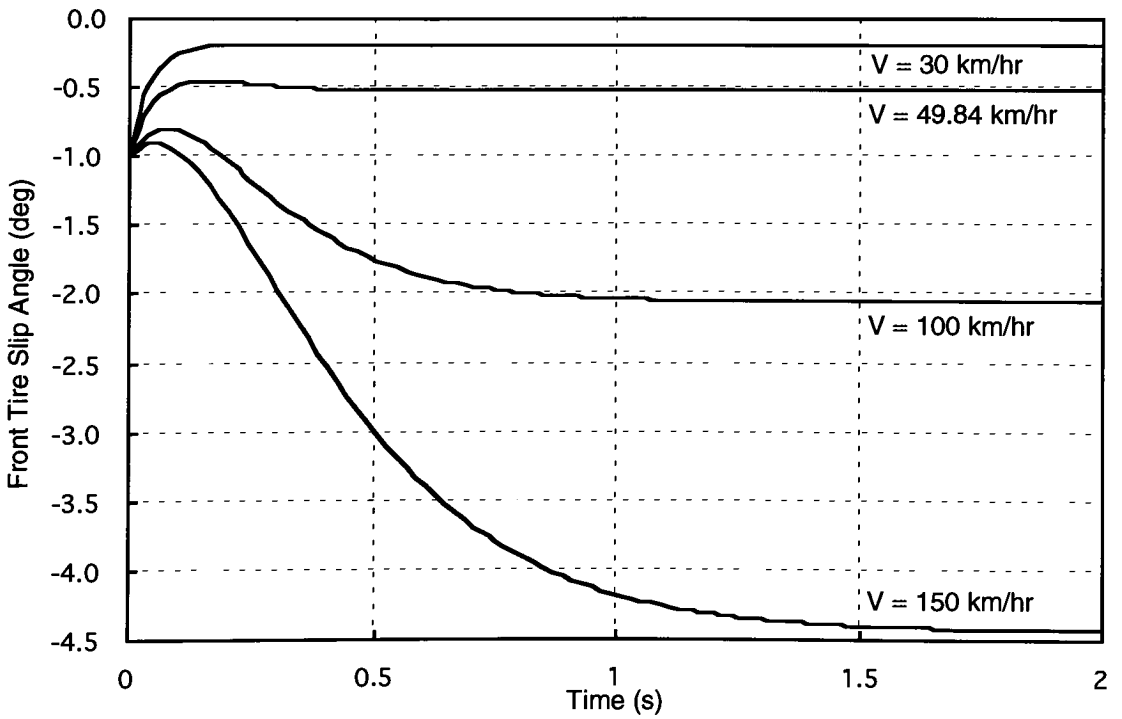

Figure 4.19: Linear Step Steer Front Tire Slip Angle Response

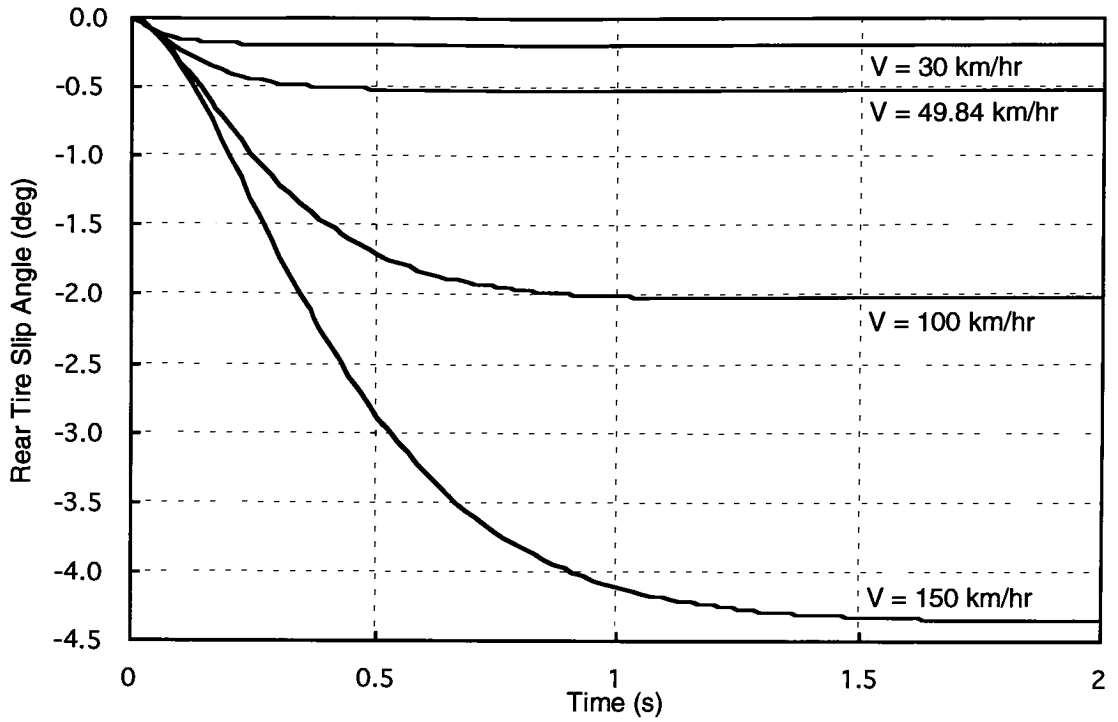

Figure 4.20: Linear Step Steer Rear Tire Slip Angle Response

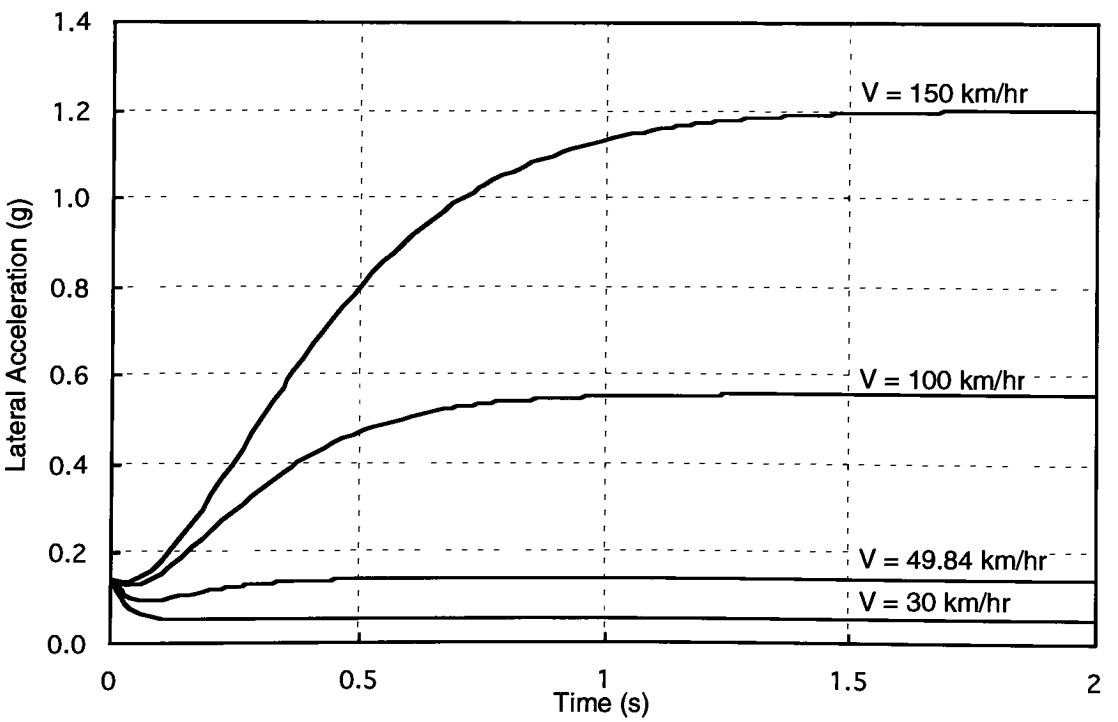

Figure 4.21: Linear Step Steer Lateral Acceleration Response

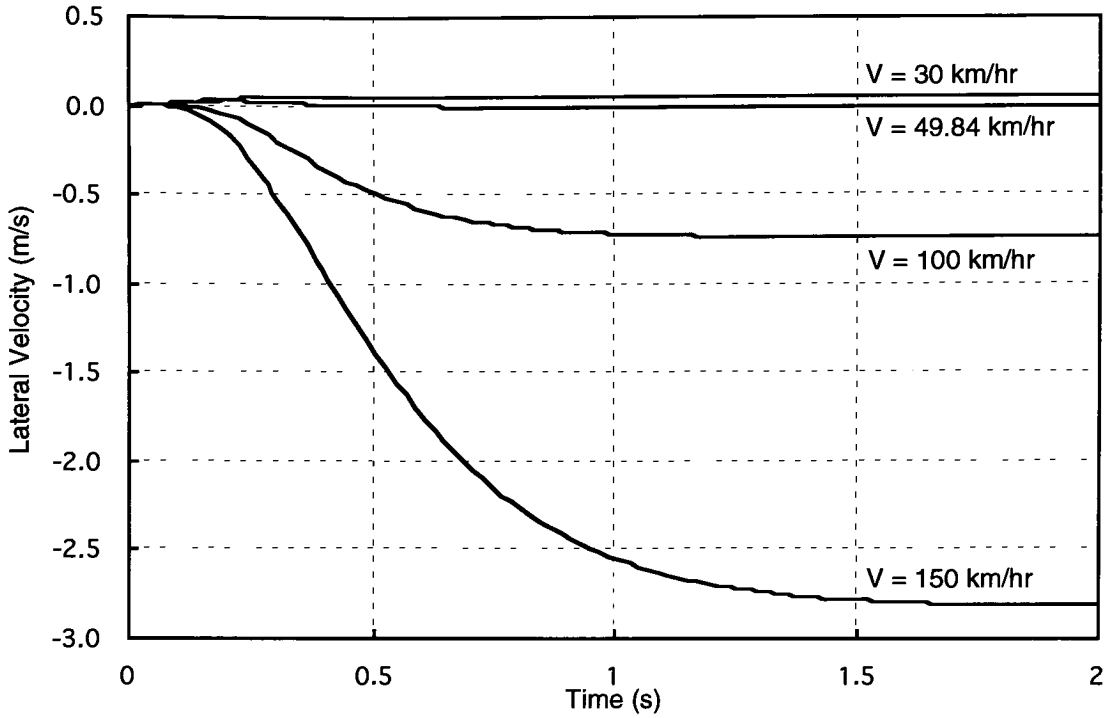

Figure 4.22: Linear Ramp Step Steer Lateral Velocity Response

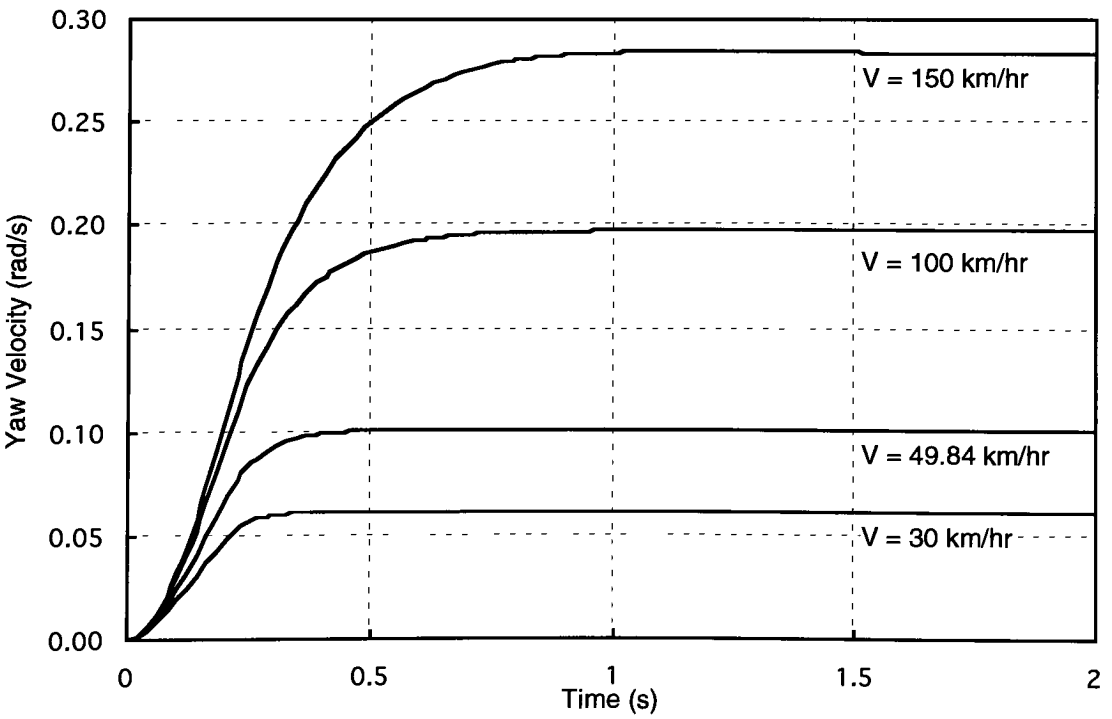

Figure 4.23: Linear Ramp Step Steer Yaw Velocity Response

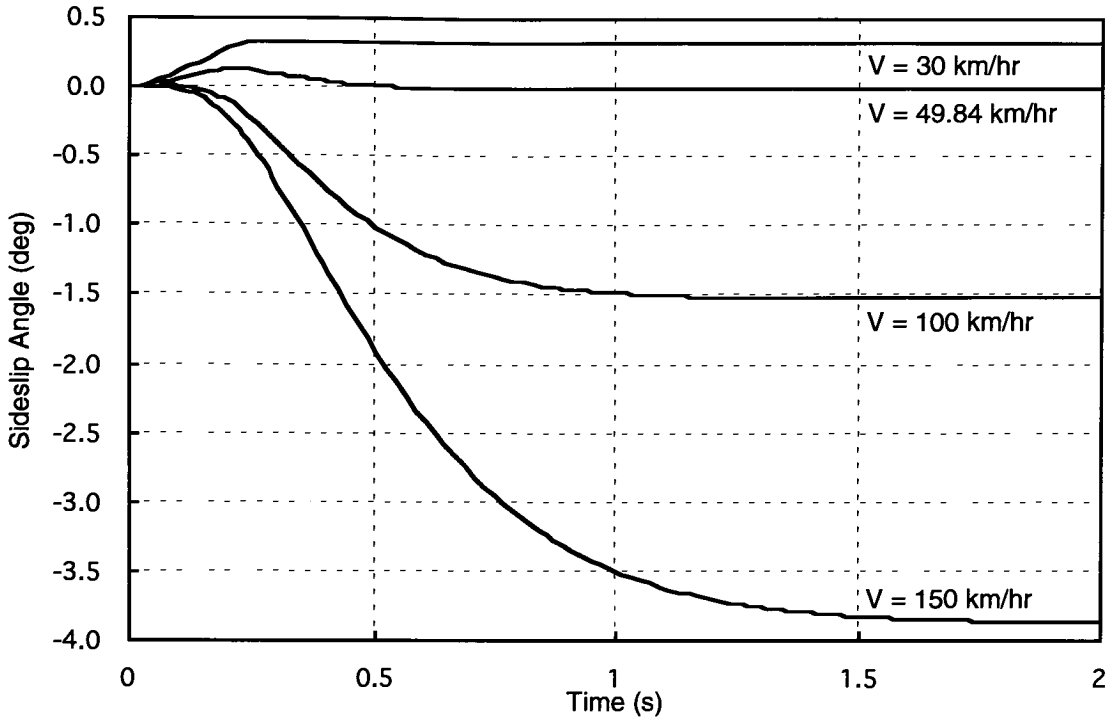

Figure 4.24: Linear Ramp Step Steer Sideslip Angle Response

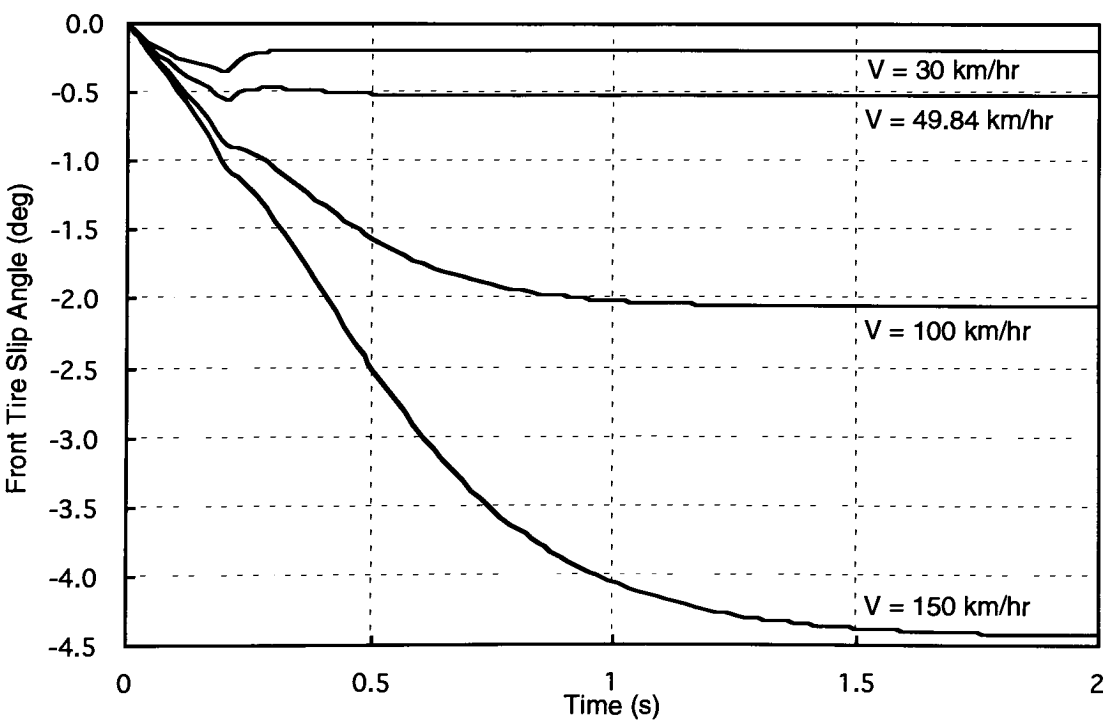

Figure 4.25: Linear Ramp Step Steer Front Tire Slip Angle Response

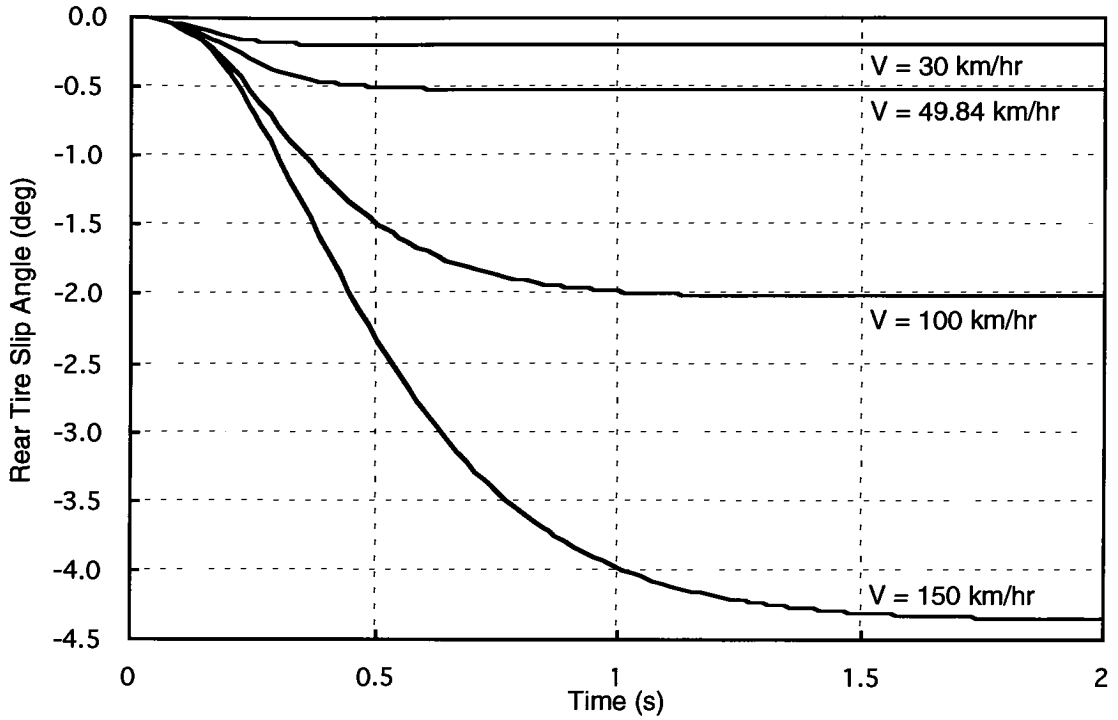

Figure 4.26: Linear Ramp Step Steer Rear Tire Slip Angle Response

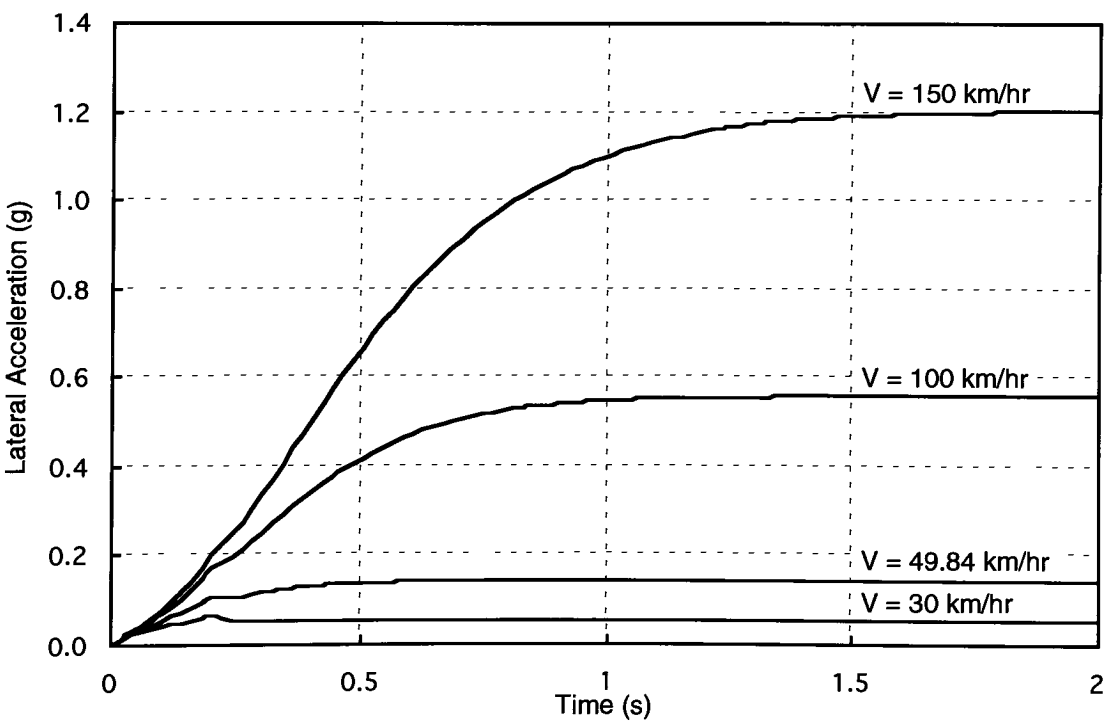

Figure 4.27: Linear Ramp Step Steer Lateral Acceleration Response

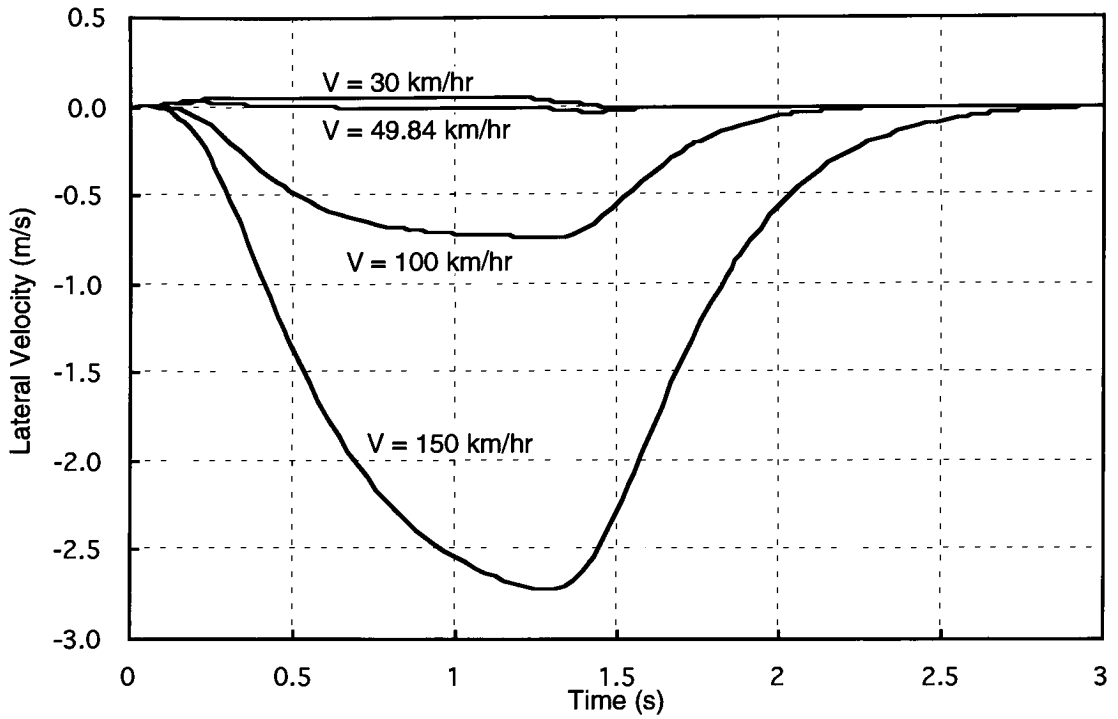

Figure 4.28: Linear Ramp Square Steer Lateral Velocity Response

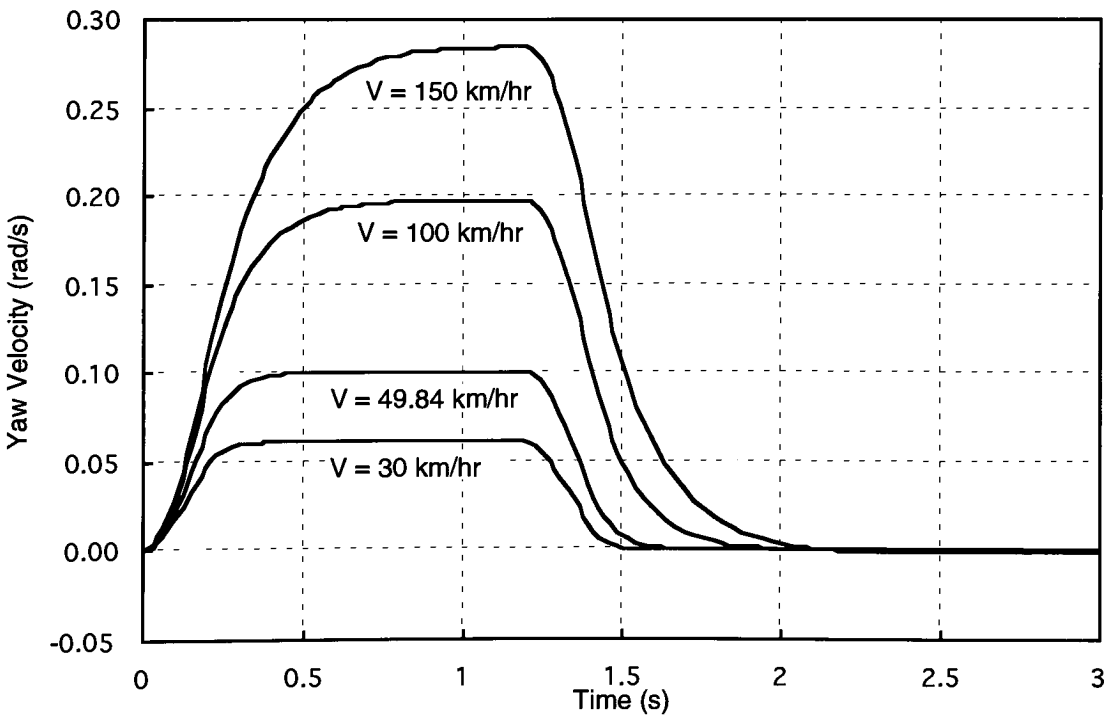

Figure 4.29: Linear Ramp Square Steer Yaw Velocity Response

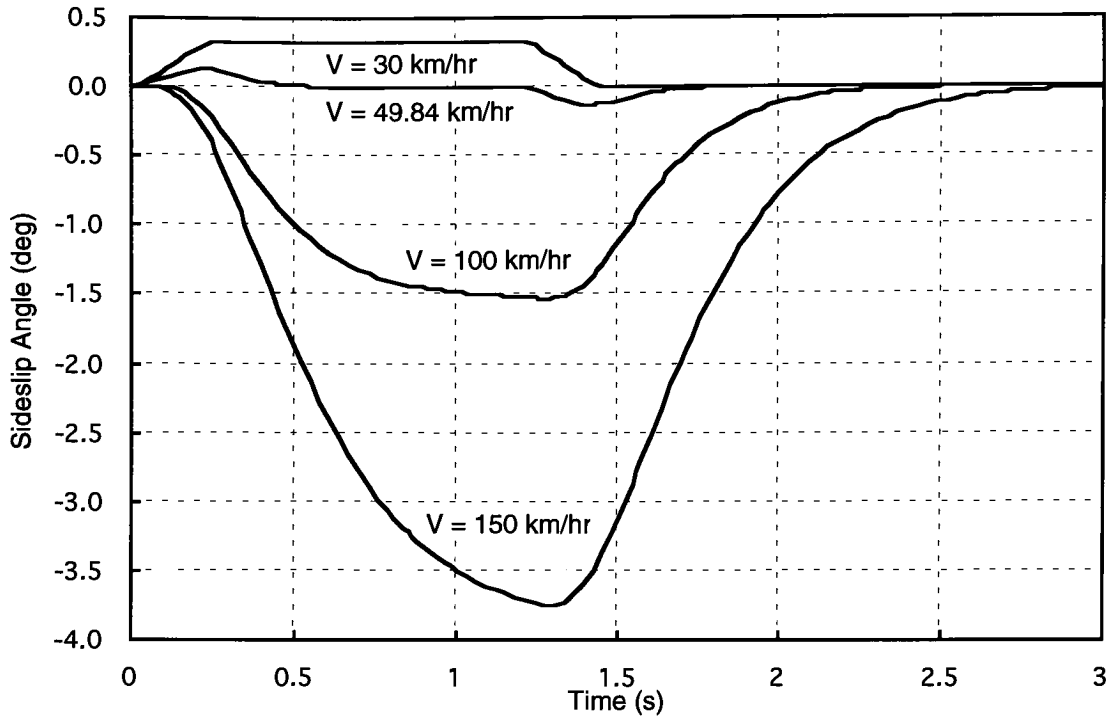

Figure 4.30: Linear Ramp Square Steer Sideslip Angle Response

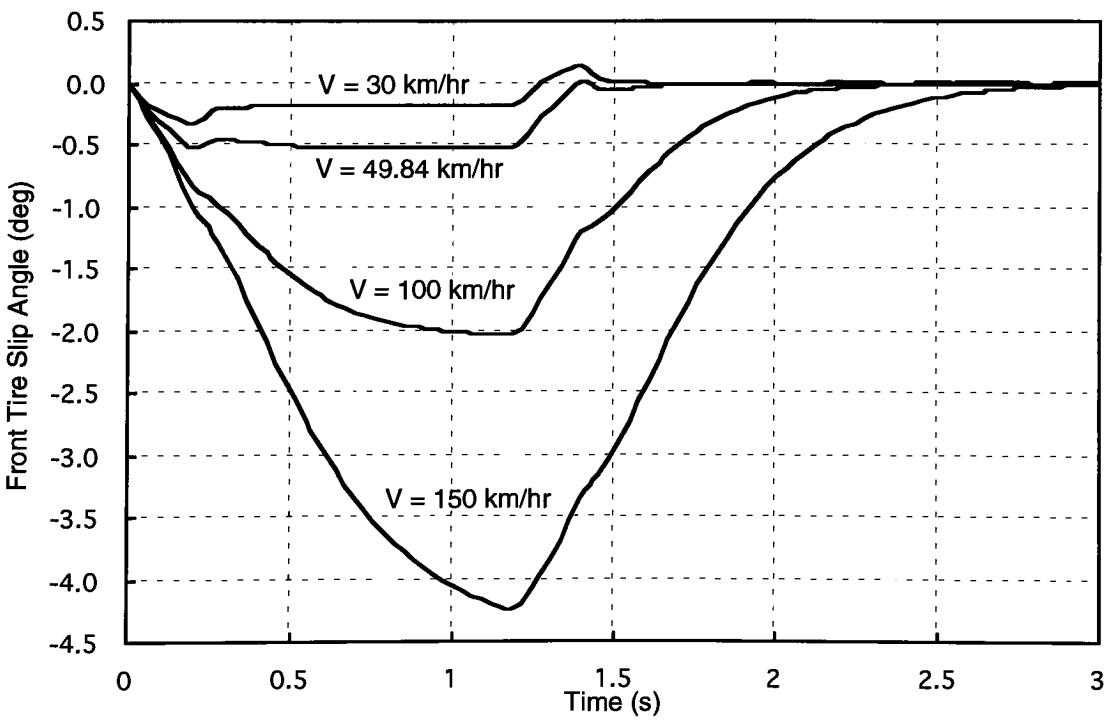

Figure 4.31: Linear Ramp Square Steer Front Tire Slip Angle Response

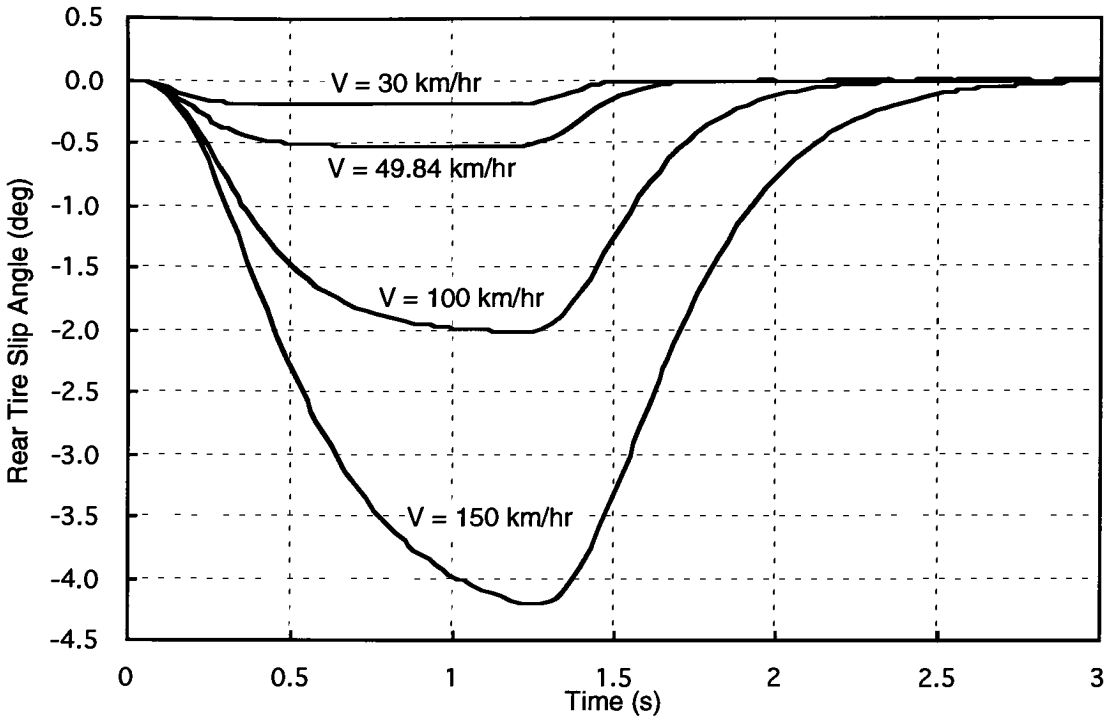

Figure 4.32: Linear Ramp Square Steer Rear Tire Slip Angle Response

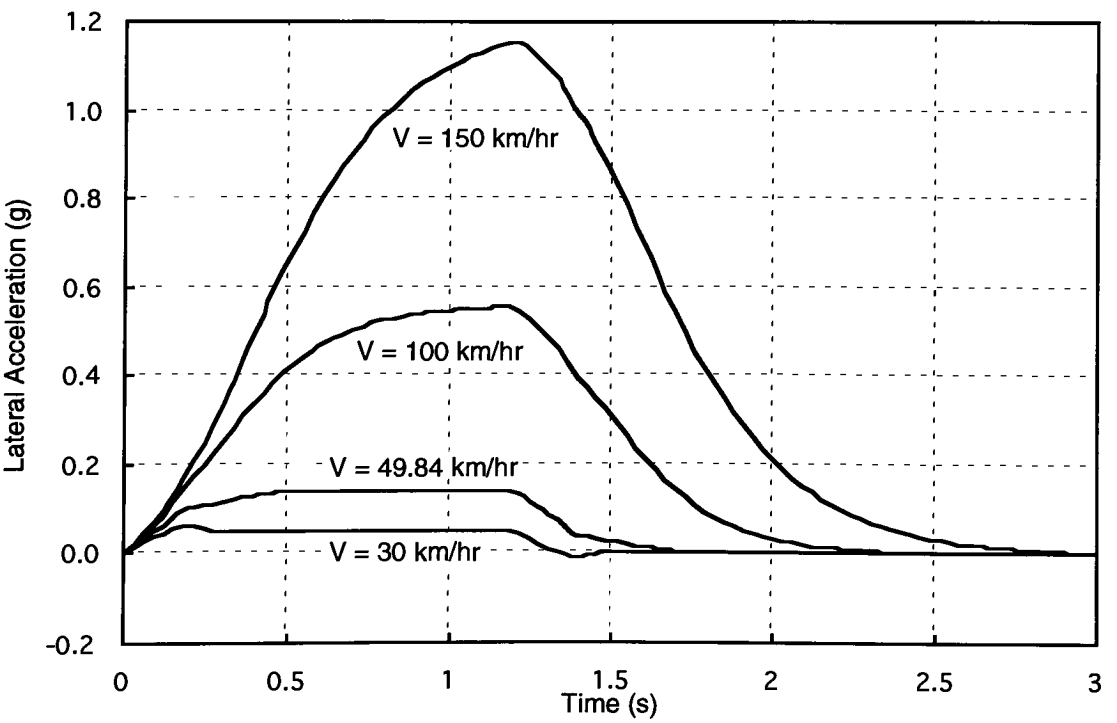

Figure 4.33: Linear Ramp Square Steer Lateral Acceleration Response

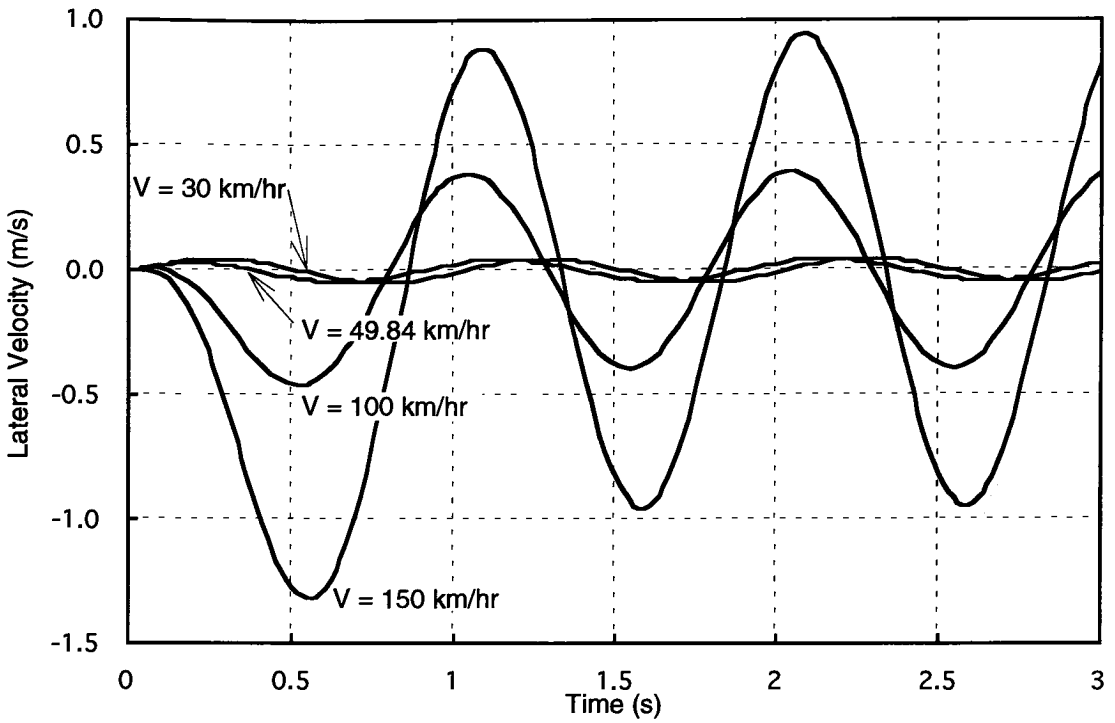

Figure 4.34: Linear 1 Hz Sine Steer Lateral Velocity Response

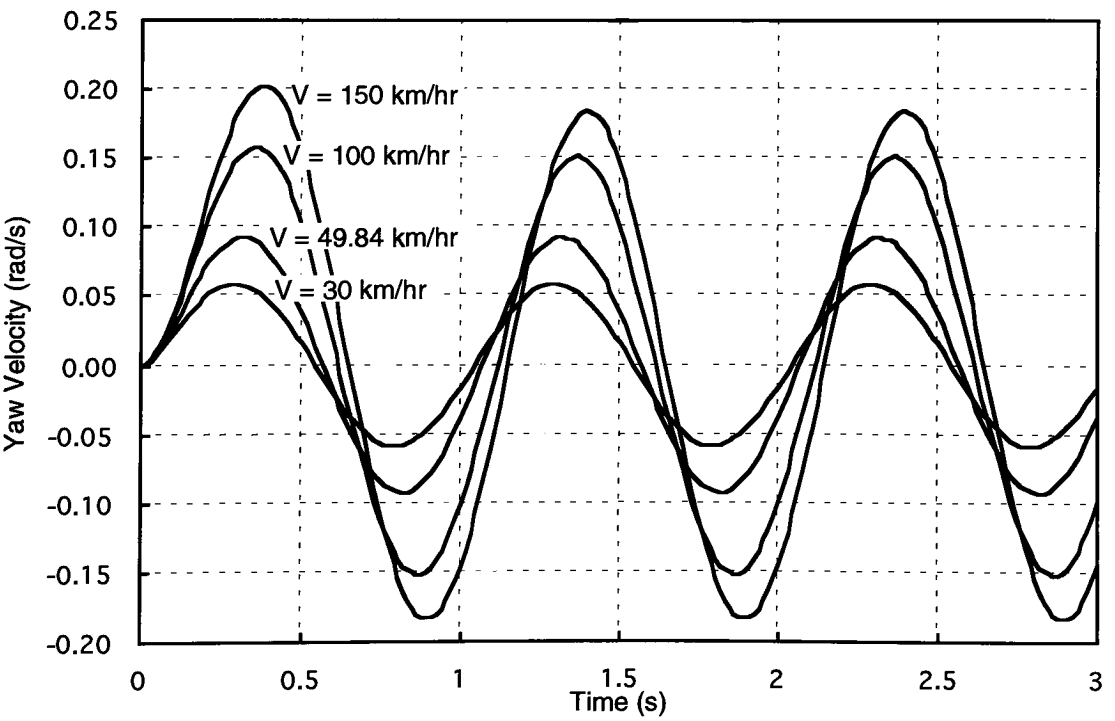

Figure 4.35: Linear 1 Hz Sine Steer Yaw Velocity Response

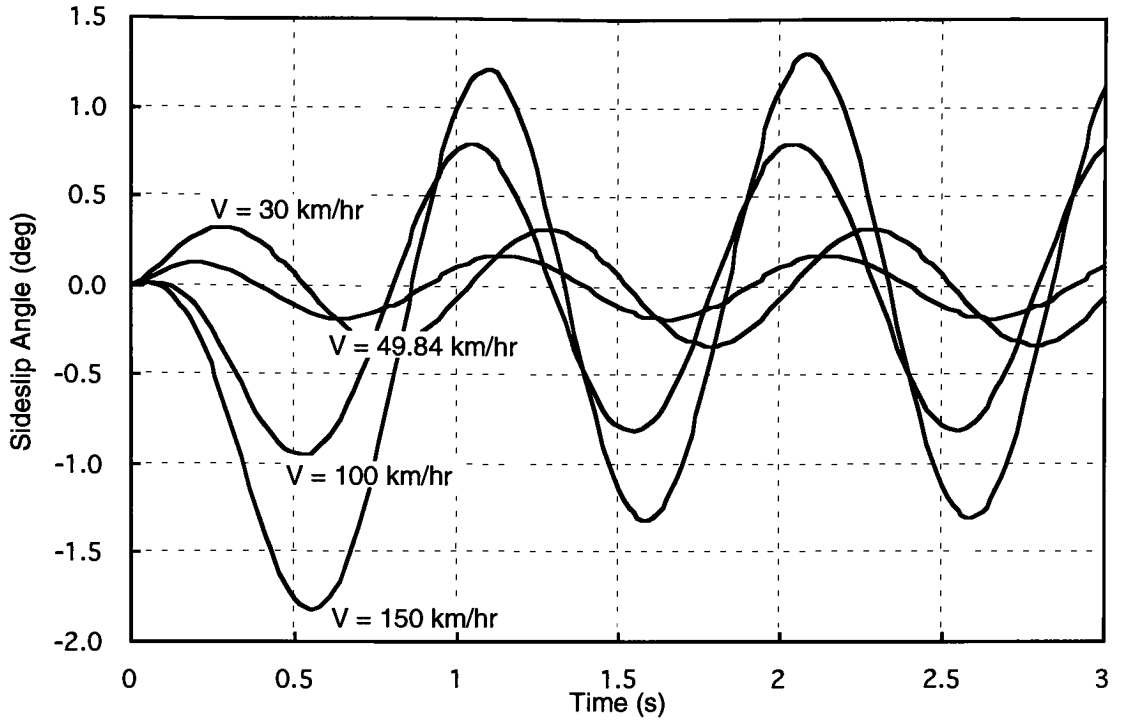

Figure 4.36: Linear 1 Hz Sine Steer Sideslip Angle Response

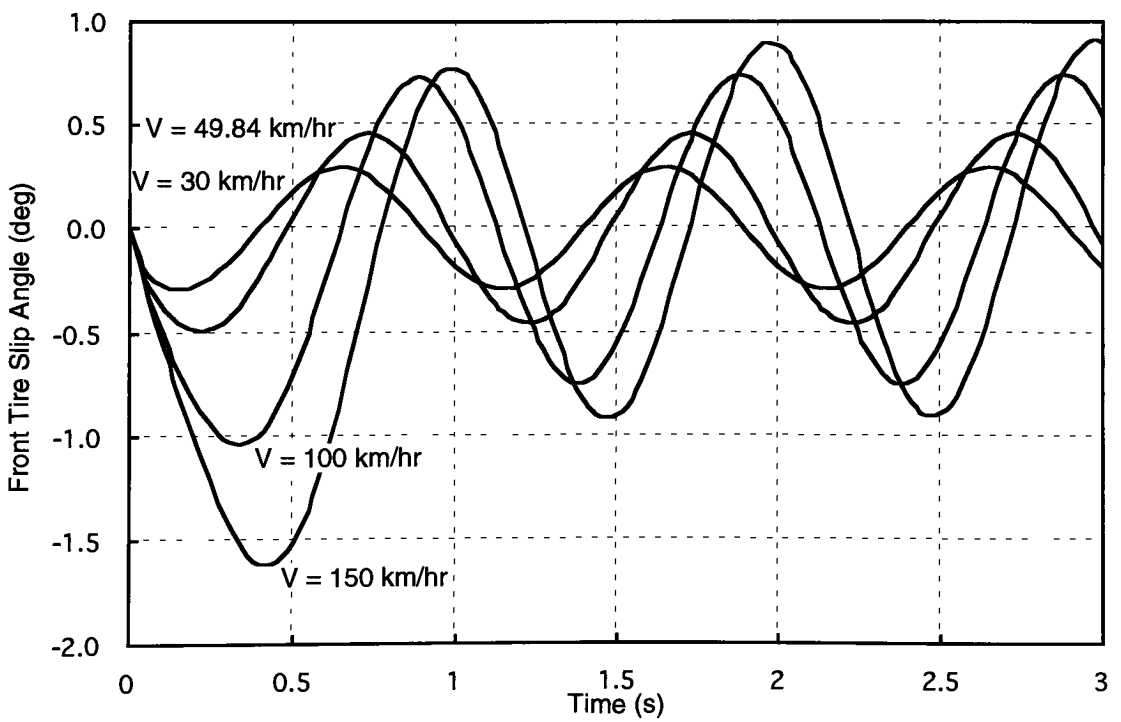

Figure 4.37: Linear 1 Hz Sine Steer Front Tire Slip Angle Response

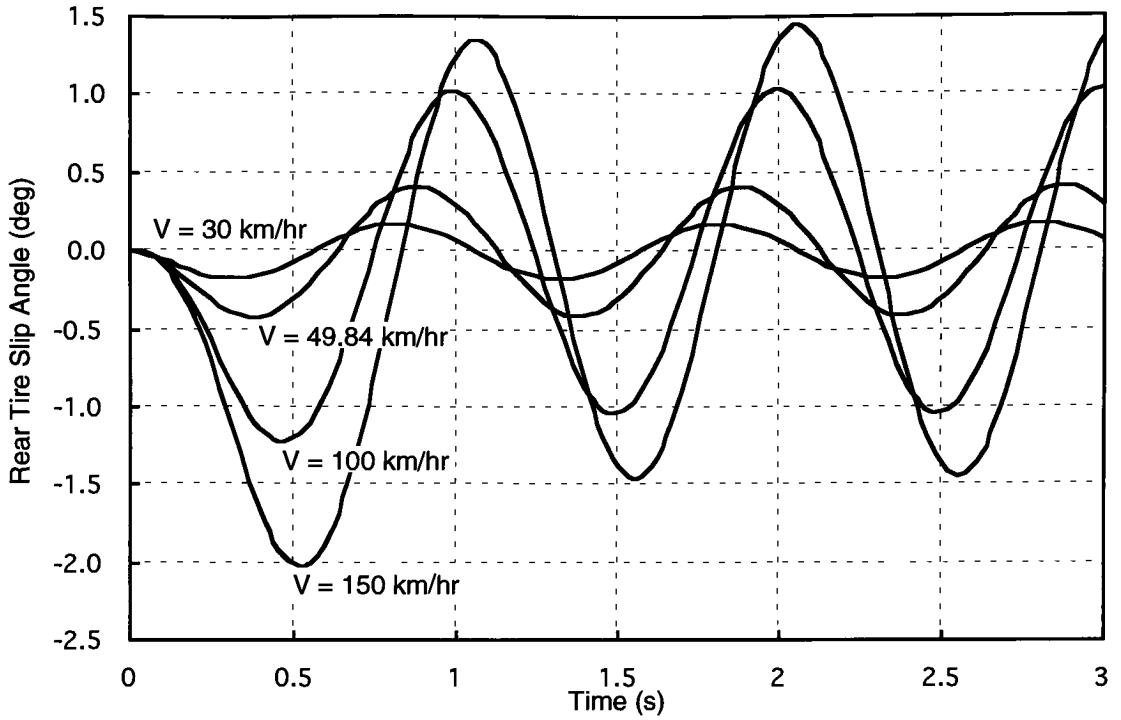

Figure 4.38: Linear 1 Hz Sine Steer Rear Tire Slip Angle Response

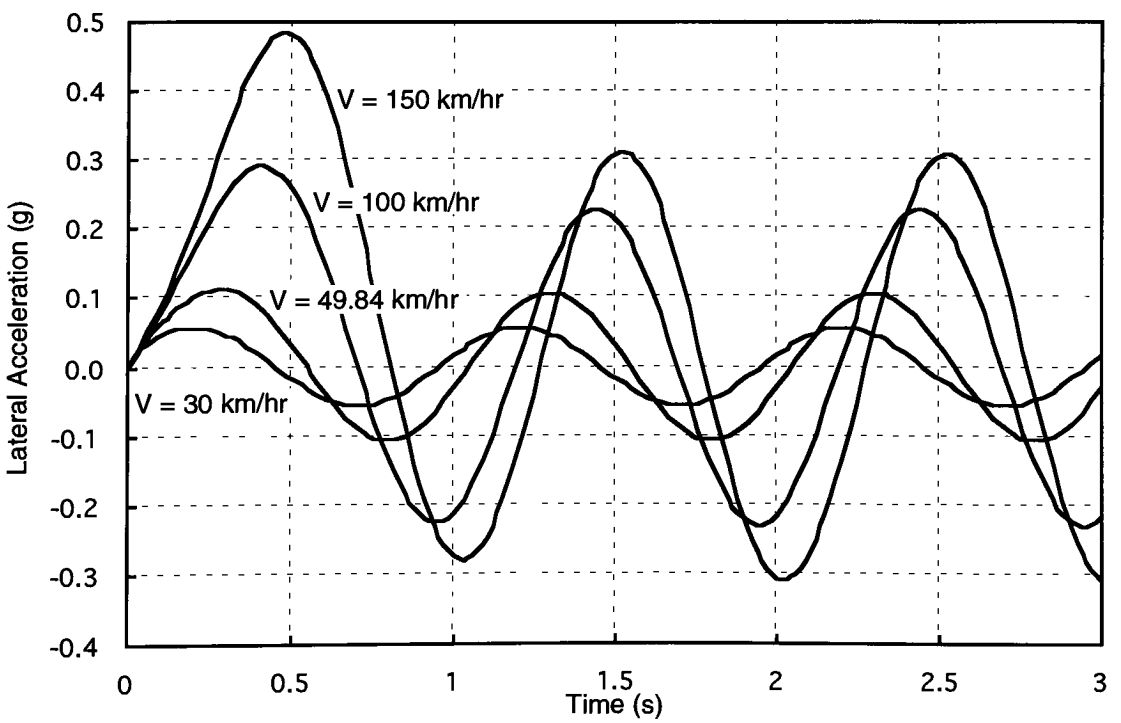

Figure 4.39: Linear 1 Hz Sine Steer Lateral Acceleration Response

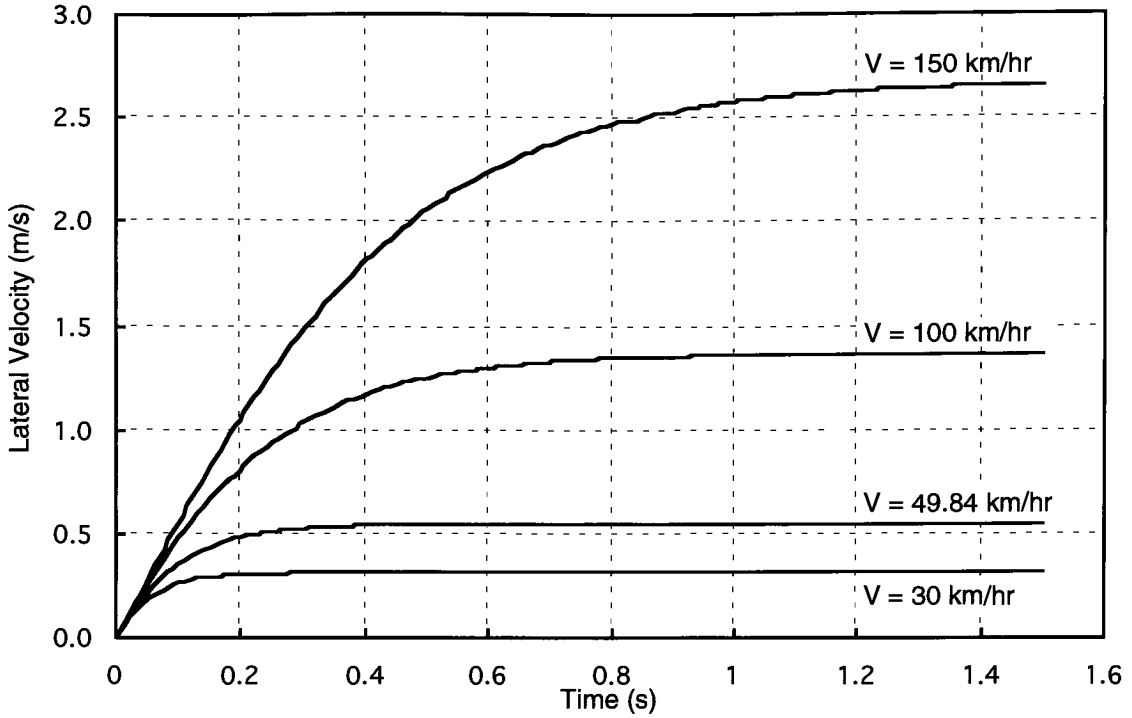

Figure 4.40: Linear Step Aero Side Force Lateral Velocity Response

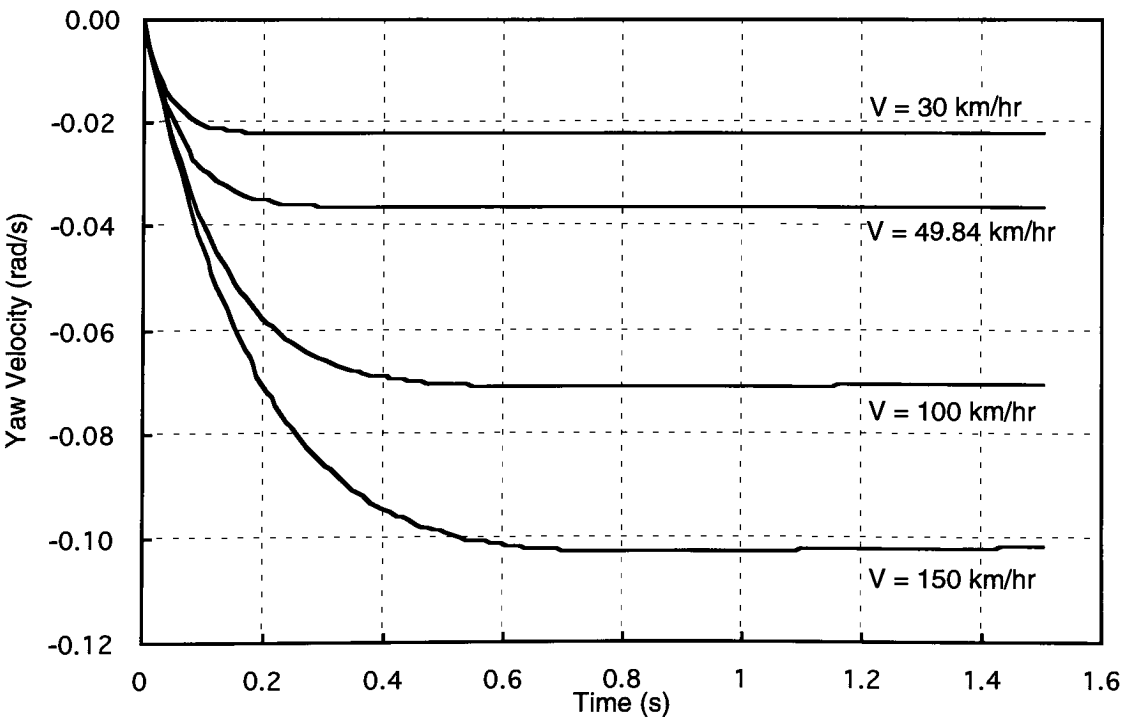

Figure 4.41: Linear Step Aero Side Force Yaw Velocity Response

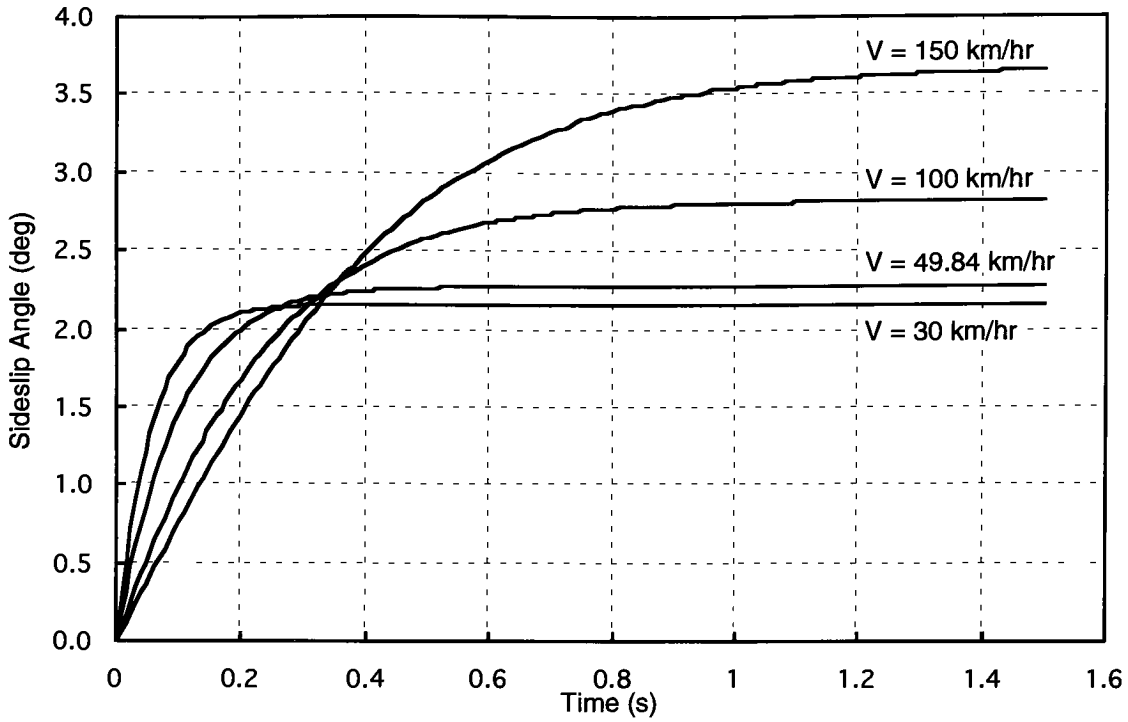

Figure 4.42: Linear Step Aero Side Force Sideslip Angle Response

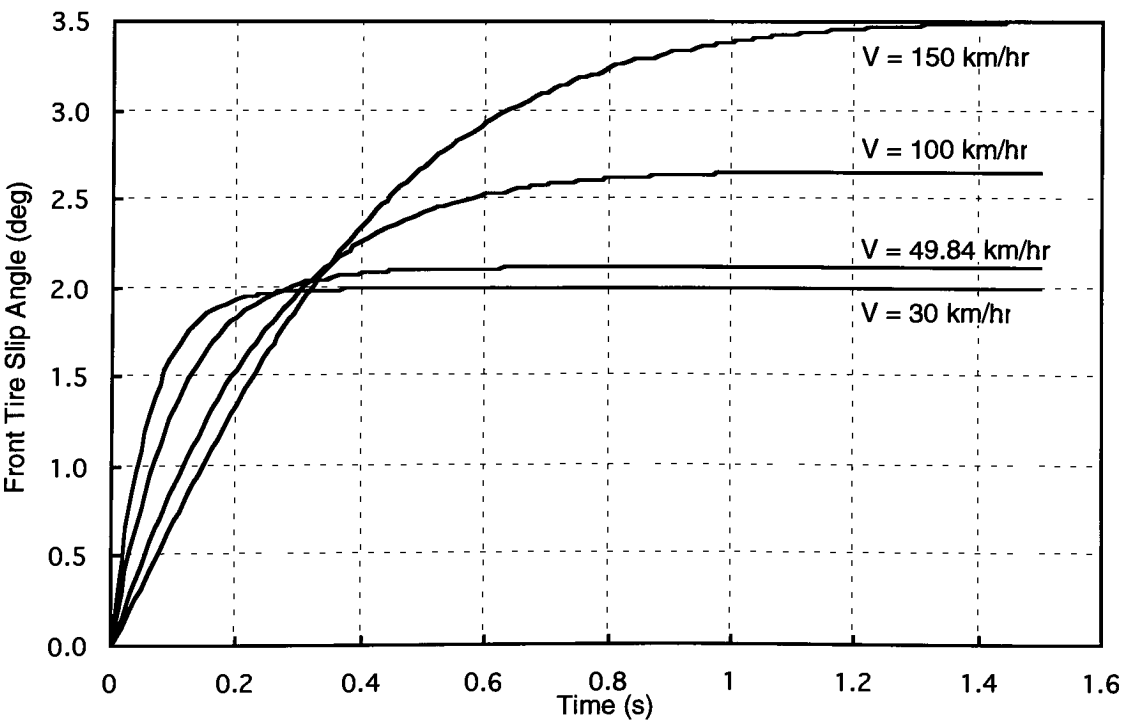

Figure 4.43: Linear Step Aero Side Force Front Tire Slip Angle Response

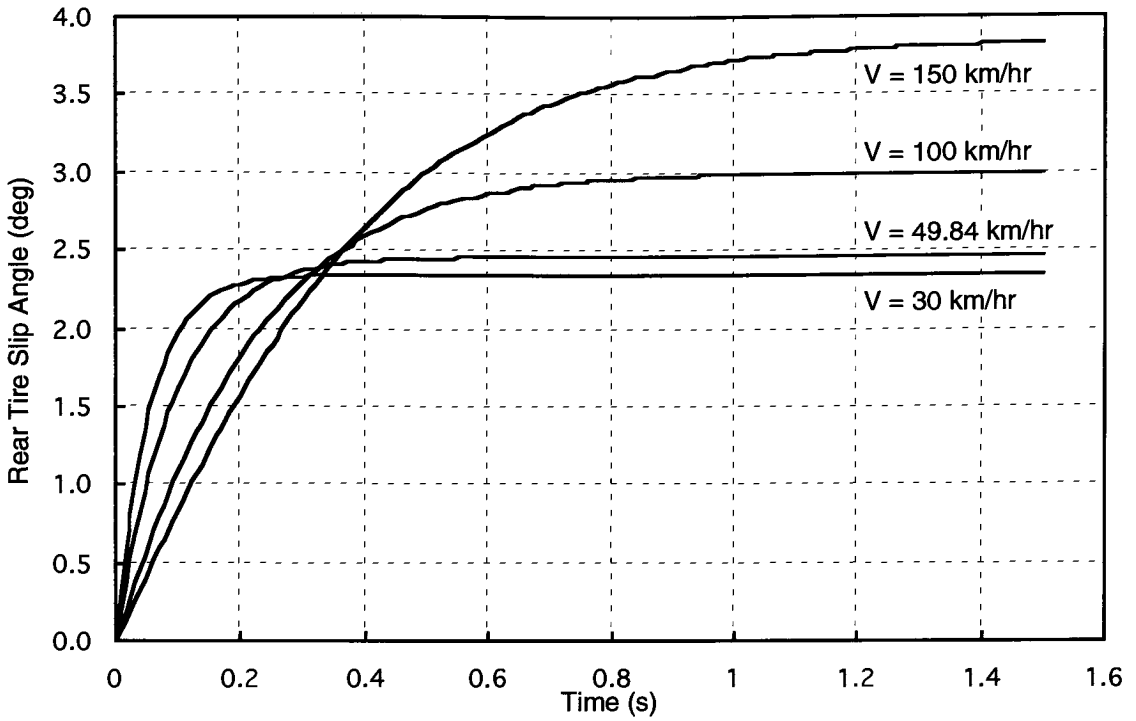

Figure 4.44: Linear Step Aero Side Force Rear Tire Slip Angle Response

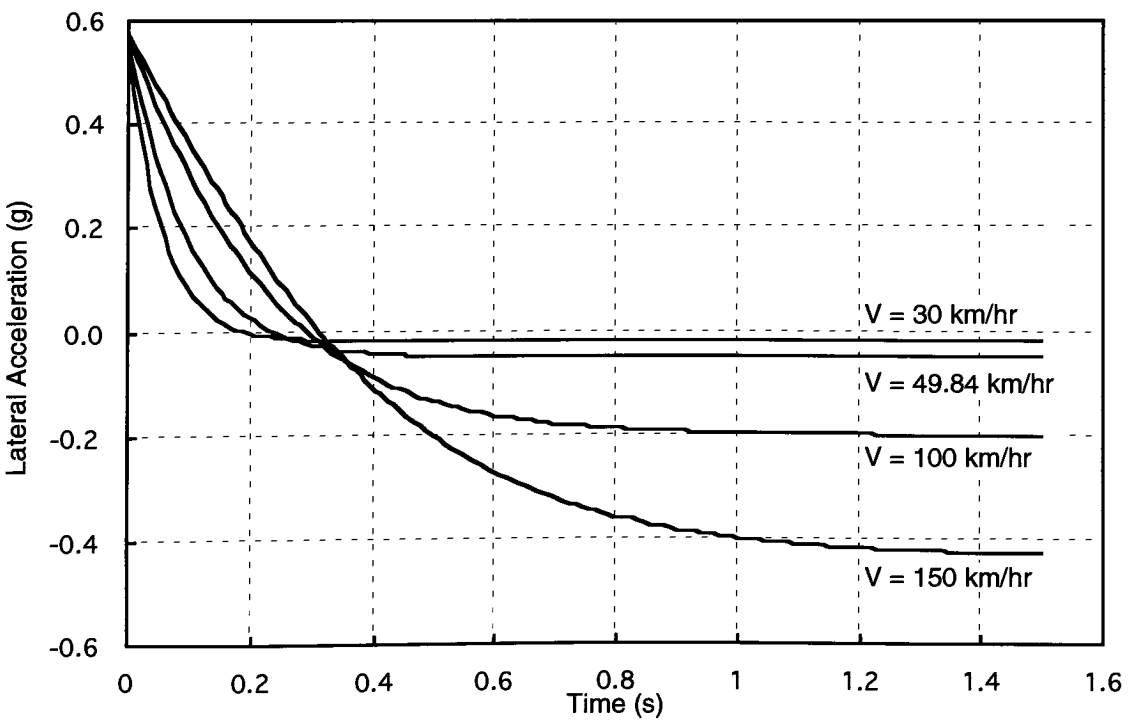

Figure 4.45: Linear Step Aero Side Force Lateral Acceleration Response

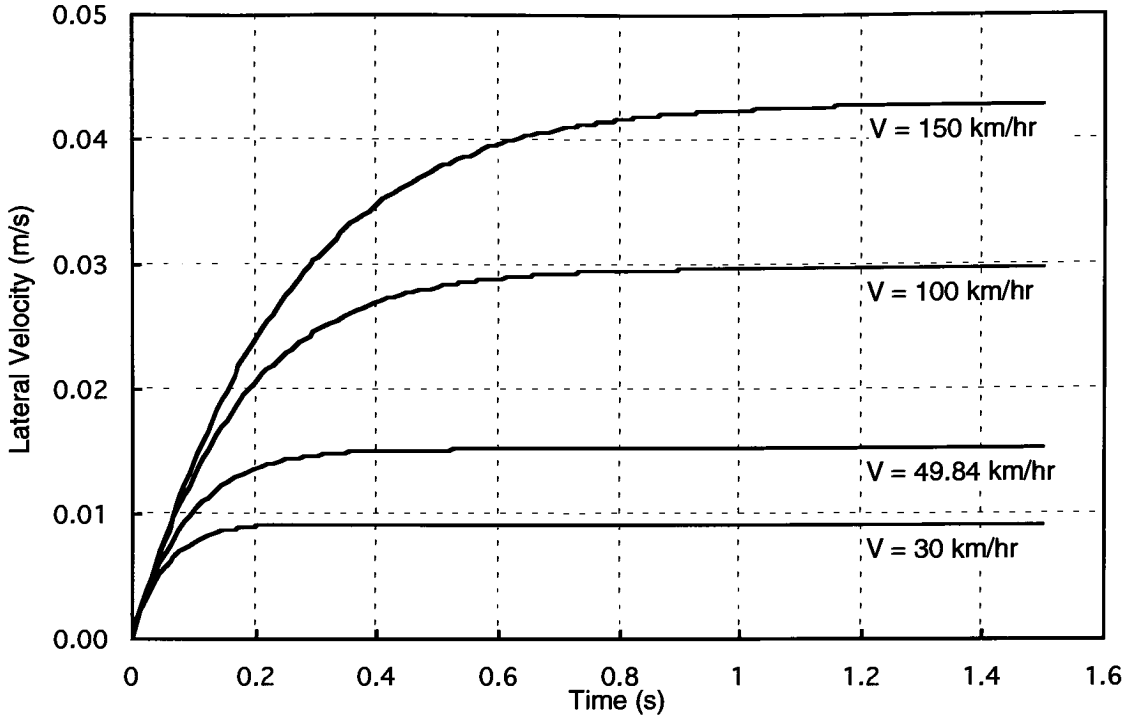

Figure 4.46: Linear Step Road Side Slope Lateral Velocity Response

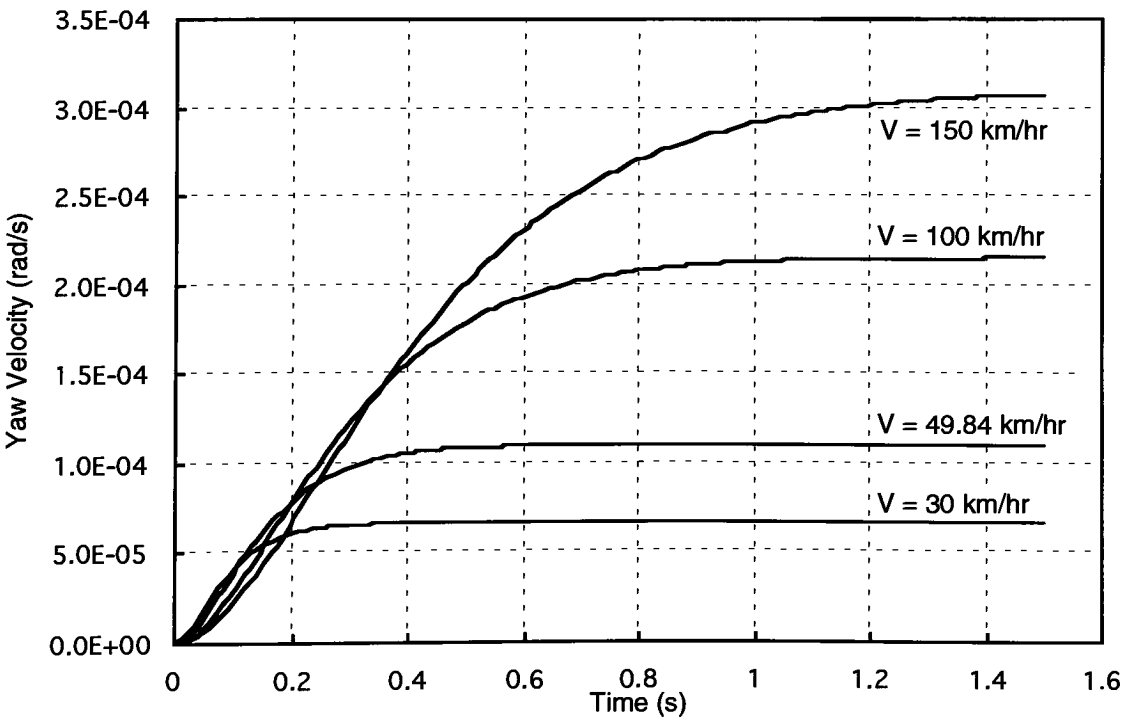

Figure 4.47: Linear Step Road Side Slope Yaw Velocity Response

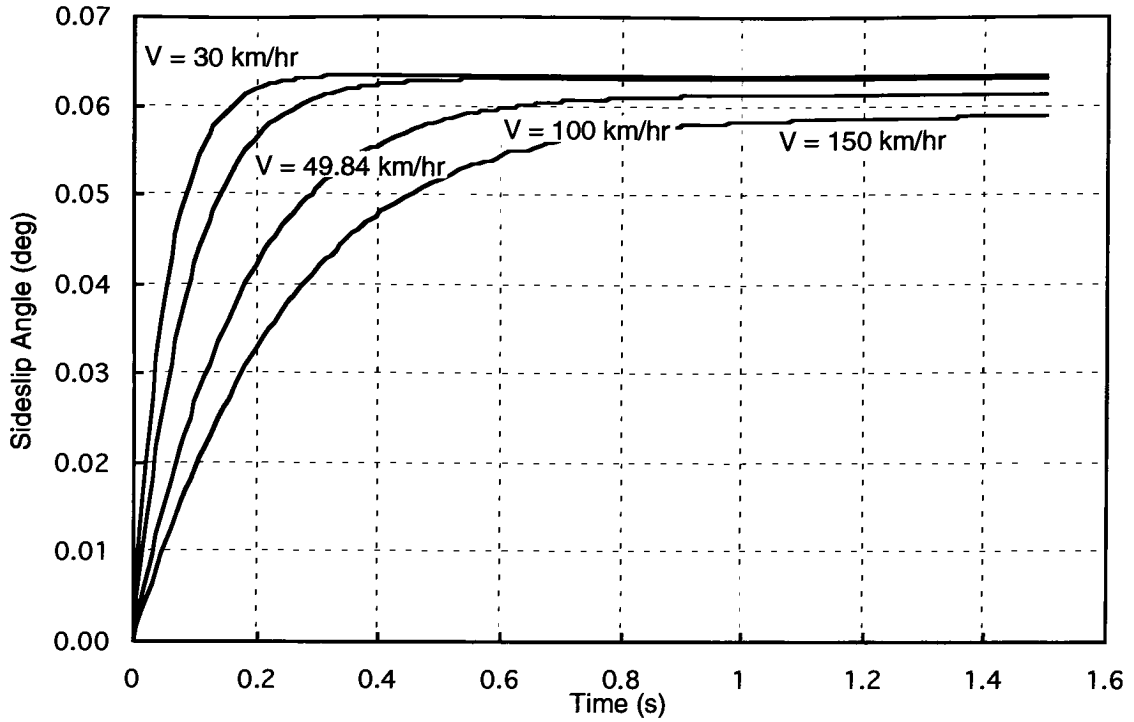

Figure 4.48: Linear Step Road Side Slope Sideslip Angle Response

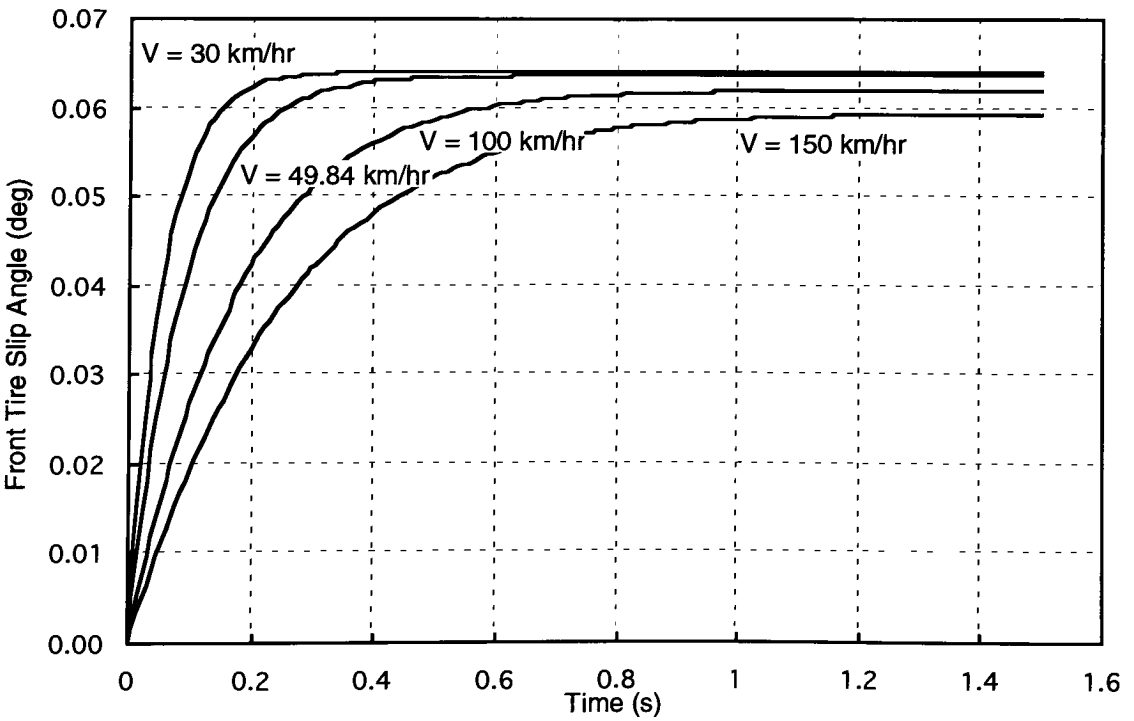

Figure 4.49: Linear Step Road Side Slope Front Tire Slip Angle Response

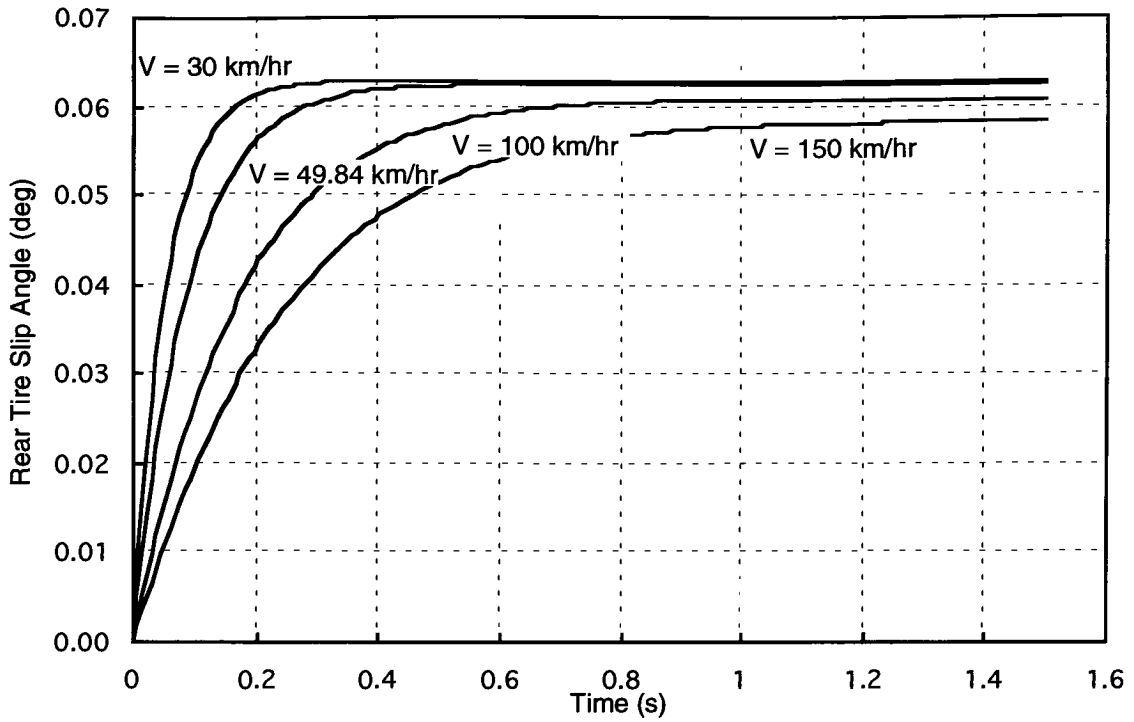

Figure 4.50: Linear Step Road Side Slope Rear Tire Slip Angle Response

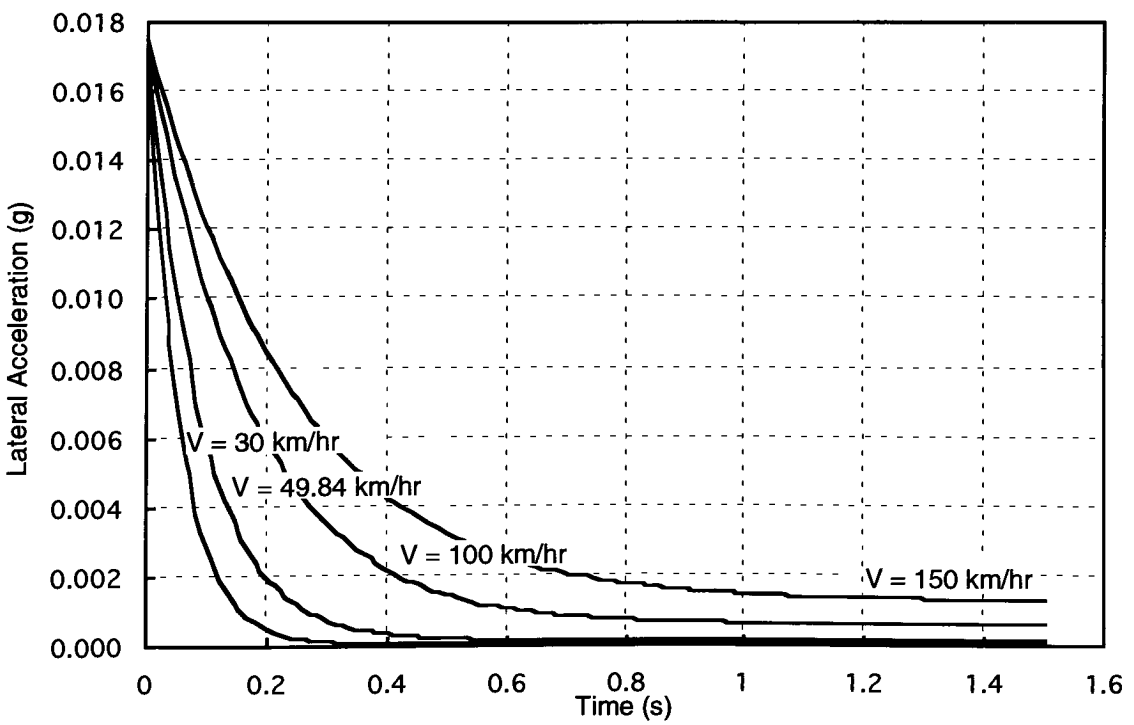

Figure 4.51: Linear Step Road Side Slope Lateral Acceleration Response

4.6 Non-Linear Model

As previously noted the linear vehicle model is valid for lateral accelerations up to approximately 0.35 g. This is primarily a result of tire lateral force being linear with respect to slip angle at small slip angles, and hence small lateral accelerations. Beyond 0.35 g when higher slip angles are being attained a non-linear tire model is usually necessary to accurately predict tire lateral forces.

As discussed in Chapter 3 many models of tire behavior exist. The tire model chosen for this work is called tire data nondimensionalization and was originated by Hugo Radt. This tire model is discussed in detail in Section 3.4.

In this section the equations describing the non-linear two degree-of-freedom vehicle model are presented. Simulation of the model is performed for selected steering inputs and the results are compared with the simulation of the linear model.

4.6.1 Model Equations

The equations of motion for the non-linear two degree-of-freedom vehicle are derived in Section 4.3 and are repeated here.

$$\begin{aligned} F_{yf}\cos\delta + F_{yr} + F_{ya} + F_{yg} &= m(\dot{v} + ur) \\ aF_{yf}\cos\delta - bF_{yr} - (c-a)F_{ya} &= I_{zz}\dot{r} \end{aligned} \tag{4.9}$$

Expressions for the tire slip angles are derived in Section 4.4.

$$\begin{aligned} \alpha_f &= \text{atan}\left(\frac{v+ar}{u}\right) - \delta \\ \alpha_r &= \text{atan}\left(\frac{v-br}{u}\right) \end{aligned} \tag{4.14}$$

The tire lateral force is given by the following expressions as described in Section 3.4 and repeated here for convenience. From these equations the tire lateral force F_y can be calculated based upon the tire vertical load F_z and the tire slip angle α.

$$C_c = B_3 + C_3 F_z \tag{3.3}$$

$$\mu_y = B_5 + C_5 F_z \tag{3.5}$$

$$\overline{\alpha} = \frac{C_c \tan(\alpha)}{\mu_y} \tag{3.6}$$

$$\overline{\psi} = (1 - E_1)\overline{\alpha} + \frac{E_1 \operatorname{atan}(B_1 \overline{\alpha})}{B_1} \tag{3.10}$$

$$\overline{\theta} = C_1 \operatorname{atan}(B_1 \overline{\psi}) \tag{3.9}$$

$$\overline{F}_y = D_1 \sin(\overline{\theta}) \tag{3.8}$$

$$F_y = \overline{F}_y \mu_y F_z \tag{3.11}$$

4.6.2 Simulation

Simulation of the non-linear two degree-of-freedom vehicle model is implemented in the MATLAB script *DOF2NLSim.m*. This script is listed in Appendix C.8 and is very similar to *DOF2LSim.m* which performs simulation of the linear model. As with the linear simulation, the scripts *DOF2Control.m*, *DOF2Param.m,* and *DOF2DependParam.m* are called at the beginning of *DOF2NLSim.m* to set simulation, vehicle, and tire parameters. The built-in MATLAB function *ode23* is used again to integrate the differential equations of motion which are contained in the function *DOF2NLDE.m*. This function calculates the state derivatives $\dot{v}$ and $\dot{r}$ based upon the instantaneous values of the state variables v and r and the current steer angle. *DOF2NLDE.m* is listed in Appendix C.9. The state derivatives are calculated as

$$\begin{aligned} \dot{v} &= \frac{2F_{yf}\cos(\delta) + 2F_{yr} + F_{ya} + F_{yg}}{m} - ur \\ \dot{r} &= \frac{2aF_{yf}\cos(\delta) - 2bF_{yr} - (c-a)F_{ya}}{I_{zz}} \end{aligned} \tag{4.89}$$

These expressions are obtained by solving Eq. (4.9) for $\dot{v}$ and $\dot{r}$.

The most significant difference between the non-linear and linear model simulations is in the calculation of tire lateral forces. The tire lateral forces are calculated by the MATLAB function *NLTire.m* which is listed in Appendix A.3. This script takes the tire vertical load and slip angle as arguments and returns the tire lateral force. Note that with the non-linear tire model the lateral forces F_{yf} and F_{yr} are for only one tire, while for simplification in the linear model they are for two tires. Thus here they are multiplied by the factor of two in Eq. (4.89) to get the lateral forces for two tires. *NLTire.m* is called at each time step by *DOF2NLDE.m*, which also calls the function *SteerAngle.m* to calculate the instantaneous steer angle.

For comparison with the linear model, simulation of the non-linear model is performed for the step steer input and the ramp square steer input. As with the linear model, simulations are performed for forward velocities of 30 km/hr, 48.94 km/hr, 100 km/hr, and 150 km/hr. The step steer and ramp square steer inputs are identical to those used for the linear model, having a magnitude of 1°. Tire parameters for the non-linear tire model are given in Table 3.1. These parameters are a result of the curve fitting of empirical tire data done in Section 3.4. The values of the linear tire comering stiffnesses used in throughout Section 4.5 are derived from these parameters, so the linear tire model and non-linear tire model agree at small slip angles. Vehicle parameters are identical to those used in the linear simulation. Results from the simulations are provided in Figure 4.52 through Figure 4.63. Included on these plots as dashed lines are the linear simulation results for comparison.

Lateral velocity, yaw velocity, sideslip angle, front tire slip angle, rear tire slip angle, and lateral acceleration results for both the non-linear and linear simulations are presented in Figure 4.52 through Figure 4.57 for the step steer input. The linear and non-

linear lateral acceleration results agree within 1% over the complete duration of the simulation for forward velocities of 30 km/hr and 49.84 km/hr. These speeds correspond to steady-state lateral accelerations of 0.05 g and 0.14 g respectively. At 100 km/hr, which produces a 0.55 g steady-state lateral acceleration, the linear model lateral acceleration results exceed those of the non-linear by 4.3% during the transient and 1.0% once steady-state is reached. At this speed the tire slip angles reach slightly more than 2°. At these slip angles the tire lateral force versus slip angle curve is still very nearly a straight line. Thus for this tire and vehicle the linear tire model is reasonably accurate and useful for lateral accelerations in excess of 0.5 g. However, at 150 km/hr the linear model lateral accelerations exceed those of the non-linear model by over 27%. At this speed the non-linear model predicts a steady-state lateral acceleration of 0.95 g while the linear model predicts 1.20 g. The tire slip angles have exceeded 6° where the lateral force versus slip angle curve is approaching its peak. The linear tire approximation is not sufficiently accurate at slip angles of this magnitude.

At high speeds the linear model predicts that the magnitudes of lateral velocities, sideslip angles, and tire slip angles are below those that the non-linear model predicts and that the yaw velocities and lateral accelerations are above those of the non-linear model. The linear model also predicts faster response than the non-linear model. At 150 km/hr the non-linear model predicts overshoot in all of the quantities examined, while the linear model predicts no overshoot.

Non-linear and linear simulation results for the ramp square steer input are plotted in Figure 4.58 through Figure 4.63. The differences between the non-linear and linear models for this input are similar to those of the step steer input. The two models agree very well for forward velocities of 30 km/hr and 49.84 km/hr. As with the step steer input, at the higher speeds the linear model predicts peak lateral velocity, sideslip angle, and tire slip angle magnitudes below those of the non-linear model and predicts peak yaw velocities and

lateral accelerations above those of the non-linear model. Differences in peak lateral acceleration reach 25%. Again, the linear model predicts faster response than the non-linear model. In particular, at 150 km/hr the response of the non-linear model lags the linear model by approximately 0.5 seconds after the steer input is ramped back down to zero. Here differences between the linear and non-linear lateral accelerations reach nearly 100%.

Comparison of the linear and non-linear model simulations shows that at low slip angles and lateral accelerations the linear vehicle and tire models can produce results comparable to the non-linear model. Even for the 100 km/hr case where slip angles exceed 2° and the lateral acceleration reaches 0.55 g the linear model produces results that are acceptable for most engineering purposes. When tire slip angles and lateral accelerations become high it is necessary to have a non-linear tire model to obtain accurate results. However, since most driving is done at low slip angles and lateral accelerations, the linear model and the linear analysis techniques presented in Section 4.5.6 through Section 4.5.26 can be used both to study vehicle behavior and to design vehicles to have desirable performance characteristics over a wide variety of operating conditions.

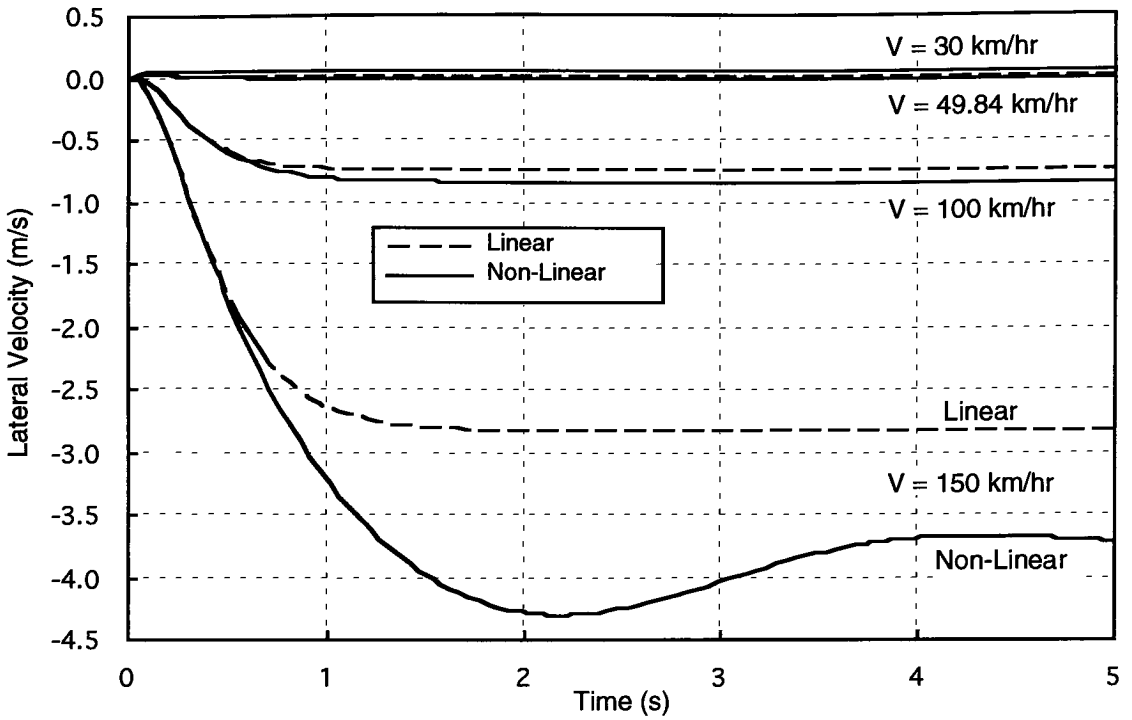

Figure 4.52: Non-Linear Step Steer Lateral Velocity Response

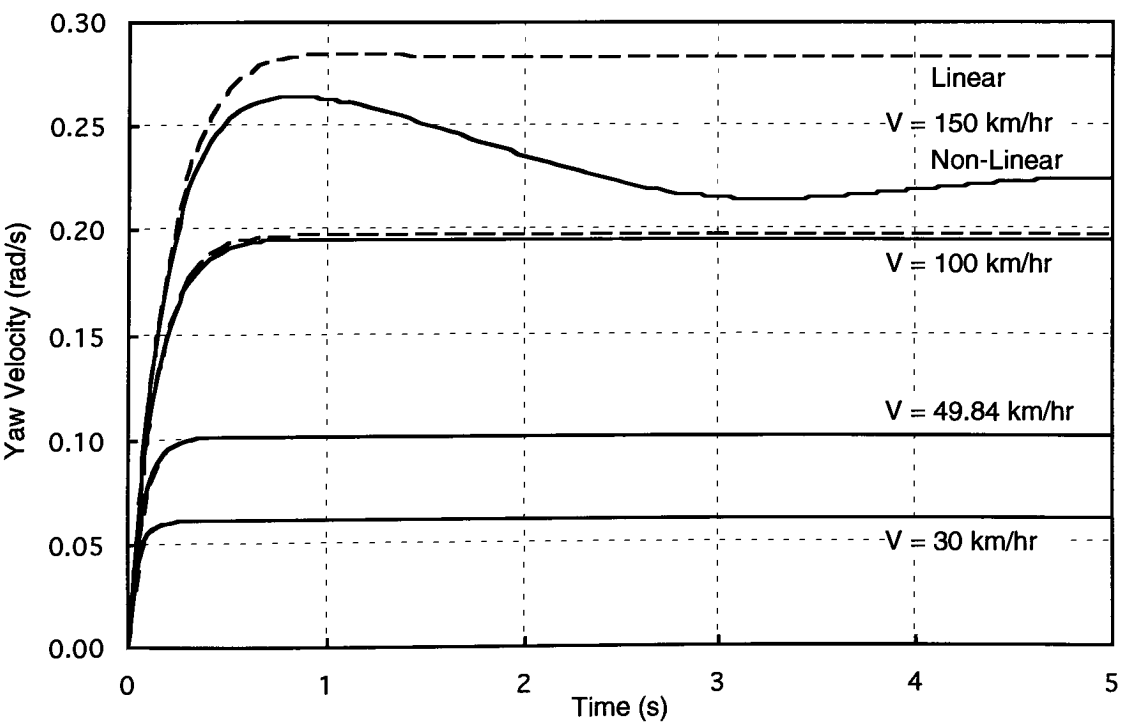

Figure 4.53: Non-Linear Step Steer Yaw Velocity Response

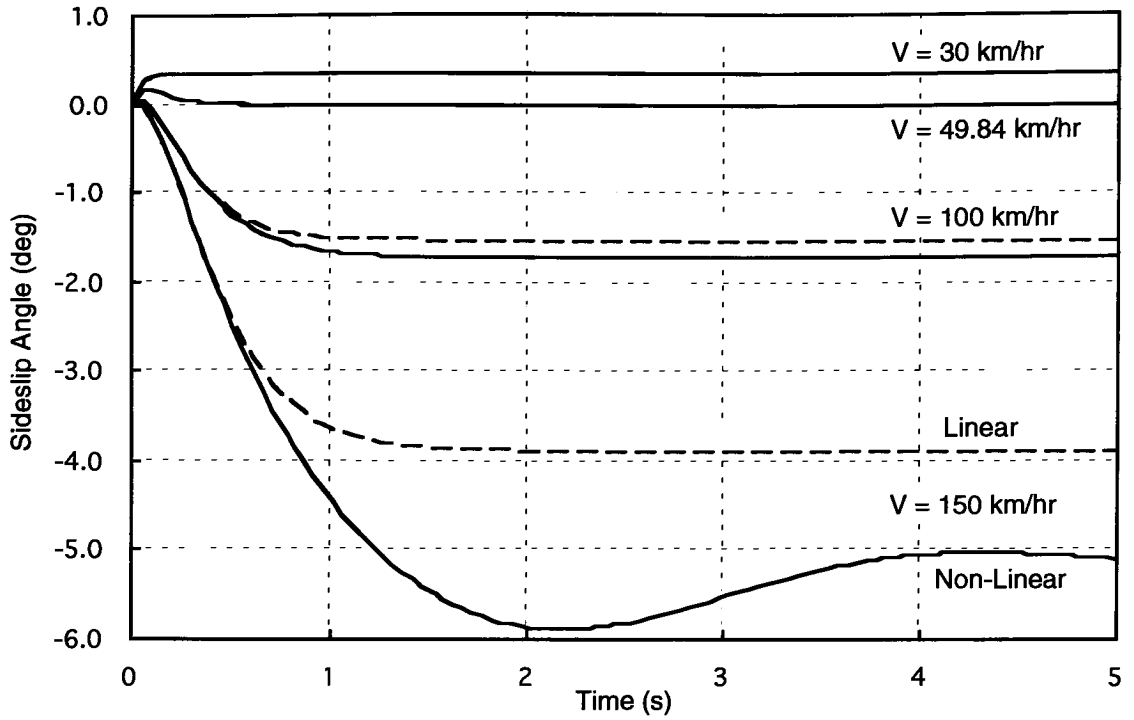

Figure 4.54: Non-Linear Step Steer Sideslip Angle Response

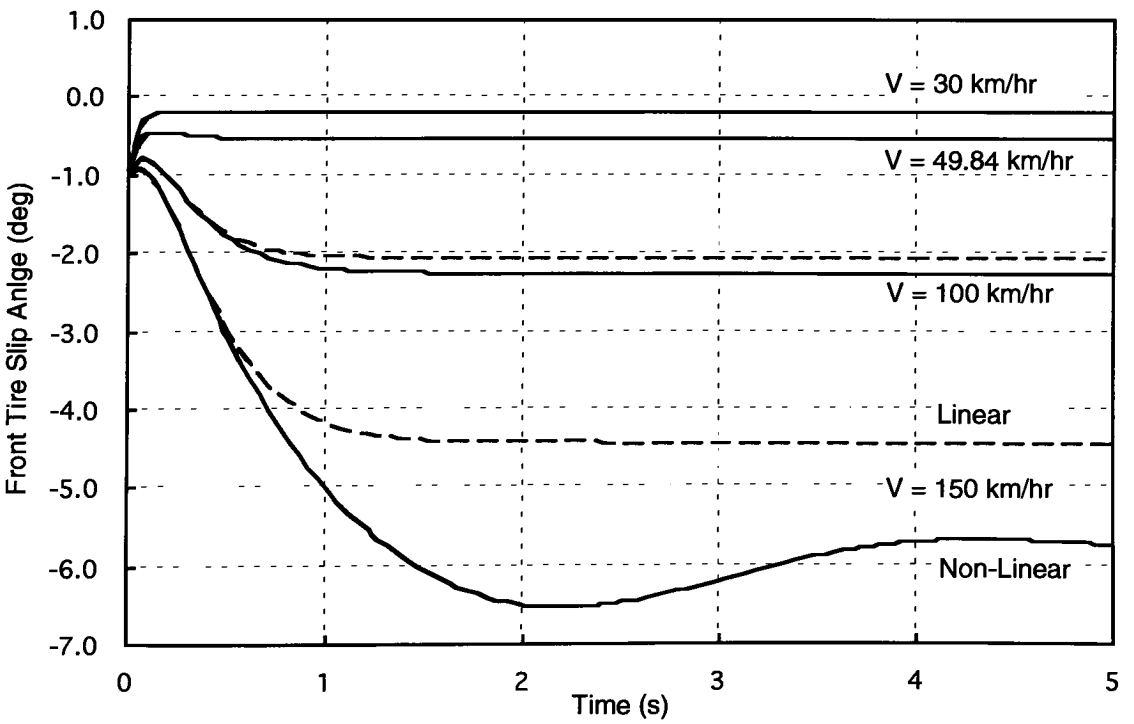

Figure 4.55: Non-Linear Step Steer Front Tire Slip Angle Response

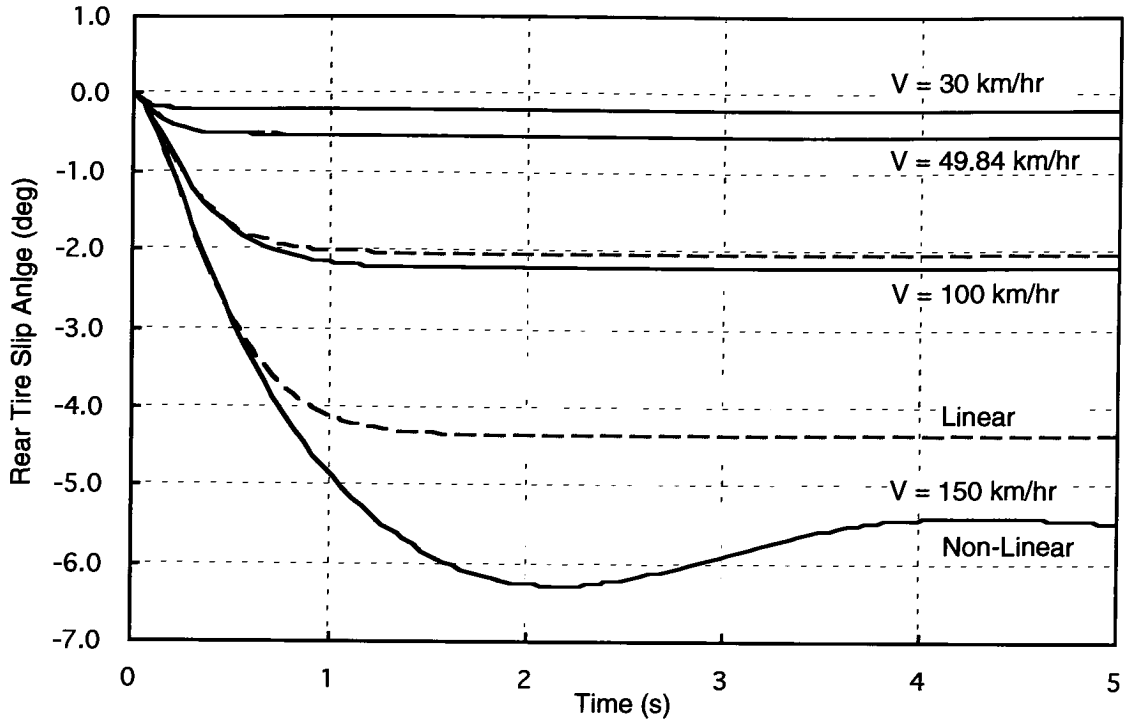

Figure 4.56: Non-Linear Step Steer Rear Tire Slip Angle Response

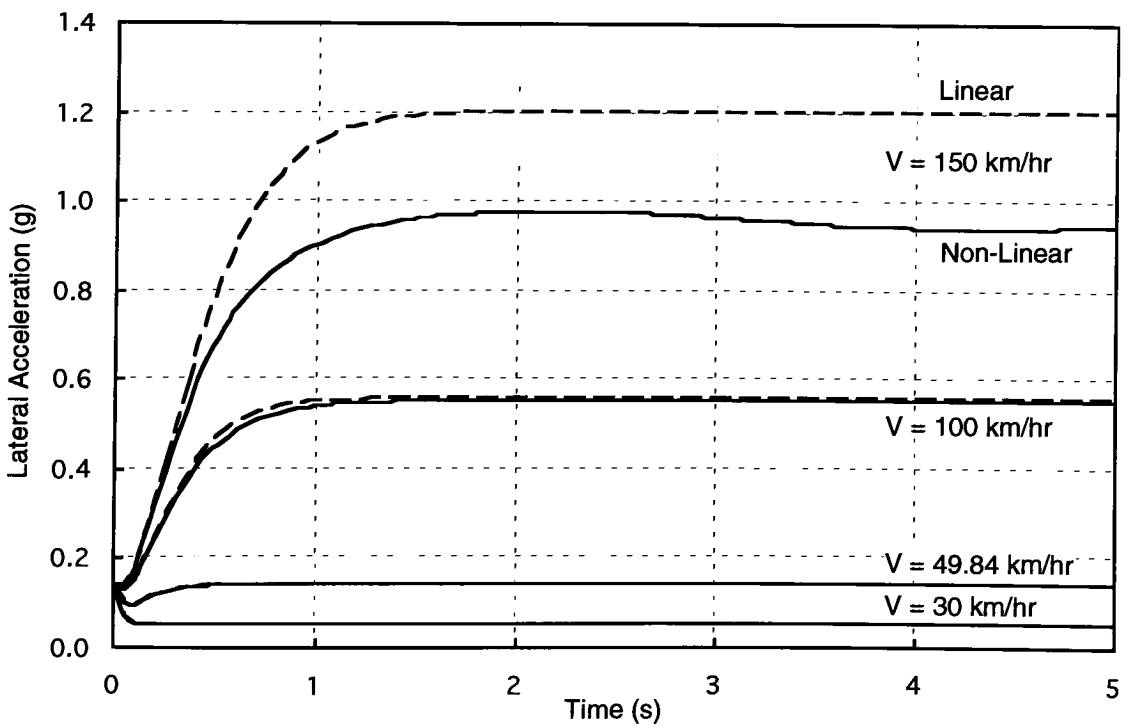

Figure 4.57: Non-Linear Step Steer Lateral Acceleration Response

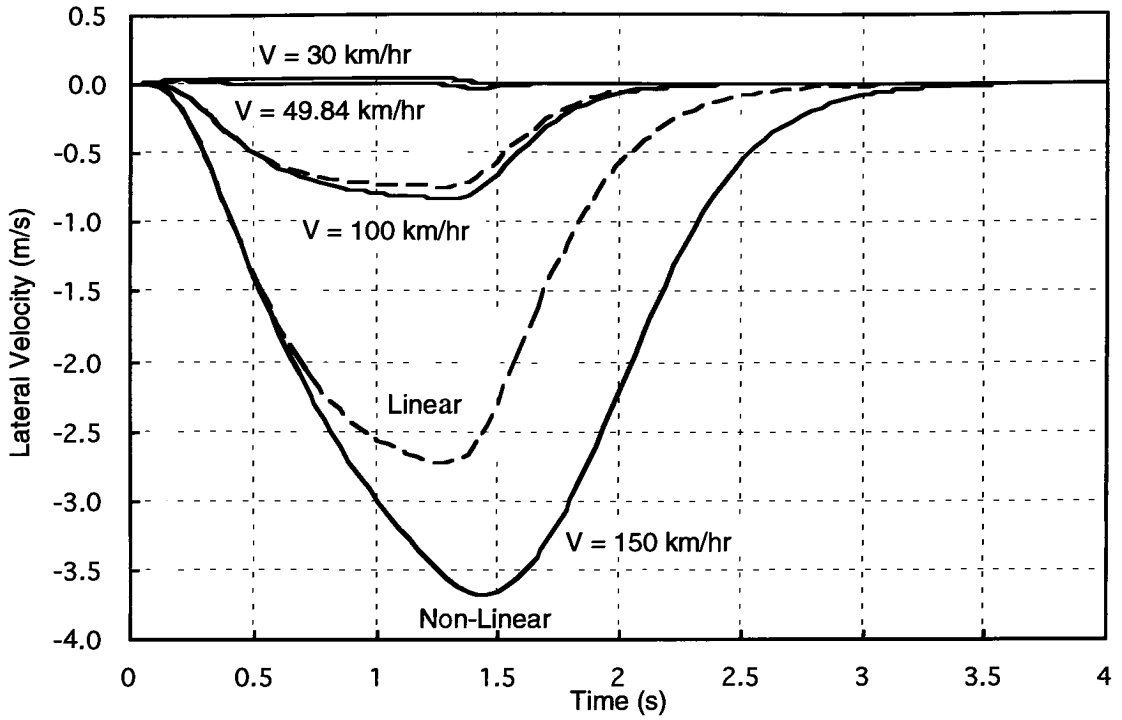

Figure 4.58: Non-Linear Ramp Square Steer Lateral Velocity Response

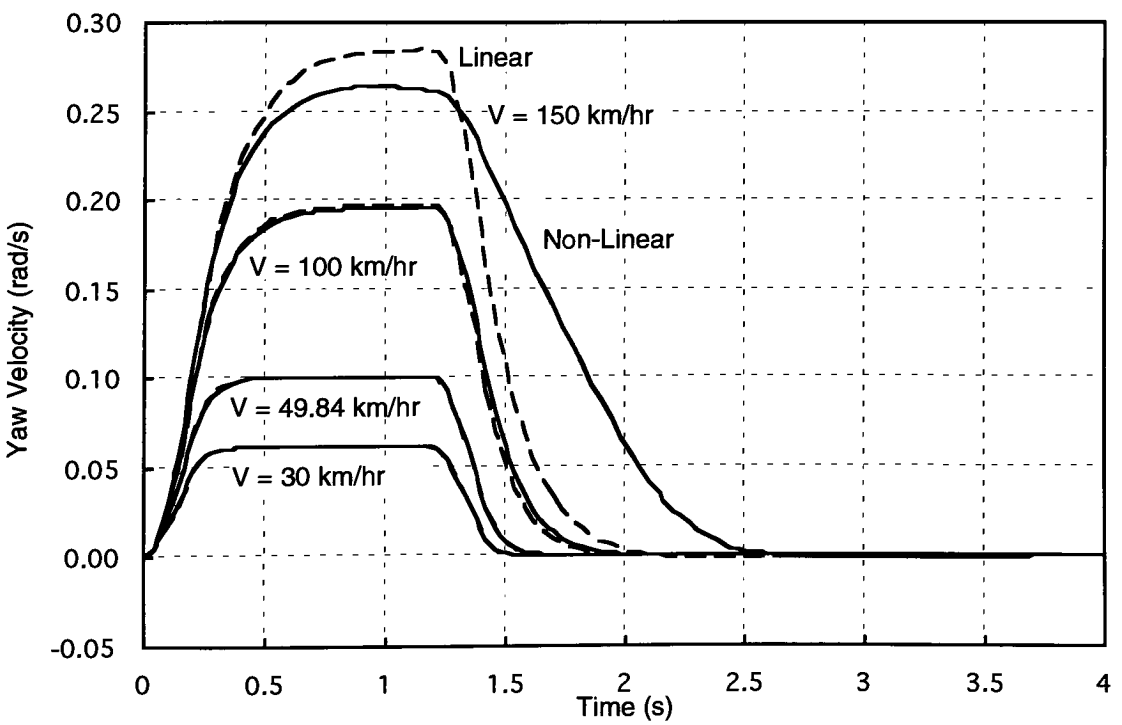

Figure 4.59: Non-Linear Ramp Square Steer Yaw Velocity Response

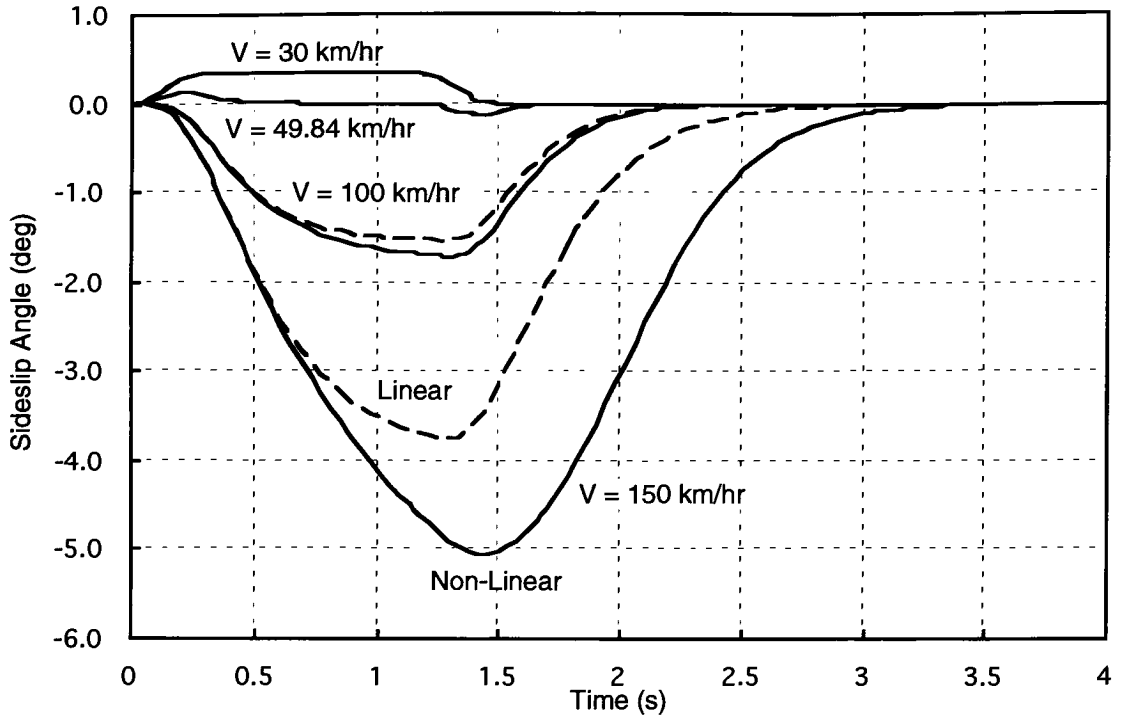

Figure 4.60: Non-Linear Ramp Square Steer Sideslip Angle Response

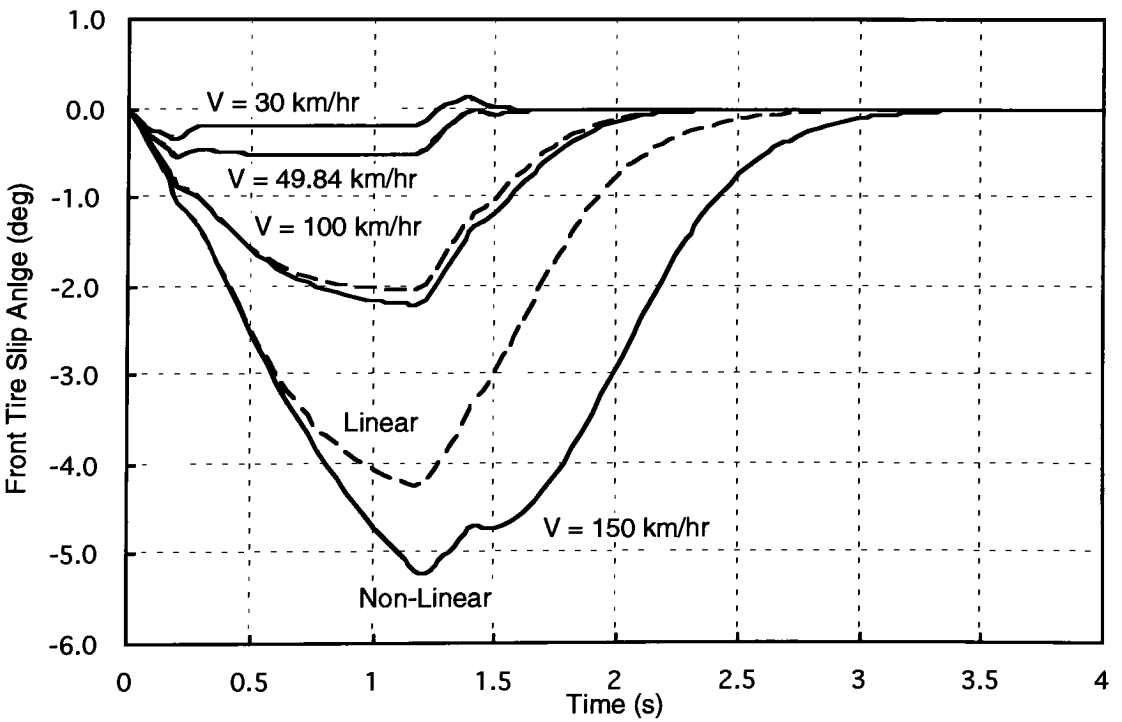

Figure 4.61: Non-Linear Ramp Square Steer Front Tire Slip Angle Response

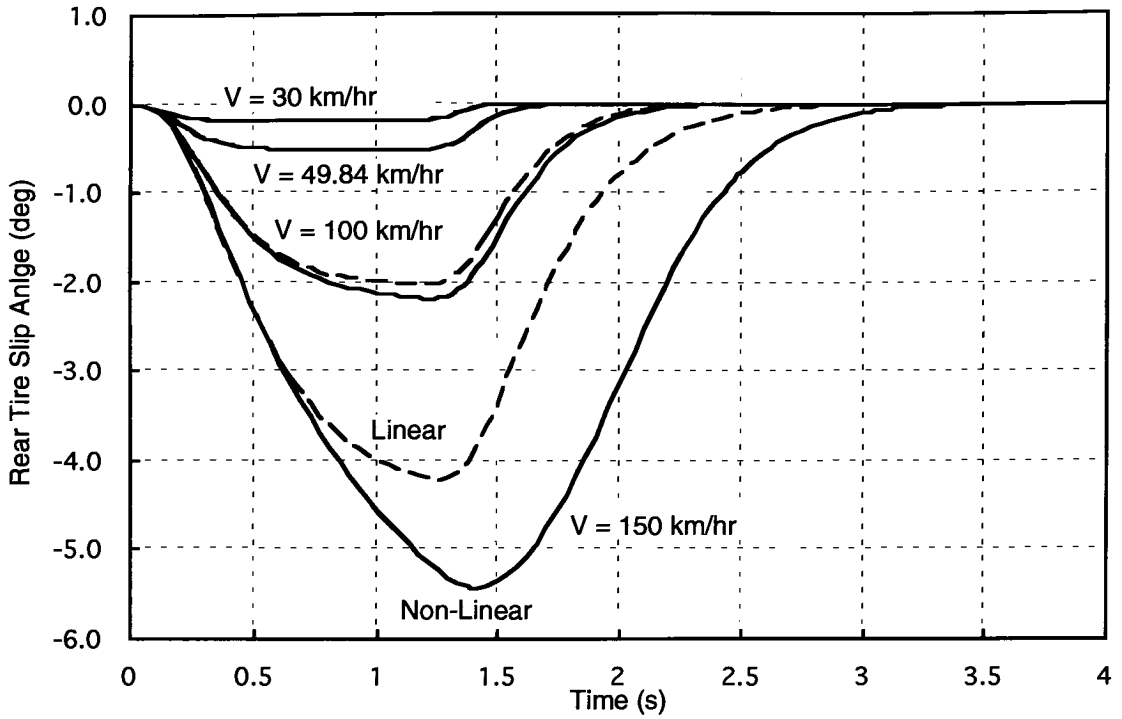

Figure 4.62: Non-Linear Ramp Square Steer Rear Tire Slip Angle Response

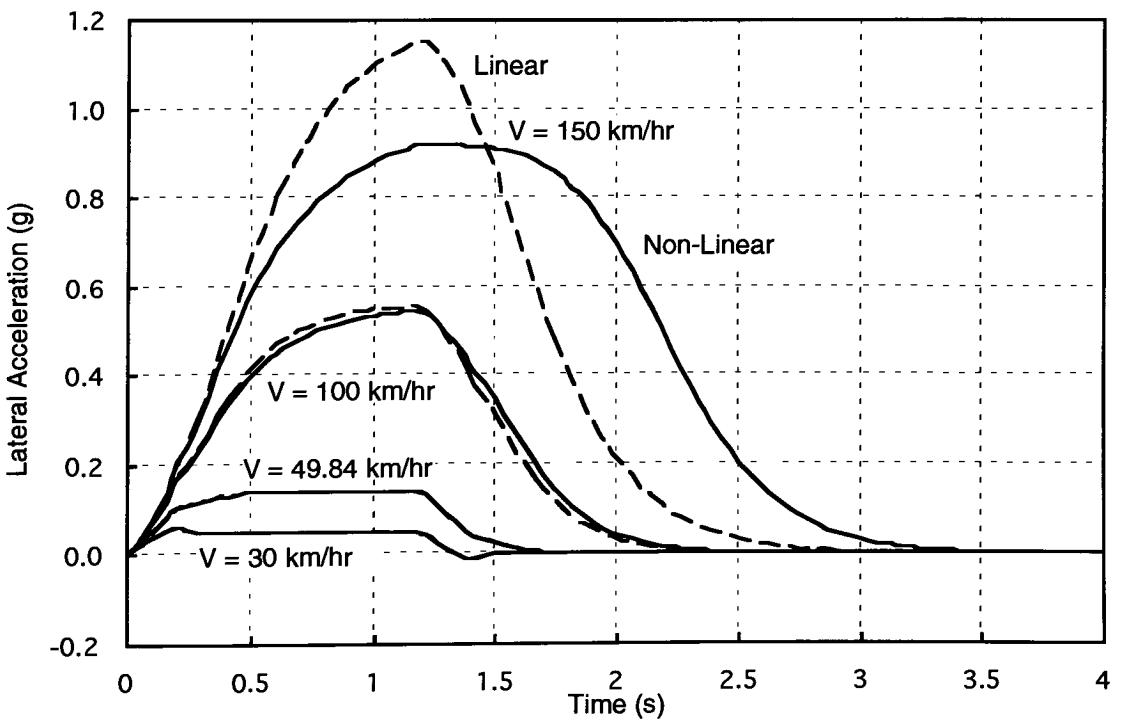

Figure 4.63: Non-Linear Ramp Square Steer Lateral Acceleration Response

5 Conclusion

In the early part of this century as the top speeds of automobiles increased vehicle dynamics became an important consideration for engineers. Manufacturers had to meet higher and higher standards of performance, particularly in the areas of safety and comfort. Mathematical modeling of vehicle dynamics has become an excellent way for engineers to study vehicle behavior and to reduce the time and cost to develop vehicles which meet performance goals. There is a great deal of literature on the topic of vehicle dynamics. Lateral vehicle dynamics in particular has been a topic of great interest due to its relationship with safety. Two areas of focus in the literature concerning the modeling of lateral dynamics have been the two degree-of-freedom vehicle model and models of tire behavior. Since tires play an extremely important role in the lateral dynamics of road vehicles, sufficiently accurate representation of tire mechanics is essential for vehicle models.

In Chapter 3 an overview of tire lateral force mechanics was given. Two representations of tire lateral forces were used. In the linear tire model the lateral force was considered to be a linear function of the tire slip angle. The non-linear tire model utilized a method called tire data nondimensionalization to predict lateral force. In this method experimentally measured tire lateral force versus slip angle curves for several vertical loads are normalized and curve fit. Tire lateral force can then be predicted as a non-linear function of both vertical load and slip angle.

In Chapter 4 the equations of motion for a two degree-of-freedom vehicle model were derived from basic principles of Newtonian mechanics. The model was then developed in two forms, linear and non-linear. The linear vehicle model utilized the linear tire model. Transfer functions were written relating both yaw velocity and sideslip angle to the inputs of steering, aerodynamic side force, and road side slope angle. Expressions for

steady-state step input response gains were derived from the transfer functions. Several other measures of steady-state stability were derived including the understeer gradient and tangent speed. Expressions for transient response characteristics such as natural frequency, damping ratio, and poles and zeros were developed. Numerical simulation of the response of the model to step steer, ramp-step steer, ramp-square steer, sine steer, step aerodynamic side force, and step road side slope inputs was performed. It was seen that the steady-state and transient response characteristics of the vehicle were very dependent upon its forward speed. In particular, when the forward speed was above the tangent speed of the vehicle, the zero associated with sideslip angle response to steer input became positive. The effect of this on the vehicle was seen clearly in the frequency response and in the simulation. For some combinations of speed and input magnitude the linear model predicted lateral accelerations higher than were actually possible due to the assumption of linear tire behavior. In all cases tested the steady-state response gains, frequency response, and simulation results were in agreement.

The non-linear vehicle model used a the non-linear tire model for predicting tire lateral forces during simulation. This model was seen to predict reasonable responses at high slip angles and lateral accelerations. Comparison with the linear model showed that for the vehicle studied the linear model was reasonably accurate for most engineering purposes up to slip angles of 2° and lateral accelerations of 0.5g. It was seen that for accurate modeling of vehicle response at high slip angles and lateral accelerations a non-linear representation of the tires was necessary.

References

1. Gillespie, Thomas D. *Fundamentals of Vehicle Dynamics.* Warrendale, PA: SAE, 1992.

2. Lanchester, F. William. "Some Reflections Peculiar to the Design of an Automobile." *Proceedings of the Institution of Mechanical Engineers,* Vol. 2, 1908, p. 187-257.

3. Olley, Maurice. "Suspension and Handling." Detroit, MI: Chevrolet Engineering Center, 1937.

4. Olley, Maurice. "Notes on Suspensions." Detroit, MI: Chevrolet Engineering Center, 1961.

5. Olley, Maurice. "Suspensions Notes II." Detroit, MI: Chevrolet Engineering Center, 1966.

6. Segal, Leonard. "Theoretical Prediction and Experimental Substantiation of the Response of the Automobile to Steering Control." *Proceedings of the Automobile Division of the Institution of Mechanical Engineers,* 1956-1957.

7. Whitcomb, David W. and William F. Milliken. "Design Implications of a General Theory of Automobile Stability and Control." *Proceedings of the Automobile Division of the Institution of Mechanical Engineers,* 1956-1957.

8. Bastow, D. and G. Howard. *Car Suspension and Handling.* Warrendale, PA: SAE, 1993.

9. Cole, D.E. *Elementary Vehicle Dynamics.* Ann Arbor, MI: University of Michigan, 1972.

10. Dixon, John C. *Tyres, Suspension and Handling,* Cambridge, England: Cambridge University Press, 1991.

11. Ellis, John R. *Vehicle Dynamics.* London: Business Books, 1969.

12. Ellis, John R. *Road Vehicle Dynamics,* Akron, OH: J.R. Ellis, 1989.

13. Milliken, William F. and Doug L. Milliken. *Race Car Vehicle Dynamics.* Warrendale, PA: SAE, 1995.

14. Mola, Simone. *Fundamentals of Vehicle Dynamics,* Detroit, MI: General Motors Institute, 1969.

15. Reimpell, Jornsen and Helmut Stoll. *The Automotive Chassis: Engineering Principles.* Warrendale, PA: SAE, 1996.

16. Taborek, Jaroslav J. *Mechanics of Vehicles.* Cleveland, OH: Penton, 1957.

17. Wong, Jo Yung. *Theory of Ground Vehicles* . New York: John Wiley & Sons, Inc., 1993.

18. Bundorf, R.T. and R.L. Leffert. "The Cornering Compliance Concept for Description of Vehicle Directional Control Properties." SAE Paper No. 760713, Oct. 1976.

19. Allen, R. Wade, Theodore J. Rosenthal, and Henry T. Szostak. "Steady State and Transient Analysis of Ground Vehicle Handling." SAE Paper No. 870495, 1987.

20. Heydinger, Gary J. "Improved Simulation and Validation of Road Vehicle Handling Dynamics." Ph.D. Dissertation, Ohio State University, Columbus, Ohio, 1990.

21. Xia, Xunmao. "A Nonlinear Analysis of Closed Loop Driver/Vehicle Performance with Four Wheel Steering Control." Ph.D. Dissertation, Department of Mechanical Engineering, Clemson University, Clemson, SC, Dec. 1990.

22. Trom, J.D., J.L. Lopex, and M.J. Vanderploeg. "Modeling of a Mid-Size Passenger Car Using a Multibody Dynamics Program." *Transactions of the ASME, Journal of Mechanisms, Transmissions, and Automation in Design*, Vol. 109, Dec. 1987.

23. Kortum, W. and W. Schiehlen. "General Purpose Vehicle System Dynamics Software Based on Multibody Formalisms." *Vehicle System Dynamics,* No. 14, 1985, p. 229-263.

24. Clarke, S.K. (Ed.). *Mechanics of Pneumatic Tires,* DOT HS-805952, US Government Printing Office, Washington, DC, 1981.

25. Gim, Gwanghun and Parviz E. Nikravesh. "An Analytical Model of Pneumatic Tyres for Vehicle Dynamic Simulations. Part 1: Pure Slips." *International Journal of Vehicle Design,* Vol. 11, No. 6, 1990.

26. Bakker, Egbert, Lars Nyborg, and Hans B. Pacejka. "Tyre Modelling for Use in Vehicle Dynamics Studies." SAE Paper No. 870421, 1987.

27. Radt, Hugo S. and D.A. Glemming. "Normalization of Tire Force and Moment Data." *Tire Science and Technology,* Vol. 21, No. 2, Apr.-June 1993.

28. Allen, R. Wade, Raymond E. Magdaleno, Theodore J. Rosenthal, David H. Klyde, and Jeffrey R. Hogue. "Tire Modeling Requirements for Vehicle Dynamics Simulation." SAE Paper No. 950312, Feb. 1995.

29. Society of Automotive Engineers. "Vehicle Dynamics Terminology." SAE J670e, 1976.

30. Radt, Hugo S. "An Efficient Method for Treating Race Tire Force-Moment Data." SAE Paper No. 942536, Dec. 1994.

31. Meriam, James L. and L. Glenn Kraige. *Engineering Mechanics: Dynamics.* New York: John Wiley & Sons, 1992.

32. Katz, Joseph. *Race Car Aerodynamics: Designing for Speed.* Cambridge, Massachusetts: Robert Bentley, Inc., 1995.

33. Franklin, Gene F., J. David Powell, and Abbas Emami-Naeini. *Feedback Control of Dynamic Systems.* New York: Addison-Wesley Publishing Company, Inc., 1994.

34. *MATLAB Reference Guide.* The MathWorks, Inc., 1994.

Appendix A Tire Model MATLAB Programs

A.1 MagicFit.m

```
%MagicFit      Curve Fitting of Tire Data to Magic Formula
%
%      Finds parameters for Magic Formula curve fit of tire lateral force or
%      aligning moment vs. slip angle data read from file TireSlip.dat
%
% Created 4/21/96
% J. Kiefer

% Initialization
clear all;
clc;

% Load Data from File
load TireSlip.dat
t = TireSlip(:,1);
y = TireSlip(:,2);

% Find Curve Fit Parameters
x0 = [.7407 1.35 1.00 -0.5];
x = leastsq('MagicError', x0, [], [], t, y)

% Construct Fit Function
t1 = linspace(0,max(t),10);
psi = (1-x(4))*t1 + x(4)/x(1)*atan(x(1)*t1);
theta = x(2)*atan(x(1)*psi);
F = x(3)*sin(theta);

% Plot Data and Fit Function
plot(t1, F, t, y, 'o')
title(['Tire Data Magic Formula Fit (B=' num2str(x(1)) ', C=' num2str(x(2))...
        ', D=' num2str(x(3)) ', E=' num2str(x(4)) ')'])
xlabel('t')
ylabel('y')
grid
```

A.2 MagicError.m

```
function e = MagicError(x, t, y)
%MagicError          Error in Magic Formula Curve Fit
%
%e = MagicError(x, t, y)
%
%       Calculates vector of errors of Magic Formula curve fit given parameters
%       x and data (t, y)
%
%       Inputs:
%             x                     Vector of curve fit parameters
%                   x(1)    B
%                   x(2)    C
%                   x(3)    D
%                   x(4)    E
%             t                     Vector of independent data
%             y                     Vector of dependent data
%       Outputs:
%             e                     Vector of errors between data and fit function
%
%       Created 4/21/96
%       J. Kiefer

psi = (1-x(4))*t + x(4)/x(1)*atan(x(1)*t);
theta = x(2)*atan(x(1)*psi);
F = x(3)*sin(theta);

e = y - F;
```

A.3 NLTire.m

```
function Fy = NLTire(Fz, alpha)
%NLTire        Non Linear Tire Model Lateral Force
%
%Fy = NLTire(Fz, alpha)
%
%       Calculates tire lateral force from inputs of tire vertical load and slip
%       angle.  Based on Radt's tire data nondimensionalization model and the
%       Magic Formula model.  Force is for one tire.  Called by the function
%       DOF2NLDE.m.
%
%       Inputs:
%              alpha                Tire slip angle (rad)
%              Fz                   Tire vertical load (N)
%       Outputs:
%              Fy                   Tire lateral force (N)
%
%       Created 2/18/96
%       J. Kiefer

global B1 C1 D1 E1 B3 C3 B5 C5;

% Normalization Parameters
Cc = B3 + C3*Fz;                                    % N/deg/N      Cornering coefficient
mu = B5 + C5*Fz;                                    % N/N          Friction coefficient

% Normalized Slip Angle
alphaN = Cc.*tan(alpha)./mu*180/pi;

% Normalized Lateral Force
psiFN = (1-E1)*alphaN + E1/B1*atan(B1*alphaN);
thetaFN = C1*atan(B1*psiFN);
FyN = D1*sin(thetaFN);

% Lateral Force
Fy = -FyN.*mu.*Fz;
```

Appendix B Two DOF Model Mathematica Session

Stability Derivatives

```
SDRules = {Yb -> Cf + Cr, Yr -> (a Cf - b Cr)/V,
           Yd -> -Cf, Nb -> a Cf - b Cr, Nr -> (a^2 Cf +
           b^2 Cr)/V, Nd -> -a Cf}
```

```
                          a Cf - b Cr
{Yb -> Cf + Cr, Yr -> -----------, Yd -> -Cf, Nb -> a Cf - b Cr,
                             V

          2       2
         a  Cf + b  Cr
  Nr -> -------------, Nd -> -(a Cf)}
               V
```

Transformed Equations of Motion

```
A = {{s-Yb/(m V), 1-Yr/(m V)},
     {-Nb/Izz,  s-Nr/Izz}};
MatrixForm[A]
```

```
      Yb          Yr
  s - ---     1 - ---
      m V         m V

    Nb          Nr
  -(---)      -(---) + s
    Izz         Izz
```

```
B1 = {Yd/(m V), Nd/Izz};
MatrixForm[B1]
```

```
  Yd
  ---
  m V

  Nd
  ---
  Izz
```

```
B2 = {1/(m V), (a-c)/Izz};
MatrixForm[B2]
```

```
   1
  ---
  m V

  a - c
  -----
   Izz
```

```
B3 = {g/V, 0};
MatrixForm[B3]
```

$$\begin{pmatrix} \frac{g}{V} \\ 0 \end{pmatrix}$$

```
B4 = {1/(m V), (a-d)/Izz};
MatrixForm[B4]
```

$$\begin{pmatrix} \frac{1}{m\,V} \\ \frac{a-d}{Izz} \end{pmatrix}$$

Transfer Function Denominator

```
Ds = Collect[Det[A],s]
```

$$\frac{Nb}{Izz} + s + \frac{Nr\ Yb}{Izz\ m\ V} + s\left(-\left(\frac{Nr}{Izz}\right) - \frac{Yb}{m\ V}\right) - \frac{Nb\ Yr}{Izz\ m\ V}$$

Transfer Function Numerators

```
Nbd =
Collect[Det[Transpose[ReplacePart[Transpose[A],B1,1]]],s]
```

$$-\left(\frac{Nd}{Izz}\right) - \frac{Nr\ Yd}{Izz\ m\ V} + \frac{s\ Yd}{m\ V} + \frac{Nd\ Yr}{Izz\ m\ V}$$

```
Nba = Collect[Det[Transpose[ReplacePart[
      Transpose[A],B2,1]]],s]
```

$$-\left(\frac{a}{Izz}\right) + \frac{c}{Izz} - \frac{Nr}{Izz\ m\ V} + \frac{s}{m\ V} + \frac{a\ Yr}{Izz\ m\ V} - \frac{c\ Yr}{Izz\ m\ V}$$

```
Nbt = Collect[Det[Transpose[ReplacePart[
      Transpose[A],B3,1]]],s]
```

$$-\left(\frac{g\ Nr}{Izz\ V}\right) + \frac{g\ s}{V}$$

```
Nrd = Collect[Det[Transpose[ReplacePart[
      Transpose[A],B1,2]]],s]
```

$$\frac{Nd\ s}{Izz} - \frac{Nd\ Yb}{Izz\ m\ V} + \frac{Nb\ Yd}{Izz\ m\ V}$$

```
Nra = Collect[Det[Transpose[ReplacePart[
      Transpose[A],B2,2]]],s]
```

$$\left(\frac{a}{Izz} - \frac{c}{Izz}\right) s + \frac{Nb}{Izz\ m\ V} - \frac{a\ Yb}{Izz\ m\ V} + \frac{c\ Yb}{Izz\ m\ V}$$

```
Nrt = Collect[Det[Transpose[ReplacePart[
      Transpose[A],B3,2]]],s]
```

$$\frac{g\ Nb}{Izz\ V}$$

```
Nrn = Collect[Det[Transpose[ReplacePart[
      Transpose[A],B4,2]]],s]
```

$$\left(\frac{a}{Izz} - \frac{d}{Izz}\right) s + \frac{Nb}{Izz\ m\ V} - \frac{a\ Yb}{Izz\ m\ V} + \frac{d\ Yb}{Izz\ m\ V}$$

Transfer Functions

Sideslip Angle

```
Gbd = Nbd/Ds
```

$$\frac{-\left(\frac{Nd}{Izz}\right) - \frac{Nr\ Yd}{Izz\ m\ V} + \frac{s\ Yd}{m\ V} + \frac{Nd\ Yr}{Izz\ m\ V}}{\frac{Nb}{Izz} + s + \frac{Nr\ Yb}{Izz\ m\ V} + s\left(-\left(\frac{Nr}{Izz}\right) - \frac{Yb}{m\ V}\right) - \frac{Nb\ Yr}{Izz\ m\ V}}$$

```
Gba = Nba/Ds
```

$$\frac{-\left(\frac{a}{Izz}\right) + \frac{c}{Izz} - \frac{Nr}{Izz\ m\ V} + \frac{s}{m\ V} + \frac{a\ Yr}{Izz\ m\ V} - \frac{c\ Yr}{Izz\ m\ V}}{\frac{Nb}{Izz} + s + \frac{Nr\ Yb}{Izz\ m\ V} + s\left(-\left(\frac{Nr}{Izz}\right) - \frac{Yb}{m\ V}\right) - \frac{Nb\ Yr}{Izz\ m\ V}}$$

Gbt = Nbt/Ds

$$\frac{\frac{g\,Nr}{Izz\,V} + \frac{g\,s}{V}}{\frac{Nb}{Izz} + s\left(\frac{2}{Izz} + \frac{Nr\,Yb}{Izz\,m\,V}\right) + \frac{Nr}{Izz} + \frac{Yb}{m\,V} + s\left(\frac{Nb\,Yr}{Izz\,m\,V}\right)}$$

Yaw Velocity

Grd = Nrd/Ds

$$\frac{\frac{Nd\,s}{Izz} - \frac{Nd\,Yb}{Izz\,m\,V} + \frac{Nb\,Yd}{Izz\,m\,V}}{\frac{Nb}{Izz} + s\left(\frac{2}{Izz} + \frac{Nr\,Yb}{Izz\,m\,V}\right) + \frac{Nr}{Izz} + \frac{Yb}{m\,V} + s\left(\frac{Nb\,Yr}{Izz\,m\,V}\right)}$$

Gra = Nra/Ds

$$\frac{\left(\frac{a}{Izz} - \frac{c}{Izz}\right)s + \frac{Nb}{Izz\,m\,V} - \frac{a\,Yb}{Izz\,m\,V} + \frac{c\,Yb}{Izz\,m\,V}}{\frac{Nb}{Izz} + s\left(\frac{2}{Izz} + \frac{Nr\,Yb}{Izz\,m\,V}\right) + \frac{Nr}{Izz} + \frac{Yb}{m\,V} + s\left(\frac{Nb\,Yr}{Izz\,m\,V}\right)}$$

Grt = Nrt/Ds

$$\frac{g\,Nb}{Izz\,V\left(\frac{Nb}{Izz} + s\left(\frac{2}{Izz} + \frac{Nr\,Yb}{Izz\,m\,V}\right) + \frac{Nr}{Izz} + \frac{Yb}{m\,V} + s\left(\frac{Nb\,Yr}{Izz\,m\,V}\right)\right)}$$

Grn = Nrn/Ds

$$\frac{\left(\frac{a}{Izz} - \frac{d}{Izz}\right)s + \frac{Nb}{Izz\,m\,V} - \frac{a\,Yb}{Izz\,m\,V} + \frac{d\,Yb}{Izz\,m\,V}}{\frac{Nb}{Izz} + s\left(\frac{2}{Izz} + \frac{Nr\,Yb}{Izz\,m\,V}\right) + \frac{Nr}{Izz} + \frac{Yb}{m\,V} + s\left(\frac{Nb\,Yr}{Izz\,m\,V}\right)}$$

Steady State Step-Input Response Gains

Sideslip Angle

```
Sbd = Simplify[Limit[Gbd, s->0]]

   -(m Nd V) - Nr Yd + Nd Yr
   -------------------------
    m Nb V + Nr Yb - Nb Yr

Sba = Simplify[Limit[Gba, s->0]]

   -Nr - a m V + c m V + a Yr - c Yr
   ---------------------------------
        m Nb V + Nr Yb - Nb Yr

Sbt = Simplify[Limit[Gbt, s->0]]

              g m Nr
   -(----------------------)
     m Nb V + Nr Yb - Nb Yr
```

Yaw Velocity

```
Srd = Simplify[Limit[Grd, s->0]]

      -(Nd Yb) + Nb Yd
   ----------------------
   m Nb V + Nr Yb - Nb Yr

Sra = Simplify[Limit[Gra, s->0]]

      Nb - a Yb + c Yb
   ----------------------
   m Nb V + Nr Yb - Nb Yr

Srt = Simplify[Limit[Grt, s->0]]

           g m Nb
   ----------------------
   m Nb V + Nr Yb - Nb Yr

Srn = Simplify[Limit[Grn, s->0]]

      Nb - a Yb + d Yb
   ----------------------
   m Nb V + Nr Yb - Nb Yr
```

Front Tire Slip Angle

```
Safd = Simplify[Sbd + a/V Srd - 1]

          2          2
   (m Nb V  + m Nd V  + a Nd Yb + Nr V Yb - a Nb Yd + Nr V Yd -

       Nb V Yr - Nd V Yr) / (V (-(m Nb V) - Nr Yb + Nb Yr))
```

```
Safa = Simplify[Sba + a/V Sra]

                                2         2    2
   (-(a Nb) + Nr V + a m V  - c m V  + a  Yb - a c Yb - a V Yr +

       c V Yr) / (V (-(m Nb V) - Nr Yb + Nb Yr))

Saft = Simplify[Sbt + a/V Srt]

       g m (a Nb - Nr V)
   --------------------------
   V (m Nb V + Nr Yb - Nb Yr)
```

Rear Tire Slip Angle

```
Sard = Simplify[Sbd - b/V Srd]

         2
   m Nd V  - b Nd Yb + b Nb Yd + Nr V Yd - Nd V Yr
   -----------------------------------------------
            V (-(m Nb V) - Nr Yb + Nb Yr)

Sara = Simplify[Sba - b/V Sra]

                          2         2
   (b Nb + Nr V + a m V  - c m V  - a b Yb + b c Yb - a V Yr +

       c V Yr) / (V (-(m Nb V) - Nr Yb + Nb Yr))

Sart = Simplify[Sbt - b/V Srt]

         g m (b Nb + Nr V)
   -----------------------------
   V (-(m Nb V) - Nr Yb + Nb Yr)
```

Path Curvature

```
Scd = Simplify[1/V Srd]

       -(Nd Yb) + Nb Yd
   --------------------------
   V (m Nb V + Nr Yb - Nb Yr)

Sca = Simplify[1/V Sra]

       Nb - a Yb + c Yb
   --------------------------
   V (m Nb V + Nr Yb - Nb Yr)

Sct = Simplify[1/V Srt]

             g m Nb
   --------------------------
   V (m Nb V + Nr Yb - Nb Yr)
```

Lateral Acceleration

```
SAd = Simplify[V/g Srd]
```

```
      V (-(Nd Yb) + Nb Yd)
   ---------------------------
   g (m Nb V + Nr Yb - Nb Yr)
```

```
SAa = Simplify[V/g Sra]
```

```
      V (Nb - a Yb + c Yb)
   ---------------------------
   g (m Nb V + Nr Yb - Nb Yr)
```

```
SAt = Simplify[V/g Srt]
```

```
            m Nb V
   ----------------------
   m Nb V + Nr Yb - Nb Yr
```

Steer Angle Response to Path Radius

```
deltaR = delta /. Solve[Scd == 1/R / delta,delta][[1,1]]
```

```
                2
     -(m Nb V ) - Nr V Yb + Nb V Yr
   -(-------------------------------)
          -(Nd R Yb) + Nb R Yd
```

```
Term1 = Coefficient[Expand[deltaR],V,2] V^2
```

```
                2
         m Nb V
   --------------------
   -(Nd R Yb) + Nb R Yd
```

```
Term1S = Simplify[Term1 /. SDRules]
```

```
                      2
    (a Cf - b Cr) m V
   ---------------------
   a Cf Cr R + b Cf Cr R
```

```
Term1Sa = Numerator[Term1S] / Simplify[Denominator[
           Term1S] /. a->L-b]
```

```
                     2
   (a Cf - b Cr) m V
   -----------------
       Cf Cr L R
```

```
Terms23  =  ExpandNumerator[Simplify[Coefficient[Expand[
            deltaR],V]  V]]
```

$$\frac{-(Nr\ V\ Yb) + Nb\ V\ Yr}{Nd\ R\ Yb - Nb\ R\ Yd}$$

```
Terms23S  =  Simplify[Terms23  /.  SDRules  /.  a->L-b]
```

$$\frac{L}{R}$$

```
deltaR1  =  Term1  +  Terms23S
```

$$\frac{L}{R} + \frac{m\ Nb\ V^2}{-(Nd\ R\ Yb) + Nb\ R\ Yd}$$

```
deltaR2  =  Term1Sa  +  Terms23S
```

$$\frac{L}{R} + \frac{(a\ Cf - b\ Cr)\ m\ V^2}{Cf\ Cr\ L\ R}$$

Understeer Gradient

```
Kus  =  Coefficient[Simplify[deltaR1  R  g],V^2]
```

$$\frac{g\ m\ Nb}{-(Nd\ Yb) + Nb\ Yd}$$

```
Kus1  =  Simplify[Kus  /.  SDRules]
```

$$\frac{(a\ Cf - b\ Cr)\ g\ m}{(a + b)\ Cf\ Cr}$$

Stability Factor

```
K1  =  Simplify[K  /.  Solve[Srd  ==  V/(L  (1+K  V^2)),  K][[1]]]
```

$$\frac{m\ Nb\ V^2 + L\ Nd\ Yb + Nr\ V\ Yb - L\ Nb\ Yd - Nb\ V\ Yr}{L\ V^2\ (-(Nd\ Yb) + Nb\ Yd)}$$

```
K2 = Simplify[Numerator[K1] - Coefficient[Numerator[K1],
     V^2] V^2 /. SDRules /. a->L-b] + Coefficient[
     Numerator[K1], V^2] V^2 / Denominator[K1]
```

$$\frac{m\ Nb}{L\ (-(Nd\ Yb) + Nb\ Yd)}$$

```
K3 = Simplify[K2 /. SDRules]
```

$$\frac{(a\ Cf - b\ Cr)\ m}{a\ Cf\ Cr\ L + b\ Cf\ Cr\ L}$$

```
K4 = Numerator[K3]/Simplify[(Denominator[K3] /.
     a -> L - b)]
```

$$\frac{(a\ Cf - b\ Cr)\ m}{Cf\ Cr\ L^2}$$

Neutral Steer Point

```
d1 = Simplify[d /. Solve[Numerator[Srn] == 0, d][[1]]]
```

$$a - \frac{Nb}{Yb}$$

```
d2 = Simplify[d1 /. SDRules]
```

$$\frac{(a + b)\ Cr}{Cf + Cr}$$

```
d3 = Simplify[d2 /. a -> L - b]
```

$$\frac{Cr\ L}{Cf + Cr}$$

Static Margin

```
SM = (d1 - a)/L
```

$$-\left(\frac{Nb}{L\ Yb}\right)$$

```
SM1 = Simplify[SM /. SDRules]
```

$$\frac{-(a\ Cf) + b\ Cr}{Cf\ L + Cr\ L}$$

Tangent Speed

```
Vtan = V /. Solve[Sbd deltaR == 0,V][[2,1]]
```

```
     Nr Yd - Nd Yr
   -(-------------)
         m Nd
```

```
Vtan1 = Sqrt[Simplify[Expand[(V /. Solve[V == Simplify[
          Vtan /. SDRules],V][[2,1]])^2]]]
```

```
          b (a + b) Cr
   Sqrt[-(------------)]
              a m
```

```
Vtan2 = Sqrt[Simplify[Numerator[Vtan1^2] /. a -> L-b]/
          Denominator[Vtan1^2]]
```

```
          b Cr L
   Sqrt[-(------)]
           a m
```

Critical Speed

```
Vcrit = V /. Solve[Denominator[Srd] == 0,V][[1]]
```

```
     Nr Yb - Nb Yr
   -(-------------)
         m Nb
```

```
Vcrit1 = Sqrt[Simplify[(V /. Solve[V == Vcrit /.
          SDRules,V][[2,1]])^2]]
```

```
                  2
          (a + b)  Cf Cr
   Sqrt[------------------]
        -(a Cf m) + b Cr m
```

```
Vcrit2 = Sqrt[Simplify[Numerator[Vcrit1^2] /. a -> L-b]/
          Denominator[Vcrit1^2]]
```

```
                    2
             Cf Cr L
   Sqrt[------------------]
        -(a Cf m) + b Cr m
```

Characteristic Speed

```
Vchar = V /. Solve[deltaR == 2 L/R,V][[2,1]]
```

```
   (-(Nr Yb) + Nb Yr + Sqrt[-4 L m Nb (2 Nd Yb - 2 Nb Yd) +

                          2
         (Nr Yb - Nb Yr) ]) / (2 m Nb)
```

```
Vchar1 = Sqrt[Simplify[(V /. Solve[V == Vchar /.
          SDRules,V][[2,1]])^2]]
```

$$\sqrt{\frac{(a+b)\,Cf\,Cr\,(a+b-2L)}{-(a\,Cf\,m)+b\,Cr\,m}}$$

```
Vchar2 = Sqrt[Simplify[Numerator[Vchar1^2] /. a -> L-b]/
          Denominator[Vchar1^2]]
```

$$\sqrt{-\frac{2\,Cf\,Cr\,L}{-(a\,Cf\,m)+b\,Cr\,m}}$$

Yaw Radius of Gyration

```
kz = Sqrt[Izz/m]
```

$$\sqrt{\frac{Izz}{m}}$$

Geometry to Inertia Ratio

```
GIR = L^2/kz^2
```

$$\frac{L^2\,m}{Izz}$$

Total Cornering Factor

```
TCF = Cf Cr/m^2
```

$$\frac{Cf\,Cr}{m^2}$$

Characteristic Equation

```
Ds == 0
```

$$\frac{Nb}{Izz} + s + \frac{Nr\,Yb}{Izz\,m\,V} + s\left(-\left(\frac{Nr}{Izz}\right) - \frac{Yb}{m\,V}\right) - \frac{Nb\,Yr}{Izz\,m\,V} == 0$$

```
a2 = Coefficient[Ds,s^2]
```

$$1$$

```
a1 = Coefficient[Ds,s]
```

```
     Nr      Yb
  -(---) - ---
     Izz     m V
```

```
a0 = Ds - a2 s^2 - a1 s
```

```
   Nb      Nr Yb      Nb Yr
  --- + ------- - -------
  Izz    Izz m V    Izz m V
```

Undamped Natural Frequency

```
wn = Simplify[Sqrt[a0]]
```

```
          m Nb V + Nr Yb - Nb Yr
  Sqrt[----------------------]
                 Izz m V
```

```
wn1 = Simplify[wn /. SDRules]
```

```
          2                          2                  2           2
         a  Cf Cr + 2 a b Cf Cr + b  Cf Cr + a Cf m V  - b Cr m V
  Sqrt[-------------------------------------------------------------]
                                     2
                                Izz m V
```

Damping Ratio

```
zeta = Simplify[a1 Izz m V/(2 Sqrt[wn^2 (Izz m V)^2])]
```

```
                -(m Nr V + Izz Yb)
  ----------------------------------------
  2 Sqrt[Izz m V (m Nb V + Nr Yb - Nb Yr)]
```

```
zeta1 = Simplify[zeta /. SDRules]
```

```
                          2         2
  -(Cf Izz + Cr Izz + a  Cf m + b  Cr m) /

                      2                          2                  2
    (2 Sqrt[Izz m (a  Cf Cr + 2 a b Cf Cr + b  Cf Cr + a Cf m V  -

                   2
          b Cr m V )])
```

Poles

```
poles = Solve[Ds==0,s];
s1 = s /. poles[[1,1]]
```

```
                                                              2
   (m Nr V + Izz Yb - Sqrt[(-(m Nr V) - Izz Yb)  -

         4 Izz m V (m Nb V + Nr Yb - Nb Yr)]) / (2 Izz m V)
```

```
s1a = Simplify[s1 /. SDRules]
```

```
                        2       2
   ((Cf + Cr) Izz + (a  Cf + b  Cr) m -

                                    2          2       2
       Sqrt[(-(Cf Izz) - Cr Izz - a  Cf m - b  Cr m)  -

                  2                                 2                  2
        4 Izz m (a  Cf Cr + 2 a b Cf Cr + b  Cf Cr + a Cf m V  -

                   2
           b Cr m V )]) / (2 Izz m V)
```

```
s2 = s /. poles[[2,1]]
```

```
                                                              2
   (m Nr V + Izz Yb + Sqrt[(-(m Nr V) - Izz Yb)  -

         4 Izz m V (m Nb V + Nr Yb - Nb Yr)]) / (2 Izz m V)
```

```
s2a = Simplify[s2 /. SDRules]
```

```
                        2       2
   ((Cf + Cr) Izz + (a  Cf + b  Cr) m +

                                    2          2       2
       Sqrt[(-(Cf Izz) - Cr Izz - a  Cf m - b  Cr m)  -

                  2                                 2                  2
        4 Izz m (a  Cf Cr + 2 a b Cf Cr + b  Cf Cr + a Cf m V  -

                   2
           b Cr m V )]) / (2 Izz m V)
```

Zeros

```
Zbd = s /. Solve[Nbd == 0, s][[1,1]]
```

```
     -(m Nd V) - Nr Yd + Nd Yr
   -(-------------------------)
              Izz Yd
```

```
Zbd1 = Simplify[Zbd /. SDRules]
```

```
              2           2
   a b Cr + b  Cr + a m V
   ----------------------
            Izz V
```

```
Zba = s /. Solve[Nba == 0, s][[1,1]]
```

```
     -Nr - a m V + c m V + a Yr - c Yr
   -(---------------------------------)
                    Izz
```

```
Zba1 = Simplify[Zba /. SDRules]
```

```
                       2                      2        2
   a c Cf + a b Cr + b  Cr - b c Cr + a m V  - c m V
   -------------------------------------------------
                          Izz V
```

```
Zbt = s /. Solve[Nbt == 0, s][[1,1]]
```

```
   Nr
   ---
   Izz
```

```
Zbt1 = Simplify[Zbt /. SDRules]
```

```
    2       2
   a  Cf + b  Cr
   -------------
       Izz V
```

```
Zrd = s /. Solve[Nrd == 0, s][[1,1]]
```

```
     -(Nd Yb) + Nb Yd
   -(----------------)
          m Nd V
```

```
Zrd1 = Simplify[Zrd /. SDRules]
```

```
   (a + b) Cr
   ----------
     a m V
```

```
Zra = s /. Solve[Nra == 0, s][[1,1]]
```

```
     Nb - a Yb + c Yb
   -(----------------)
       (a - c) m V
```

```
Zra1 = Simplify[Zra /. SDRules]
```

```
   -(c Cf) + a Cr + b Cr - c Cr
   ----------------------------
          a m V - c m V
```

```
Zrt = Solve[Nrt == 0, s]
```

```
{{}}
```

Appendix C Two DOF Model MATLAB Programs

C.1 DOF2Control.m

```
%DOF2Control          2 DOF Model Execution Control
%
%      Controls execution of 2 DOF model.  Sets control input type (step, step
%      ramp, ramp step / ramp down, or sine steer).  Sets simulation parameters.
%
% Created 1/11/96
% J. Kiefer

% Control Input Type
step = 1;                          % Step steer
ramp = 2;                          % Ramp step steer
rampsquare = 3;                    % Ramp square steer
sine = 4;                          % Sine steer

input = 1;                         % Select which control input to use

% Simulation Parameters
t0 = 0.0;                          % s    Initial time for steer input
tr = 0.2;                          % s    Ramp time
td = 1.0;                          % s    Dwell time
ts = 1.0;                          % s    Period for sine steer
tf = 4.0;                          % s    Final time for simulation
tol = 1e-5;                        %      Simulation accuracy (default = 1e-3)
```

C.2 DOF2Param.m

```
%DOF2Param          2 DOF Model Independent Parameters and Simulation Control
%
%       Sets independendent vehicle, tire, control, and disturbance parameters
%       for 2 DOF model.
%
% Created 1/7/96
% J. Kiefer

% Initialization
clear all;
clc;
global m Izz L a b c u Cf Cr d0 Fzf Fzr Fyg Fya t0 tr td ts tf input;
global B1 C1 D1 E1 B3 C3 B5 C5;

% Constants
g = 9.81;                           % m/s^2       Acceleration due to gravity

% Vehicle Independent Parameters
m = 1775;                           % kg          Gross vehicle mass
Izz = 1960;                         % kg-m^2      Yaw inertia
f = 0.52;                           %             Fraction of weight on front axle
L = 2.372;                          % m           Wheelbase
u = 100;                            % km/hr       Vehicle forward speed

% Control and Disturbance Inputs
d0 = 1;                             % deg         Steer input magnitude
theta = 0;                          % deg         Side slope
Fya = 0;                            % N           Aerodynamic side force
c = 1.25;                           % m           Distance from front axle to
                                    %                   aerodynamic side force

% Linear Tire Model Parameters
Cf = -1230.5;                       % N/deg       Front cornering stiffness (one tire)
Cr = -1155.5;                       % N/deg       Rear cornering stiffness (one tire)

% Non Linear Tire Model Parameters
%       Normalized Lateral Force Magic Formula Parameters
B1 = 0.5835;
C1 = 1.7166;
D1 = 1.0005;
E1 = 0.2517;

%       Cornering Coefficient Parameters
B3 = 0.333;
C3 = -1.352e-5;

%       Friction Coefficient Parameters
B5 = 1.173;
C5 = -3.696e-5;


% Unit Conversions
u = u*1000/3600;            % m/s         Vehicle forward speed
```

```
d0 = d0*pi/180;                 % rad          Step steer input
Cf = Cf*180/pi*2;               % N/rad        Front tire cornering stiffness (two tires)
Cr = Cr*180/pi*2;               % N/rad        Rear tire cornering stiffness (two tires)
```

C.3 DOF2DependParam.m

```
%DOF2DependParam      2 DOF Model Dependent Parameter Calculation
%
%      Calculates values of dependent parameters for 2 DOF model.
%
% Created 1/7/96
% J. Kiefer

% Dependent Parameters
a = (1-f)*L;                                % m     Distance from front tire to C.G.
b = f*L;                                    % m     Distance from rear tire to C.G.
V = u;                                      % m/s   Vehicle speed
Fyg = m*g*sin(theta*pi/180);                % N     Side slope lateral force
Fzf = m*g*f/2*cos(theta*pi/180);            % N     Front tire normal load (one tire)
Fzr = m*g*(1-f)/2*cos(theta*pi/180);        % N     Rear tire normal load (one tire)

% Stability Derivatives
Yb = Cf + Cr;                               % N/rad       Damping-in-sideslip
Yr = (a*Cf-b*Cr)/V;                         % N-s/rad     Lateral force / yaw coupling
Yd = -Cf;                                   % N/rad       Control force
Nb = a*Cf-b*Cr;                             % N-m/rad     Directional stability
Nr = (a^2*Cf+b^2*Cr)/V;                     % N-m-s/rad   Yaw damping
Nd = -a*Cf;                                 % N-m/rad     Control moment
```

C.4 SteerAngle.m

```
function delta = SteerAngle(t,input,t0,tr,td,ts,tf,d0)
%SteerAngle          Calculate Steer Angle Based on Time and Control Input Selection
%
%delta = SteerAngle(t,input,t0,tr,td,ts,tf,d0)
%
%       Determines steer angle based on current time, input selection, and
%       simulation parameters.  Input selection may be step, ramp, ramp square, or
%       sine.  Called by functions DOF2LDE.m, DOF2NLDE.m, DOF3LDE.m, DOF3NLDE.m.
%
%       Inputs:
%              t              Time (s)
%              input          Flag for input selection
%                                     1 = step
%                                     2 = ramp
%                                     3 = rampsquare
%                                     4 = sine
%              t0             Initial time for simulation (s)
%              tr             Ramp time (s)
%              td             Dwell time (s)
%              ts             Period for sine steer (s)
%              tf             Final time for simulation (s)
%              d0             Steer input magnitude (rad)
%
%       Outputs:
%              delta          Steer angle (rad)
%
%       Created 1/7/96
%       J. Kiefer

% Crash Through Result
delta = 0;

% Step Steer
if input == 1
       delta = d0;
       if t < t0
              delta = 0;
       end
end

% Ramp Step Steer
if input == 2
       delta = d0;
       if t < t0 + tr
              delta = d0*(t-t0)/tr;
       end
       if t < t0
              delta = 0;
       end
end

% Ramp Square Steer
if input == 3
```

```
        delta = 0;
        if t < t0 + 2*tr + td
                delta = d0*(t0+td+2*tr-t)/tr;
        end
        if t < t0 + tr + td
                delta = d0;
        end
        if t < t0 + tr
                delta = d0*(t-t0)/tr;
        end
        if t < t0
                delta = 0;
        end
end

% Sine Steer
if input == 4
        delta = d0*sin(2*pi*(t-t0)/ts);
        if t < t0
                delta = 0;
        end
end
```

C.5 DOF2LFreq.m

```
%DOF2LFreq            Frequency Response of Linear 2 DOF Model
% For a Single Set of Parameters
%
%       Generates bode plot data for linear 2 DOF model for outputs of
%       sideslip angle and yaw speed, and for inputs of steer angle control,
%       aerodynamic side force disturbance, and road side slope disturbance.
%
% Created 2/4/96
% J. Kiefer

DOF2Param;                              % Set independent parameters
DOF2Control;                            % Set execution control parameters
DOF2DependParam;                        % Calculate dependent parameters

% Transfer Function Denominator
D = [1 -Nr/Izz-Yb/(m*V) Nb/Izz+(Nr*Yb-Nb*Yr)/(Izz*m*V)];

% Transfer Function Numerators
Nbd = [Yd/(m*V) (Nd*Yr-Nr*Yd-Nd*m*V)/(Izz*m*V)];
Nba = [1/(m*V) (c-a)/Izz+((a-c)*Yr-Nr)/(Izz*m*V)];
Nbt = [g/V -g*Nr/(Izz*V)];
Nrd = [Nd/Izz (Nb*Yd-Nd*Yb)/(Izz*m*V)];
Nra = [(a-c)/Izz ((c-a)*Yb+Nb)/(Izz*m*V)];
Nrt = [g*Nb/(Izz*V)];

% Bode Plot Data
w = logspace(-1,2)*2*pi;
[Mbd,Pbd,w] = bode(Nbd,D,w);
[Mba,Pba,w] = bode(Nba,D,w);
[Mbt,Pbt,w] = bode(Nbt,D,w);
[Mrd,Prd,w] = bode(Nrd,D,w);
[Mra,Pra,w] = bode(Nra,D,w);
[Mrt,Prt,w] = bode(Nrt,D,w);
```

C.6 DOF2LSim.m

```
%DOF2LSim      Simulation of Linear 2 DOF Model Response to Control and Disturbance
%                    Inputs
%
%       Performs simulation of linear 2 DOF model response to control and
%       disturbance inputs.  Determines yaw speed, lateral speed, sideslip angle,
%       front and rear tire slip angles, front and rear tire lateral forces, and
%       lateral acceleration.  Plots these responses versus time.  Reads data from
%       DOF2Param, DOF2DependParam.
%
% Created 1/7/96
% J. Kiefer

DOF2Param;                          % Set independent parameters
DOF2Control;                        % Set execution control parameters
DOF2DependParam;                    % Calculate dependent parameters

% Perform simulation
[t,x] = ode23('DOF2LDE',0,tf,[0 0]',tol);
v = x(:,1);
r = x(:,2);

% Steer Angle
delta = zeros(length(t), 1);
for i = 1:length(t)
       delta(i) = SteerAngle(t(i),input,t0,tr,td,ts,tf,d0);      % rad  Steer angle
end

% Vehicle and Tire Slip Angles
beta = v/u;                                 % rad       Vehicle sideslip angle
alphaF = (v+a*r)/u-delta;                   % rad       Front tires slip angle
alphaR = (v-b*r)/u;                         % rad       Rear tires slip angle

% External Forces and Moments
Fyf = Cf*alphaF;                            % N         Front tires lateral force
Fyr = Cr*alphaR;                            % N         Rear tires lateral force

% State Derivatives
vdot = (Fyf + Fyr + Fya + Fyg)/m - u*r;
rdot = (a*Fyf - b*Fyr - (c-a)*Fya)/Izz;

% Lateral Acceleration
ay = vdot + u*r;                            % m/s^2     Lateral acceleration

% Do Plots
subplot(2,2,1)
plot(t,v)
grid
title('Lateral Speed')
xlabel('Time (s)')
ylabel('Speed (m/s)')

subplot(2,2,2)
plot(t,r*180/pi)
```

```
grid
title('Yaw Speed')
xlabel('Time (s)')
ylabel('Speed (deg/s)')

subplot(2,2,3)
plot(t,beta*180/pi,t,alphaF*180/pi,'--',t,alphaR*180/pi,'-.',t,delta*180/pi,':')
grid
title('Vehicle Sideslip Angle, Tire Slip Angles, Steer Angle')
xlabel('Time (s)')
ylabel('Slip Angle (deg)')

subplot(2,2,4)
plot(t,ay/g)
grid
title('Lateral Acceleration')
xlabel('Time (s)')
ylabel('Acceleration (g)')
```

C.7 DOF2LDE.m

```
function xdot = DOF2NLDE(t,x)
%DOF2NLDE              Non Linear Differential Equations for 2 DOF Model
%
%xdot = DOF2NLDE(t,x)
%
%       Determines derivatives of lateral speed and yaw speed given time and
%       state vector.  Non linear tire and non linear slip angles. Used with ode23
%       for simulation.
%
%       Inputs:
%              t              Time (s)
%              x(1)           Lateral speed (m/s)
%              x(2)           Yaw speed (rad/s)
%       Outputs:
%              xdot(1)        Derivative of lateral speed (m/s^2)
%              xdot(2)        Derivative of yaw speed (rad/s^2)
%
%       Created 2/18/96
%       J. Kiefer

global m Izz L a b c u d0 Fzf Fzr Fyg Fya t0 tr td ts tf input;

delta = SteerAngle(t,input,t0,tr,td,ts,tf,d0);
alphaF = atan((x(1)+a*x(2))/u)-delta;
alphaR = atan((x(1)-b*x(2))/u);
[Fyf, Mzf] = NLTire(Fzf, alphaF);
[Fyr, Mzr] = NLTire(Fzr, alphaR);

xdot = [-u*x(2) + (2*Fyf*cos(delta)+2*Fyr+Fya+Fyg)/m
        (2*a*Fyf*cos(delta)-2*b*Fyr+(a-c)*Fya)/Izz];
```

C.8 DOF2NLSim.m

```
%DOF2NLSim     Simulation of Non-Linear 2 DOF Model Response to Control and Disturbance
%                      Inputs
%
%       Performs simulation of non linear 2 DOF model response to control and
%       disturbance inputs.  Determines yaw speed, lateral speed, sideslip angle,
%       front and rear tire slip angles, front and rear tire lateral forces, and
%       lateral acceleration.  Plots these responses versus time.  Reads data from
%       DOF2Param, DOF2DependParam.
%
% Created 2/18/96
% J. Kiefer

DOF2Param;                              % Set independent parameters
DOF2Control;                            % Set execution control parameters
DOF2DependParam;                        % Calculate dependent parameters

% Perform simulation
[t,x] = ode23('DOF2NLDE',0,tf,[0 0]',tol);
v = x(:,1);
r = x(:,2);

% Steer Angle
delta = zeros(length(t), 1);
for i = 1:length(t)
       delta(i) = SteerAngle(t(i),input,t0,tr,td,ts,tf,d0);      % rad  Steer angle
end

% Vehicle and Tire Slip Angles
beta = atan(v/u);                               % rad          Vehicle sideslip angle
alphaF = atan((v+a*r)/u)-delta;                 % rad          Front tires slip angle
alphaR = atan((v-b*r)/u);                       % rad          Rear tires slip angle

% External Forces and Moments
Fyf = NLTire(Fzf, alphaF);                      % N     Front tire lateral force (one tire)
Fyr = NLTire(Fzr, alphaR);                      % N     Rear tire lateral force (one tire)

% State Derivatives
vdot = (2*Fyf.*cos(delta) + 2*Fyr + Fya + Fyg)/m - u*r;
rdot = (2*a*Fyf.*cos(delta) - 2*b*Fyr - (c-a)*Fya)/Izz;

% Lateral Acceleration
ay = vdot + u*r;                                % m/s^2        Lateral acceleration

% Do Plots
subplot(2,2,1)
plot(t,v)
grid
title('Lateral Speed')
xlabel('Time (s)')
ylabel('Speed (m/s)')

subplot(2,2,2)
plot(t,r*180/pi)
```

```
grid
title('Yaw Speed')
xlabel('Time (s)')
ylabel('Speed (deg/s)')

subplot(2,2,3)
plot(t,beta*180/pi,t,alphaF*180/pi,'--',t,alphaR*180/pi,'-.',t,delta*180/pi,':')
grid
title('Vehicle Sideslip Angle, Tire Slip Angles, Steer Angle')
xlabel('Time (s)')
ylabel('Slip Angle (deg)')

subplot(2,2,4)
plot(t,ay/g)
grid
title('Lateral Acceleration')
xlabel('Time (s)')
ylabel('Acceleration (g)')
```

C.9 DOF2NLDE.m

```
function xdot = DOF2NLDE(t,x)
%DOF2NLDE              Non Linear Differential Equations for 2 DOF Model
%
%xdot = DOF2NLDE(t,x)
%
%       Determines derivatives of lateral speed and yaw speed given time and
%       state vector.  Non linear tire and non linear slip angles. Used with ode23
%       for simulation.
%
%       Inputs:
%              t              Time (s)
%              x(1)           Lateral speed (m/s)
%              x(2)           Yaw speed (rad/s)
%       Outputs:
%              xdot(1)        Derivative of lateral speed (m/s^2)
%              xdot(2)        Derivative of yaw speed (rad/s^2)
%
%       Created 2/18/96
%       J. Kiefer

global m Izz L a b c u d0 Fzf Fzr Fyg Fya t0 tr td ts tf input;

delta = SteerAngle(t,input,t0,tr,td,ts,tf,d0);
alphaF = atan((x(1)+a*x(2))/u)-delta;
alphaR = atan((x(1)-b*x(2))/u);
Fyf = NLTire(Fzf, alphaF);
Fyr = NLTire(Fzr, alphaR);

xdot = [-u*x(2) + (2*Fyf*cos(delta)+2*Fyr+Fya+Fyg)/m
       (2*a*Fyf*cos(delta)-2*b*Fyr+(a-c)*Fya)/Izz];
```

Appendix D Relevant Literature

"Control of Vehicle Dynamics." *Automotive Engineering*, May 1995, p. 87-93.

"Road Vehicles -- Lateral Transient Response Test Methods." ISO 7401, May 1988.

"Road Vehicles -- Steady State Circular Test Procedure." ISO 4138, Aug. 1982.

"Road Vehicles -- Vehicle Dynamics and Road-Holding Ability -- Vocabulary." ISO 8855, Dec. 1991.

"Vehicle Dynamics Terminology." SAE J670e, Warrendale, PA: SAE, 1976.

1994 Motor Sports Engineering Conference Proceedings: Volume 1: Vehicle Design Issues. SAE Publication No. P-287, Dec. 1994.

Allen, R. Wade and Theodore J. Rosenthal. "A Computer Simulation Analysis of Safety Critical Maneuvers for Assessing Ground Vehicle Dynamic Stability." SAE Paper No. 930760, Mar. 1993.

Allen, R. Wade and Theodore J. Rosenthal. "Requirements for Vehicle Dynamics Simulation Models." SAE Paper No. 940175, Feb. 1994.

Allen, R. Wade, Raymond E. Magdaleno, Theodore J. Rosenthal, David H. Klyde, and Jeffrey R. Hogue. "Tire Modeling Requirements for Vehicle Dynamics Simulation." SAE Paper No. 950312, Feb. 1995.

Allen, R. Wade, Thomas T. Myers, and Theodore J. Rosenthal. "Vehicle Stability Considerations with Automatic and Four Wheel Steering Systems." SAE Paper No. 931979, Nov. 1993.

Allen, R. Wade, Theodore J. Rosenthal, and Jeffrey R. Hogue. "Modeling and Simulation of Driver/Vehicle Interaction." SAE Paper No. 960177, Feb. 1996.

Allen, R. Wade, Theodore J. Rosenthal, and Henry T. Szostak. "Steady State and Transient Analysis of Ground Vehicle Handling." SAE Paper No. 870495, 1987.

Allen, R. Wade, Theodore J. Rosenthal, David H. Klyde, Keith J. Owens, and Henry T. Szostak. "Validation of Ground Vehicle Computer Simulations Developed for Dynamics Stability Analysis." SAE Paper No. 920054, Feb. 1992.

Allen, R. Wade, Henry T. Szostak, Theodore J. Rosenthal, David H. Klyde, and Keith J. Owens. "Characteristics Influencing Ground Vehicle Lateral/Directional Dynamic Stability." SAE Paper No. 910234, Feb. 1991.

Antoun, R.J, P.B. Hackert, M.C. O'Leary, and A. Sitchin. "Vehicle Dynamic Handling Computer Simulation -- Model Development, Correlation, and Application Using ADAMS." SAE Paper No. 860574, 1986.

Araki, Kazuo and Hideo Sakai. "Study of Tire Model Consisting of Theoretical and Experimental Equations for Vehicle Dynamics Analysis - Part 2: Under the Condition of Various Velocity on the Asphaltic Road Surface." SAE Paper No. 960996, Feb. 1996.

Ashley, Steven. "Spin Control for Cars." *Mechanical Engineering,* Vol. 117, No. 6, June 1995, p. 66-68.

Bakker, Egbert, Lars Nyborg, and Hans B. Pacejka. "Tyre Modelling for Use in Vehicle Dynamics Studies." SAE Paper No. 870421, 1987.

Bakker, Egbert, Hans B. Pacejka, and Lars Lidner. "A New Tire Model with an Application in Vehicle Dynamics Studies." SAE Paper No. 890087, 1989.

Barak, Pinhas. "Magic Numbers in Design of Suspensions for Passenger Cars." SAE Paper No. 911921, 1991.

Barbieri, Nilson. "Suspensions Optimization." SAE Paper No. 921491, 1992.

Bastow, D. and G. Howard. *Car Suspension and Handling.* Warrendale, PA: SAE, 1993.

Bernard, James E. and C.L. Clover. "Tire Modeling for Low-Speed and High-Speed Calculations." SAE Paper No. 950311, Feb. 1995.

Bernard, James E. and C.L. Clover. "Validation of Computer Simulations of Vehicle Dynamics." SAE Paper No. 940231, Feb. 1994.

Bixel, Ronald A., Gary J. Heydinger, N.J. Durisek, and Dennis A. Guenther. "New Developments in Vehicle Center of Gravity and Inertial Parameter Estimation and Measurement." SAE Paper No. 950356, Feb. 1995.

Blank, Matthew and Donald Margolis. "The Effect of Normal Force Variation on the Lateral Dynamics of Automobiles." SAE Paper No. 960484, Feb. 1996.

Bowman, J. Eric and E.H. Law. "A Feasibility Study of an Automotive Slip Control Braking System." SAE Paper No. 930762, Mar. 1993.

Breuer, Bert, Thomas Bachmann, Stefan Ernesti, and Jorg Stocker. "Methods and Instruments for On-Board Measurement of Tyre/Road Friction." SAE Paper No. 942470, Dec. 1994.

Bundorf, R.T. and R.L. Leffert. "The Cornering Compliance Concept for Description of Vehicle Directional Control Properties." SAE Paper No. 760713, Oct. 1976.

Cambiaghi, Danilo and Marco Gadola. "Computer-Aided Racing Car Design and Development at the University of Brescia, Italy." SAE Paper No. 942507, Dec. 1994.

Captain, K.M., A.B. Boghani, and D.N. Wormley. "Analytical Tire Models for Dynamic Vehicle Simulation." *Vehicle System Dynamics,* Vol. 8, 1979, p. 1-32.

Car Suspension Systems and Vehicle Dynamics. SAE Publication No. SP-878, Sept. 1991.

Chen, H. Fred and Dennis A. Guenther. "The Effects of Suspension Stiffness on Handling Responses." SAE Paper No. 911928, 1991.

Chocholek, S.E. "The Development of a Differential for the Improvement of Traction Control." IMechE Paper No. C368/88, 1988.

Chrstos, Jeffrey P. "A Simplified Method for the Measurement of Composite Suspension Parameters." SAE Paper No. 910232, 1991.

Clover, Chris L. and James E. Bernard. "The Influence of Lateral Load Transfer Distribution on Directional Response." SAE Paper No. 930763, Mar. 1993.

Cole, D.E. *Elementary Vehicle Dynamics.* Ann Arbor, MI: University of Michigan, 1972.

Crahan, Thomas C. "Modeling Steady-State Suspension Kinematics and Vehicle Dynamics of Road Racing Cars - Part I: Theory and Methodology." SAE Paper No. 942505, Dec. 1994.

Crahan, Thomas C. "Modeling Steady-State Suspension Kinematics and Vehicle Dynamics of Road Racing Cars - Part II: Examples." SAE Paper No. 942506, Dec. 1994.

Crolla, D.A. and M.B.A. Abdel-Hady. "Semi-Active Suspension Control for a Full Vehicle Model." SAE Paper No. 911904, Sept. 1991.

Day, Terry D. "An Overview of the HVE Vehicle Model." SAE Paper No. 950308, Feb. 1995.

Dickison, J.G. and A.J. Yardley. "Development and Application of a Functional Model to Vehicle Development." SAE Paper No. 930835, Mar. 1993.

Dixon, John C. *Tyres, Suspension and Handling,* Cambridge, England: Cambridge University Press, 1991.

Dreyer, Andreas and Heinz-Dieter Heitzer. "Control Strategies for Active Chassis Systems with Respect to Road Friction." SAE Paper No. 910660, Feb. 1991.

Egnaczak, Bernard C. "Supplement to: 'The Development of a Differential for the Improvement of Traction Control." Auto Tech 89, Session 5 Traction Control, Nov. 14, 1989.

ElBeheiry, ElSayed M. and Dean C. Karnopp. "Optimization of Active and Passive Suspensions Based on a Full Car Model." SAE Paper No. 951063, Feb. 1995.

Ellis, John R. *Road Vehicle Dynamics,* Akron, OH: J.R. Ellis, 1989.

Ellis, John R. *Vehicle Dynamics.* London: Business Books, 1969.

Floyd, R. Scott and E. Harry Law. "Simulation and Analysis of Suspension and Aerodynamic Interactions of Race Cars." SAE Paper No. 942537, Dec. 1994.

Franklin, Gene F., J. David Powell, and Abbas Emami-Naeini. *Feedback Control of Dynamic Systems.* New York: Addison-Wesley Publishing Company, Inc., 1994.

Garrot, W. Riley, Douglas L. Wilson, and Richard A. Scott. "Digital Simulation for Automobile Maneuvers." *Simulation,* Sept. 1981, p. 83-91.

Gillespie, T.D. *Fundamentals of Vehicle Dynamics.* Warrendale, PA: SAE, 1992.

Gim, Gwanghun and Namcheol Kang. "Requirements of a Tire Model for Practical Cornering Simulations of Vehicles." SAE Paper No. 960179, Feb. 1996.

Gim, Gwanghun and Parviz E. Nikravesh. "A Three-Dimensional Tire Model for Steady-State Simulations of Vehicles." SAE Paper No. 931913, Nov. 1993.

Gim, Gwanghun and Parviz E. Nikravesh. "An Analytical Model of Pneumatic Tyres for Vehicle Dynamic Simulations. Part 1: Pure Slips." *International Journal of Vehicle Design,* Vol. 11, No. 6, 1990.

Gim, Gwanghun and Parviz E. Nikravesh. "An Analytical Model of Pneumatic Tyres for Vehicle Dynamic Simulations. Part 2: Comprehensive Slips." *International Journal of Vehicle Design,* Vol. 12, No. 1, 1991.

Gruening, James and James E. Bernard. "Verification of Vehicle Parameters for Use in Computer Simulation." SAE Paper No. 960176, Feb. 1996.

Gruening, James, Keith A. Williams, Kurt Hoffmeister, and James E. Bernard. "Tire Force and Moment Processor." SAE Paper No. 960182, Feb. 1996.

Guntur, R. and S. Sankar. "A Friction Circle Concept for Dugoff's Tyre Friction Model." *International Journal of Vehicle Design,* Vol. 1, No. 4, 1980.

Haney, Paul and Jeff Braun. *Inside Racing Technology.* Redwood City, CA: TV Motorsports, 1995.

Heydinger, Gary J. "Improved Simulation and Validation of Road Vehicle Handling Dynamics." Ph.D. Dissertation, Ohio State University, Columbus, Ohio, 1990.

Heydinger, Gary J., W. Riley Garrot, and Jeffrey P. Chrstos. "The Importance of Tire Lag on Simulated Transient Vehicle Response." SAE Paper No. 910235, 1991.

Heydinger, Gary J., Paul A. Grygier, and Seewoo Lee. "Pulse Testing Techniques Applied to Vehicle Handling Dynamics." SAE Paper No. 930828, Mar. 1993.

Holmes, H. and D. Alexander. *Formula Car Technology.* Santa Ana, CA: Steve Smith Autosports, 1980.

Hopkins, Patrick and L. Daniel Metz. "Oversteer/Understeer Characteristics of a Locked Differential." SAE Paper No. 942485, Dec. 1994.

Howard, Geoffrey. *Chassis & Suspension Engineering,* London, England: Osprey Publishing Limited, 1987.

Huang, Feng, J. Roger Chen, and Lung-Wen Tsai. "The Use of Random Steer Test Data for Vehicle Parameter Estimation." SAE Paper No. 930830, Mar. 1993.

Huchtkoetter, Heinrich and Heinz Klein. "The Effect of Various Limited-Slip Differentials in Front-Wheel Drive Vehicles on Handling and Traction." SAE Paper No. 960717, Feb. 1996.

Ikushima, Y. and K Sawase. "A Study on the Effects of the Active Yaw Moment Control." SAE Paper No. 950303, Feb. 1995.

Jung, Shinsub and Dennis A. Guenther. "An Examination of the Maneuverability of an All Wheel Steer Vehicle at Low Speed." SAE Paper No. 910241, Feb. 1991.

Kaminaga, M., M. Murata, and Y. Tateishi. "Factoring Nonlinear Kinematics into New Suspension Design: A CAE Approach to Vehicle Roll Dynamics." SAE Paper No. 940871, Feb. 1994.

Karnopp, Dean. "Active Damping in Road Vehicle Suspension Systems." *Vehicle System Dynamics,* Vol. 12, 1983, p. 291-316.

Kasprzak, James L. and R. Scott Floyd. "Use of Simulation to Tune Race Car Dampers." SAE Paper No. 942504, Dec. 1994.

Katz, Joseph. *Race Car Aerodynamics.* Cambridge, MA: Robert Bentley, Inc., 1995.

Klein, Richard H., Gary L. Teper, and James D. Fait. "Lateral/Directional Stability of Tow Dolly Type Combination Vehicles." SAE Paper No. 960184, Feb. 1996.

Ko, Y. and T. Oh. "Motion Control of the Vehicle with an Active Suspension System." SAE Paper No. 940865, Feb. 1994.

Koibuchi, Ken, Masaki Yamamoto, Yoshiki Fukada, and Shoji Inagaki. "Vehicle Stability Control in Limit Cornering by Active Brake." SAE Paper No. 960487, Feb. 1996.

Kortum, W. and W. Schiehlen. "General Purpose Vehicle System Dynamics Software Based on Multibody Formalisms." *Vehicle System Dynamics,* No. 14, 1985, p. 229-263.

Kramer, Kenneth D. and Dale E. Calkins. "Lateral Response of Formula SAE Race Car." SAE Paper No. 942523, Dec. 1994.

La Joie, Joseph C. "Race Car Performance Optimization." SAE Paper No. 942492, Dec. 1994.

Langer, William. "Vehicle Testing with Flat Surface Roadway Technology." SAE Paper No. 960731, Feb. 1996.

Lee, Allan Y. "Emulating the Lateral Dynamics of a Range of Vehicles Using a Four-Wheel-Steering Vehicle." SAE Paper No. 950304, Feb. 1995.

Lee, Allan Y. "Performance of Four-Wheel-Steering Vehicles in Lane Change Maneuvers." SAE Paper No. 950316, Feb. 1995.

Lee, Seewoo, Jeffrey P. Chrstos, and Dennis A. Guenther. "Modeling of Dynamic Characteristics of Tire Lateral and Longitudinal Force Responses to Dynamic Inputs." SAE Paper No. 950314, Feb. 1995.

Lee, Seewoo, Gary J. Heydinger, and Dennis A. Guenther. "The Application of Pulse Input Techniques to the Study of Tire Lateral Force and Self-Aligning Moment Dynamics in the Frequency Domain." SAE Paper No. 950317, Feb. 1995.

Lund, Yvonne I. and James E. Bernard. "The Relationship Between the Complexity of Linear Models and the Utility of the Computer Results." SAE Paper No. 920052, Feb. 1992.

Maalej, Aref Y. "Application of Suspension Derivative Formulation to Ground Vehicle Modeling and Simulation." Ph.D. Dissertation, The Ohio State University, Columbus, OH, 1988.

Mabrouka, Hani, H. Fred Chen, Aref Y. Maalej, and Dennis A. Guenther. "Effect of Lateral Tire Flexibility on the Steering Dynamic Behavior." SAE Paper No. 910239, Feb. 1991.

Mashadi, Behrooz and David A. Crolla. "Vehicle Handling Analysis Using Linearization Around Non-Linear Operating Conditions." SAE Paper No. 960482, Feb. 1996.

McConville, James B. and John C. Angell. "The Dynamic Simulation of a Moving Vehicle Subject to Transient Steering Inputs Using the ADAMS Computer Program." ASME Paper No. 84-DET-2, 1984.

Metz, L. Daniel and D.M. Alter. "Transient and Steady State Performance Characteristics of a Two-Wheel-Steer and Four-Wheel-Steer Vehicle Model." SAE Paper No. 911926, 1991.

Metz, L. Daniel, Michael Dover, John Fisher, Victoria McCleary, and Errol Shavers. "Comparison of Linear Roll Dynamics Properties for Various Vehicle Configurations." SAE Paper No. 920053, 1992.

Metz, L. Daniel, Troy S. Torbeck, Kevin H. Forbes, and L. Gregory Metz. "Evasive Maneuver Capability Without and In the Presence of a Flat Tire." SAE Paper No. 942469, Dec. 1994.

Metz, L. Daniel. "Dynamics of Four-Wheel Steer Off-Highway Vehicles." SAE Paper No. 930765, Mar. 1993.

Milliken, William F. and Doug L. Milliken. *Race Car Vehicle Dynamics.* Warrendale, PA: SAE, 1995.

Milliken, William F. and R.S. Rice. "Moment Method." IMechE Paper No. C113/83, 1983, p. 31-60.

Milliken, William F., Peter G. Wright, and Douglas L. Milliken. "Moment Method -- A Comprehensive Tool for Race Car Development." SAE Paper No. 942538, Dec. 1994.

Mimuro, Tetsushi, Masayoshi Ohsaki, Hiromichi Yasunaga, and Kohji Satoh. "Four Parameter Evaluation Method of Lateral Transient Response." SAE Paper No. 901734, 1990.

Mola, Simone. *Fundamentals of Vehicle Dynamics,* Detroit, MI: General Motors Institute, 1969.

Moline, D., S. Floyd, S. Vaduri, and E.H. Law. "Simulation and Evaluation of Semi-Active Suspensions." SAE Paper No. 940864, Feb. 1994.

Mori, Yoshinori, Hironobu Matsushita, Takashi Yonekawa, Yoshihisa Nagahara, and Hiroshi Shimomura. "A Simulation System for Vehicle Dynamics Control." SAE Paper No. 910240, Feb. 1991.

Nalecz, Andrzej G. "Analysis of the Dynamic Response of a Four Wheel Steering Vehicles at High Speed." *International Journal of Vehicle Design,* Vol. 9, No. 2, 1988.

Nalecz, Andrzej G. "Development and Validation of Light Vehicle Dynamics Simulation (LVDS)." SAE Paper No. 920056, Feb. 1992.

Nalecz, Andrzej G. and Alan C. Bindemann. "Investigation into the Stability of Four Wheel Steering Vehicles." *International Journal of Vehicle Design,* Vol. 9, No. 2, 1988, p. 159-178.

Naude, Alwyn F. and Jasper L. Steyn. "Objective Evaluation of the Simulated Handling Characteristics of a Vehicle in a Double Lane Change Manoeuvre." SAE Paper No. 930826, Mar. 1993.

Negrut, D. and J.S. Freeman. "Dynamic Tire Modelling for Application with Vehicle Simulations Incorporating Terrain." SAE Paper No. 940223, Feb. 1994.

Neto, Mauro Speranza, Fernando Riberio da Silva, and Jose Francisco Martinex. "Design Methodology in Vehicle Dynamics, Using the Procedures of Modeling, Simulation, and Analysis of System Dynamics." SAE Paper No. 921480, 1992.

New Developments in Vehicle Dynamics, Simulation, and Suspension Systems. SAE Publication No. SP-1074, Feb. 1995.

Nikravesh, Parviz E. and Jong-Nyun Lee. "Optimal Four-Wheel Steering Strategy Using Nonlinear Analytical Vehicle Models." SAE Paper No. 931915, Nov. 1993.

Olley, Maurice. "Suspension and Handling." Detroit, MI: Chevrolet Engineering Center, 1937.

Olley, Maurice. "Notes on Suspensions." Detroit, MI: Chevrolet Engineering Center, 1961.

Olley, Maurice. "Suspensions Notes II." Detroit, MI: Chevrolet Engineering Center, 1966.

Palmeri, Paolo S., Alberto Moschetti, and Luigi Gortan. "H-Infinity Control for Lancia Thema Full Active Suspension System." SAE Paper No. 950583, Feb. 1995.

Petersen, Michael R. and John M. Starkey. "Nonlinear Vehicle Performance Simulation with Test Correlation and Sensitivity Analysis." SAE Paper No. 960521, Feb. 1996.

Post, J.W. and E.H. Law. "Modeling, Characterization and Simulation of Automobile Power Steering Systems for the Prediction of On-Center Handling." SAE Paper No. 960178, Feb. 1996.

Radt, Hugo S. "An Efficient Method for Treating Race Tire Force-Moment Data." SAE Paper No. 942536, Dec. 1994.

Radt, Hugo S. and D.A. Glemming. "Normalization of Tire Force and Moment Data." *Tire Science and Technology,* Vol. 21, No. 2, Apr.-June 1993, p. 91-119.

Radt, Hugo S. and Donald J. Van Dis. "Vehicle Handling Responses Using Stability Derivatives." SAE Paper No. 960483, Feb. 1996.

Reichelt, Werner. "Correlation Analysis of Open/Closed Loop Data for Objective Assessment of Handling Characteristics of Cars." SAE Paper No. 910238, Feb. 1991.

Reimpell, Jornsen and Helmut Stoll. *The Automotive Chassis: Engineering Principles.* Warrendale, PA: SAE, 1996.

Rice, R.S. and William F. Milliken. "Static Stability and Control of the Automobile Utilizing the Moment Method." SAE Paper No. 800847, June 1980.

Sayers, Micheal W. and C. Mink. "A Simulation Graphical User Interface for Vehicle Dynamics Models." SAE Paper No. 950169, Feb. 1995.

Sayers, Michael W. and Stephen M. Riley. "Modeling Assumptions for Realistic Multibody Simulations of the Yaw and Roll Behavior of Heavy Trucks." SAE Paper No. 960173, Feb. 1996.

Schuring, Dieterich J., Wolfgang Pelz, and Marion G. Pottinger. "A Model for Combined Tire Cornering and Braking Forces." SAE Paper No. 960180, Feb. 1996.

Schuring, Dieterich J., Wolfgang Pelz, and Marion G. Pottinger. "An Automated Implementation of the 'Magic Formula' Concept." SAE Paper No. 931909, Nov. 1993.

Segal, Leonard. "Theoretical Prediction and Experimental Substantiation of the Response of the Automobile to Steering Control." *Proceedings of the Automobile Division of the Institution of Mechanical Engineers*, No. 7, 1956-1957, p. 310-330.

Sharp, R.S. and D.A. Crolla. "Road Vehicle Suspension System Design -- A Review." *Vehicle System Dynamics,* Vol. 16, 1987, p. 167-192.

Shimada, K. and Y. Shibahata. "Comparison of Three Active Chassis Control Methods for Stabilizing Yaw Moments." SAE Paper No. 940870, Feb. 1994.

Smith, C. *Engineer to Win.* Osceola, WI: Motorbooks International, 1984.

Smith, C. *Prepare to Win.* Fallbrook, CA: Aero Publishers, Inc., 1975.

Smith, C. *Tune to Win.* Fallbrook, CA: Aero Publishers, Inc., 1978.

Smith, Norman. "Transient Control Response of Automobiles." *Vehicle System Dynamics,* Vol. 6, No. 2-3, Sept. 1977, p. 63-67.

Sohn, H.S., S.C. Lee, M.W. Suh, and Y.M. Song. "The Influences of Chassis Geometric Characteristics on Vehicle Dynamic Performances." SAE Paper No. 940872, Feb. 1994.

Song, Jun-gyu and Yong-San Yoon. "Design of Two-Wheel Steer Vehicle Using Optimal Control Algorithm of Four-Wheel Steer." SAE Paper No. 931914, 1993.

Staniforth, A. *Competition Car Suspension.* Newbury Park, CA: Haynes Publications Inc., 1991.

Sultan, Mohammad O., Gary J. Heydinger, Nicholas J. Durisek, and Dennis A. Guenther. "A Study of Vehicle Class Segregation Using Linear Handling Models." SAE Paper No. 950307, Feb. 1995.

Taborek, Jaroslav J. *Mechanics of Vehicles.* Cleveland, OH: Penton, 1957.

Thomas, D.W. "Vehicle Modeling and Service Loads Analysis." SAE Paper No. 871940, Oct. 1987.

Trom, J.D., J.L. Lopex, and M.J. Vanderploeg. "Modeling of a Mid-Size Passenger Car Using a Multibody Dynamics Program." *Transactions of the ASME, Journal of Mechanisms, Transmissions, and Automation in Design*, Vol. 109, Dec. 1987.

Trom, J.D., M.J. Vanderploeg, and James E. Bernard. "Application of Inverse Models to Vehicle Optimization Problems." *Vehicle System Dynamics,* Vol. 19, 1990, p. 97-110.

Turpin, D.R. and D.F. Evans. "High-Fidelity Road/Tire Interaction Models for Real Time Simulation." SAE Paper No. 950170, Feb. 1995.

Van Valkenburgh, P. *Race Car Engineering and Mechanics.* Seal Beach, CA: Paul Van Valkenburgh, 1986.

van Zanten, Anton Th., Rainer Erhardt, Albert Lutz, Wilfried Neuwald, and Harmut Bartels. "Simulation for the Development of the Bosch-VDC." SAE Paper No. 960486, Feb. 1996.

Vanderlploeg, M.J., J.D. Trom, and James E. Bernard. "Evaluation of Four-Wheel Steer Path Follow Performance Using a Linear Inverse Vehicle Model." SAE Paper No. 880644, 1988.

Vedamuthu, S. and E.H. Law. "An Investigation of the Pulse Steer Method for Determining Automobile Handling Qualities." SAE Paper No. 930829, Mar. 1993.

Vehicle Dynamics and Electronic Controlled Suspensions. SAE Publication No. SP-861, Feb. 1991.

Vehicle Dynamics and Rollover Propensity Research. SAE Publication No. SP-909, Feb. 1992.

Vehicle Dynamics and Simulation. SAE Publication No. SP-950, Mar. 1993.

Vehicle Suspension System Advancements. SAE Publication No. SP-1031, Feb. 1994.

Whatmough, K.J. "Real-Time Wheel Brake and Tire Lateral Force Models Refined for Low Speeds." SAE Paper No. 940178, Feb. 1994.

Whitcomb, David W. and William F. Milliken. "Design Implications of a General Theory of Automobile Stability and Control." *Proceedings of the Automobile Division of the Institution of Mechanical Engineers* , Aug. 1956, p. 83-107.

Wilson, D.A., R.S. Sharp, and S.A. Hassan. "Application of Linear Optimal Control Theory to the Design of Automobile Suspension." *Vehicle System Dynamics,* Vol. 15, 1986, p. 105-118.

Wong, Jo Yung. *Theory of Ground Vehicles.* New York: John Wiley & Sons, Inc., 1993.

Wright, Peter. "Out at the Edge!" *Racecar,* Vol. 5, No. 3, 1995, p. 15-18.

Xia, Xunmao. "A Nonlinear Analysis of Closed Loop Driver/Vehicle Performance with Four Wheel Steering Control." Ph.D. Dissertation, Department of Mechanical Engineering, Clemson University, Clemson, SC, Dec. 1990.

Xia, Xunmao and E.H. Law. "Nonlinear Analysis of Closed Loop Driver/Automobile Performance with Four Wheel Steering Control." SAE Paper No. 920055, 1992.

Xia, Xunmao and J.N. Willis. "The Effects of Tire Cornering Stiffness on Vehicle Linear Handling Performance." SAE Paper No. 950313, Feb. 1995.

Yamamoto, Masaki. "Active Control Strategy for Improved Handling and Stability." SAE Paper No. 911902, Sept. 1991.

Yasui, Yoshiyuki, Kenji Tozu, Noriaki Hattori, and Masakazu Sugisawa. "Improvement of Vehicle Directional Stability for Transient Steering Maneuvers Using Active Brake Control." SAE Paper No. 960485, Feb. 1996.